

The behavior of shallow arches subjected to static and dynamic loads
by Johnson Liao

A thesis submitted to the Graduate Faculty in partial fulfillment of the requirements for the degree of
DOCTOR OF PHILOSOPHY in Civil Engineering
Montana State University
© Copyright by Johnson Liao (1973)

Abstract:
The behavior of hinged shallow circular arches respectively under arbitrary static loading and under a moving load is studied.

The first part of this thesis deals with the static stability problem, the second part with the dynamic instability, and the last part with the deflection and the stresses on the arch rib. The results respectively due to various types of loading are obtained and examined. It is found that the smallest static buckling loads for the hinged shallow circular arches occur when the point load lies between the support and the center of the span. In the dynamic case the results show that except for a small range of v/L (speed-span ratio) the dynamic buckling loads are greater as v increases. For some range of v/L, the dynamic buckling load is found to be less than the corresponding static buckling load.

For large geometric parameter λ, the effect of λ upon the deflection and the static stresses is negligible. However, the effect of the section stiffness upon the static deflection as well as static stresses is quite significant.

THE BEHAVIOR OF SHALLOW ARCHES SUBJECTED TO STATIC AND DYNAMIC LOADS

by

JOHNSON LIAO

A thesis submitted to the Graduate Faculty in partial fulfillment of the requirements for the degree

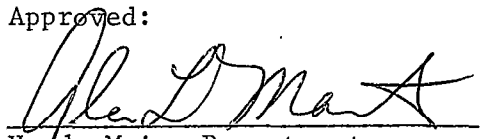
of

DOCTOR OF PHILOSOPHY

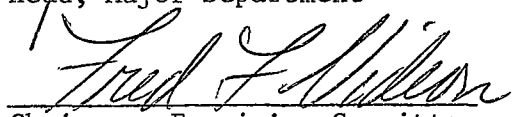
in

Civil Engineering

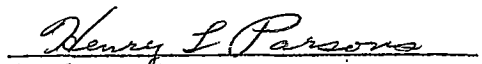
Approved:



Head, Major Department



Chairman, Examining Committee



Graduate Dean

MONTANA STATE UNIVERSITY
Bozeman, Montana

March, 1973

ACKNOWLEDGEMENT

The author wishes to express his sincere appreciation to Dr. Fred. F. Videon under whose guidance this research was conducted. Great gratitude goes to Dr. Theodore E. Lang whose suggestions and assistance have been helpful in the completion of this work.

The author is also indebted to Dr. Robert L. Brown for his help in solving part of the equations. Thanks are due to Dr. Donald R. Reichmuth and Dr. Harry W. Townes for their valued opinions.

The author deeply thanks the Civil Engineering and Engineering Mechanics Department headed by Dr. Glen L. Martin for its financial support with which this research is made possible.

Finally, acknowledgement is extended to Mrs. Peggy Humphrey, Miss Linda Van Dyken, and Mrs. Dee Strong for their help in typing the dissertation.

TABLE OF CONTENTS

	Page
NOTATION	
CHAPTER 1: INTRODUCTION	1
1.1 General Introduction and Scope	1
1.2 Historical Background	3
CHAPTER 2: DERIVATION OF EQUATIONS	5
2.1 Introduction	5
2.2 Arch Equations in General	5
2.3 Equations for Shallow Arches	16
2.4 Equations of Motion for Shallow Arches	20
CHAPTER 3: THE STATIC STABILITY OF SHALLOW ARCHES	21
3.1 Introduction	21
3.2 Point Load	21
3.3 Point Load and Uniformly Distributed Pressure Acting Simultaneously	33
CHAPTER 4: DYNAMIC STABILITY OF SHALLOW ARCHES SUBJECT TO MOVING LOAD	44
4.1 Introduction	44
4.2 Point Load	45
4.3 Point Load Plus Uniform Pressure	58
4.4 Damping Effects	62
4.5 The New Concept About Dynamic Instability	63
CHAPTER 5: THE DEFLECTION AND THE STRESSES OF PINNED-END SHALLOW CIRCULAR ARCHES	87
5.1 Introduction	87
5.2 Static Deflection and Dynamic Deflection	88
5.3 Static Stresses and Dynamic Stresses	109
CHAPTER 6: DISCUSSIONS AND CONCLUSIONS	122
APPENDICES	126
BIBLIOGRAPHY	169

LIST OF TABLES

Table		Page
3-1	Critical Load Parameter $\bar{P}_{cr}$ for Pinned-end Shallow Circular Arches Under Point Load Only.	127
3-2	Critical Load Parameter $\bar{P}_{cr}$ for Pinned-end Shallow Circular Arches Under Point Load and Uniform Pressure ($\bar{\phi}$ = 1.0). . . .	128
3-3	Critical Load Parameter $\bar{P}_{cr}$ for Pinned-end Shallow Circular Arches under Point Load and Uniform Pressure ($\bar{\phi}$ = 0.1). . . .	129
3-4	Critical Load Parameter $\bar{P}_{cr}$ for Pinned-end Shallow Circular Arches Under Point Load and Uniform Pressure ($\bar{\phi}$ = 0.05) . . .	130
3-5	Critical Load Parameter $\bar{P}_{cr}$ for Pinned-end Shallow Circular Arches Under Point Load and Uniform Pressure ($\bar{\phi}$ = 0.01) . . .	131
3-6	Critical Load Parameter $\bar{P}_{cr}$ for Pinned-end Shallow Circular Arches Under Point Load and Uniform Pressure ($\bar{\phi}$ = 0.001). . .	132
3-7	Critical Load Parameter $\bar{P}_{cr}$ for Pinned-end Shallow Circular Arches Under Point Load and Uniform Pressure ($\bar{\phi}$ = 0.0001) . .	133
3-8	Critical Load Parameter $\bar{P}_{cr}$ for Pinned-end Shallow Circular Arches Under Point Load and Uniform Pressure ($\bar{\phi}$ = 0.00001). .	134
4-1	Critical Load Parameter P_{2cr} for Pinned-end Shallow Circular Arches Under Point Load Only.	135
4-2	Critical Load Parameter P_{2cr} for Pinned-end Shallow Circular Arches Under Point Load and Uniform Pressure ($\bar{\phi}$ = 1.0). . . .	136
4-3	Critical Load Parameter P_{2cr} for Pinned-end Shallow Circular Arches Under Point Load and Uniform Pressure ($\bar{\phi}$ = 0.1). . . .	136
4-4	Critical Load Parameter P_{2cr} for Pinned-end Shallow Circular Arches Under Point Load and Uniform Pressure ($\bar{\phi}$ = 0.001). . .	137
4-5	Critical Load Parameter P_{2cr} for Pinned-end Shallow Circular Arches Under Point Load and Uniform Pressure ($\bar{\phi}$ = 0.00001). .	137
4-6	Critical Load Parameter P_{2cr} for Pinned-end Shallow Circular Arches Under Uniform Pressure Only.	137

LIST OF TABLES (Cont'd.)

Table		Page
4-7	Critical Load Parameter P_{2cr} for Pinned-end Shallow Circular Arches Under Point Load Only (Damping Effects Included) . . .	138
5-1	Relationship among λ, L, H/L, H, β and $\bar{R}$.	139
5-2	Deflection of Pinned-end Shallow Circular Arches (E = 475200 psf, I = 1/96 ft^4, A = 1/2 ft^2, b = 1 ft, and L = 50 ft). . .	140
5-3	Maximum Stresses of Pinned-end Shallow Circular Arches (E = 475200 psf, I = 1/96 ft^4, A = 1/2 ft^2, b = 1 ft, and L = 50 ft).	153
5-4	Maximum Stresses Computed by the Elastic Theory (E.T.) and by the Deflection Theory (D.T.)	166

LIST OF FIGURES

Figure		Page
2-1a	Pin-Pin Circular Arches Under Uniform Pressure q.	6
2-1b	Equilibrium State of the Element ΔS	6
2-2	An Arch Section Before and After Deformation.	9
2-3	Deformation of a Small Arch Element	9
3-1	Load-Displacement Curve	25
3-2	Load-Displacement Curve (Bifurcation Instability)	25
3-3	Relation Between $\bar{P}$, the External Load Parameter and μ, the Axial Load Parameter.	28
3-4	Relation Between $\bar{P}$, the External Load Parameter and μ, the Axial Load Parameter (the Bifurcation Point Lying in the Unstable Region).	28
3-5	Effect of the Load Position η_o/μ and the Geometric Parameter λ upon the Critical Loads $\bar{P}_{cr}$	34
3-6	Relation Among the Geometric Parameter λ, the Radius of Gyration R^* and the Arch rise H	35
3-7	Effect of Uniform Pressure on the Critical Loads $\bar{P}_{cr}$.	37
4-1 a-e	Response Curves of A_1, A_2, A_3, A_4 and A_5.	48
4-1f	Effect of Number of Modes Upon Buckling Loads P_{2cr}.	53
4-2	Critical Load Parameter P_{2cr} Corresponding to Various Values of the Geometric Parameter λ_1 and Speed-Span Ratio v/L	56
4-3	Effect of the Speed-Span Ratio upon the Buckling Load P_{2cr}.	57
4-4	Comparison of Critical Values for Pin-Pin Shallow Circular Arches Subject to Uniform Pressure and Combined Loading Respectively, ($\bar{\phi}$ = 1.0)	59

LIST OF FIGURES (Cont'd.)

Figure		Page
4-5	Comparison of Critical Values for Pin-Pin Shallow Circular Arches Subject to Uniform Pressure and Combined Loading Respectively, ($\bar{\phi}$ = 0.00001)	61
4-6	Response Curves of A_1 Associated with D = 0.0, 0.1 and 1.0 Respectively.	64
4-7	Effect of Damping (D = 0.1)	65
4-8	Response Curve of A_1 (One Mode Approximation)	68
4-9	Response Curve of A_1 (One Mode Approximation)	69
4-10	Response Curve of A_1 (One Mode Approximation)	70
4-11	Response Curve of A_1 (One Mode Approximation)	71
4-12	Relation Between the Equivalent Frequency and A_1	74
4-13	Response History of A_1 (One Mode Approximation: A_1 Only)	79
4-14	Response History of A_1 (Two-Modes Approximation: A_1 plus A_2)	80
4-15	Response History of A_1 (One Mode Approximation: A_1 Only)	81
4-16	Response History of A_1 (Two-Modes Approximation: A_1 plus A_2)	82
4-17	Response History of A_1 (One Mode Approximation: A_1 Only)	83
5-1	Deformed Shapes of Pin-Pin Shallow Circular Arches.	90
5-2	Influence Lines for Deflection (λ = 10) (at x/L = .1, .3, .5, .7, .9)	100
5-3	Influence Lines for Deflection (λ = 30) (at x/L = .1, .3, .5, .7, 19)	101
5-5	Effect of λ Upon Abs. Max. Deflection	107
5-4a	Effect of Speed-Span Ratio Upon Abs. Max. Displacement.	103

LIST OF FIGURES (Cont'd.)

Figure		Page
5-4b	Enlargement of a Part of Fig. 5-4a.	104
5-4c	Effect of Speed Upon the Abs. Max. Displacement	105
5-6	Effect of Radius of Gyration on Deflection ($\lambda = 50$)	108
5-7	Comparison for Max. Deflection for (a) static case, (b) v = 1.0, (c) v = 5.0, (d) v = 10.0 ft/sec	110
5-8	Influence Lines for Stress.	112
5-9	Comparison of σ_{max}.	112
5-10	Effect of λ Upon Stresses	115
5-11	Effect of the Geometric Parameter λ Upon Abs. M_{max} and N_{max}	117
5-12	Effect of Radius of Gyration Upon Stresses.	118
5-13	Variation of the Axial Thrust Due to v.	119
5-14	Maximum Stresses Computed by the Elastic Theory (E.T.) and by the Deflection Theory (D.T.)	121

ABSTRACT

The behavior of hinged shallow circular arches respectively under arbitrary static loading and under a moving load is studied.

The first part of this thesis deals with the static stability problem, the second part with the dynamic instability, and the last part with the deflection and the stresses on the arch rib. The results respectively due to various types of loading are obtained and examined. It is found that the smallest static buckling loads for the hinged shallow circular arches occur when the point load lies between the support and the center of the span. In the dynamic case the results show that except for a small range of v/L (speed-span ratio) the dynamic buckling loads are greater as v increases. For some range of v/L, the dynamic buckling load is found to be less than the corresponding static buckling load.

For large geometric parameter λ, the effect of λ upon the deflection and the static stresses is negligible. However, the effect of the section stiffness upon the static deflection as well as static stresses is quite significant.

NOTATION

A cross-sectional area of the arch

$\bar{a}$ unit tangential vector

$\bar{A}_n, A_n$ the amplitude of the n^{th} harmonic; $A_n = \frac{\bar{A}_n}{2R^*}$

A_1^*, A_1^{**} critical amplitude associated with the first mode

A_{nin} value of A_n at $T = 0$

b width of the arch

C the distance between the point load and the left support

D damping coefficient

$\bar{D} = DL^4/EI\pi^4$

E Young's modulus

$e = \sqrt{N_1}$

$e_{\alpha\alpha}$ axial strain component

$e_{\zeta\zeta}$ strain component in the radial direction

$e_{\alpha\zeta}$ shearing strain component

e_c defined in Eq. (2.23) $[= \frac{du}{ds} - \frac{w}{R} + \frac{1}{2}(\frac{dw}{ds})^2]$

$\bar{g}$ a vector defined in Eq. (2.25)

H rise of the undeformed arch

I moment of inertia of the arch section

$I^* = \int_A (\zeta^2/1 - \zeta/R)\, dA$

$J(\ )$ indicating unit step function

K_c defined in Eq. (2.23a) $[= \frac{d^2w}{ds^2} - \frac{w}{R^2}]$

$k = H/L$

L span length of the arch

M_{max} maximum moment corresponding to a point of application of the point load

Abs. M_{max} the largest value of M_{max} for an arch

M bending moment of an arch section

ΔM small increment of M

m mass per unit length of the arch axis

N_{max} absolute maximum axial thrust

N axial thrust

ΔN small increment of N

N_o constant axial thrust

$N_1 = -A \epsilon \bar{R}^2/2$

$\bar{n}$ unit normal vector

P external point load

$P_1 = P\bar{R}^3/EI$; $P_2 = \dfrac{PL^3}{2EI\pi^4 R^*}$; $\bar{P} = P_1\beta/\bar{R}$

$\bar{P}^A_{cr}$ antisymmetric buckling load parameter

Q shear force resultant

ΔQ small increment of Q

q uniform pressure per unit length of the arch axis

R radius of the deformed arch

$\bar{R}$ radius of the undeformed arch

R^* radius of gyration of an arch section

$\bar{R}_o, \bar{R}^*$ position vectors explained in Section 2-2

$\bar{r}_o$, $\bar{r}$ position vectors explained in Section 2-2

$S = \dfrac{N_o L^2}{EI\pi^2}$

s distance measured along the arch axis from the left support

Δs curved length of an arch element

$\Delta s'$, $\Delta s''$ see Figure 2-3

$\bar{s} = s/R$

T time

t thickness of the arch rib

$U \quad u/\bar{R}\beta^2$

u tangential displacement of the arch axis

$\bar{u} = Ru/t^2$

v speed

$W = w/\bar{R}\beta^2$

w radial displacement of the arch axis

$\bar{w} = w/t$

w^* displacement increment associated with the antisymmetric mode

x a spatial coordinate

y_o vertical coordinate of the undeformed arch shape

y vertical corrdinate of the deformed arch shape

α angular coordinate

$\Delta\alpha$ central angle of an arch element

α_o angular position where the point load is acting

β angle subtended by the arch

$\delta(\ )$ indicating Dirac delta function

ϵ axial strain

$\overset{*}{\epsilon}$ infinitesimal increment of ϵ

ζ length of PQ (see Fig. 2-2)

$\bar{\zeta} = \zeta/t$

$\eta = e\alpha$

η_o position of application of the point load

λ, λ_n geometric parameter of the arch

$\mu = e\beta$

$\bar{\phi} = q/P$

Ω angle $Q\bar{P}\bar{Q}$ (See Fig. 2-2)

$\bar{\Omega} = R\Omega/t$

ω_n natural frequency of a linear system

ω_e equivalent natural frequency associated with A_1

$\sigma_{\alpha\alpha}$ axial stress

σ the combined stress of the extreme fiber of the section

σ_{max} maximum combined stress corresponding to a point of application of the point load

Abs. $\dot{\sigma}_{max}$ the largest value of σ_{max} for an arch

(abs. = absolute; max. = maximum; and cr = critical)

CHAPTER I

INTRODUCTION

1.1 General Introduction and Scope

Arches are a common type of structure. They are usually divided into two categories: shallow and high arches, depending upon the arch rise. The analysis of high arches is a linear problem since the axial strain can be taken as zero. Shallow arches, however, behave in a non-linear character. Many papers dealing with the static stability of shallow arches may be seen in the literature. These papers are limited to the special case of symmetric loading. Since most practical loading cases are non-symmetric, a part of this thesis is devoted to the investigation of the static stability problem of hinged shallow circular arches under arbitrary loading. The investigation is made by first solving the governing equations and then studying the load-displacement curves. The buckling loads are obtained either from the load-displacement curves or from external load parameter vs. axial load parameter curves. The critical (buckling) loads corresponding to a point load and combined loads (point load plus uniform load) respectively are tabulated, plotted and compared.

For shallow arches subjected to dynamic loads, the behavior is expected to be different from the static case. The behavior of shallow arches under step loads or impulsive loads is well documented in the literature. To the knowledge of this writer there has been no paper in the past that studied shallow arches under moving loads. Thus,

an additional objective of this thesis is to examine the dynamic stability of shallow arches under moving loads. This study is of practical interest in many applications of arches. The dynamic investigation uses a numerical method for solving the governing equations. The critical (buckling) loads are determined by observing the sudden great change in the displacement due to a small increase in the external load. The critical loads are expected to be different for various arch geometric parameters. They are also a function of the velocity of the moving load. The effects of geometry and load velocity are investigated. These results are included in Chapter 4. In addition, the effects of the dead weight treated as a uniform pressure in addition to the moving load are investigated.

The deflection and the stresses on the arch rib are of concern to the structural engineer. To get an insight into how the moving load affects the deflection and the stresses of the arches, the influence lines for the deflection and the maximum stresses respectively corresponding to various cases are drawn and compared. Some study about the effects of the section stiffness and the arch geometry upon the maximum deflection and the maximum stresses are also carried out. Chapter 5 gives the results of this investigation.

Throughout this work, the following assumptions are made:

1) The material obeys Hooke's law;

2) The section remains plane after deformation;

3) Shear and rotary intertia effect is neglected; and

4) The undeformed arch shape is perfect.

1.2 Historical Background

In the study of the stability of shallow arch, as early as 1935, Timoshenko [1] investigated a sinusoidal arch under sinusoidal loading. In his simple solution, the buckling mode was restricted to the symmetrical one. In 1952, Fung and Kaplan [10] worked out the same problem by using a series solution. They also examined pin-supported circular arches with a point load acting at the crown. Later, Gjelsvik and Bodner [5] used energy criteria in investigating snap buckling of fixed arches under a central point load. It was not until 1966 when an exact solution was obtained [4] by directly solving the governing differential equations. The closed form solution worked out by Masur and Shreyer for fix-ended arches under a uniformly distributed load and a central point load was experimentally verified by Cheung and Babcock in 1970 [15]. In 1967, Lo and Conway [43,44] analyzed pinned-end arches under opposite end moments and under central point load and found that the inextensional theory cannot be applied to the shallow arch problem. By verification from experiments, Kennedy and Aggarwal [48] found that for longer arches the arch weight has a profound effect upon the buckling loads. To compare the results by exact solutions, series solutions and by experimental work, Dickie and Broughton [46] carried out investigation of circular arches with different boundary conditions and under various types of loading.

As for an arch under dynamic loading, Hoff and Bruce [9], Hsu [14,21,23,26,27,50] used an energy approach to study shallow arches under a step load, as well as an impulsive pressure. Hoff and Bruce used a two-mode approximation while Hsu obtained the results by the exact solution. In 1966, Humphreys [22] used the analog computer to solve the problem. In the same year, Lock [51] analyzed a pinned-end arch under step pressure by direct integration.

There are several articles concerning the stresses and the deflection. The most noted one probably began with the report [32] in which the Rainbow Arch Bridge over the Niagara Gorge was designed and analyzed. The difference between the so-called elastic theory and the deflection theory was presented and discussed. Earlier, Newmark [28] studied the interaction between the rib and the superstructure. About the same time Hall [29] examined the effect of the deflection.

CHAPTER 2

DERIVATION OF GOVERNING EQUATIONS

2.1 Introduction

The arch problem, characteristic of its nonlinearity in the relationship between load and displacement may not be treated in the same way as in the beam problem. With an aim to clarify this problem thoroughly, and under the assumptions made in Chapter I, the equations governing the arches in general are to be derived in the following sections.

2.2 Arch Equations in General

Consider the small element of a deformed arch as shown in Fig. 2-1. Summing all the forces in the radial direction gives:

$$bq\Delta s - Q \cos\frac{\Delta\alpha}{2} + (Q + \Delta Q) \cos\frac{\Delta\alpha}{2} + N \sin\frac{\Delta\alpha}{2}$$

$$+ (N + \Delta N) \sin\frac{\Delta\alpha}{2} = 0 \qquad \text{---------- (2.1)}$$

in which b = the width of the arch

q = distributed load per unit area

Δs = axial length of the arch element

Q = shear force resultant of the section

ΔQ = small increment of Q

$\Delta\alpha$ = central angle of the arch element

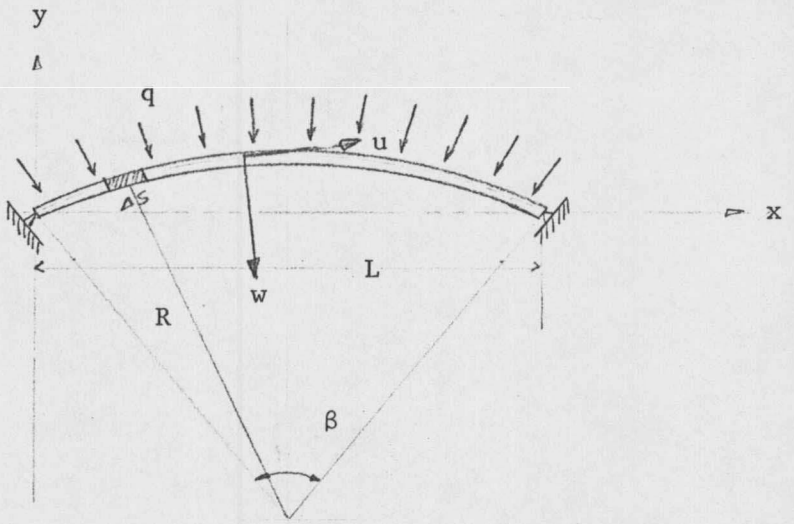


Fig. 2-1a. Pin-Pin Circular Arches Under Uniform Pressure q

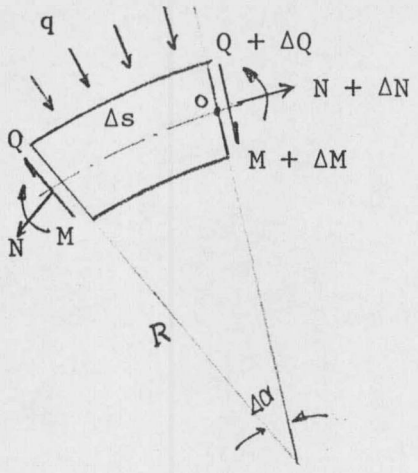


Fig. 2-1b. Equilibrium State of the Element Δs

N = axial thrust

ΔN = small increment of N

Divide the equation by Δs. Note that $\Delta s = R\ \Delta\alpha$, where R is the radius of the arch in its deformed shape, $\text{Cos}\ \frac{\Delta\alpha}{2} \doteq 1$ and $\text{Sin}\ \frac{\Delta\alpha}{2} \doteq \frac{\Delta\alpha}{2}$. Take the limit as Δs approaches zero and one obtains the following equation:

$$bq + \frac{dQ}{ds} + \frac{N}{R} = 0 \qquad \text{---------- (2.2)}$$

Similarly, summing all the forces in the tangential direction gives:

$$\frac{Q}{R} - \frac{dN}{ds} = 0 \qquad \text{---------- (2.3)}$$

Taking the moment of all the forces about point 0 and applying the equilibrium conditions gives:

$$-bq\ \Delta s\ R\ \text{Sin}\ \frac{\Delta\alpha}{2} + M - (M + \Delta M) + Q\ \text{Cos}\ \frac{\Delta\alpha}{2}$$

$$(2R\ \text{Sin}\ \frac{\Delta\alpha}{2}) - N\ \text{Sin}\ \frac{\Delta\alpha}{2}\ (2R\ \text{Sin}\ \frac{\Delta\alpha}{2}) = 0 \qquad \text{---------- (2.4)}$$

in which M = bending moment

ΔM = small increment of M

As before, rearranging and taking the limit as $\Delta s \to 0$, the last equation becomes:

$$Q - \frac{dM}{ds} = 0 \qquad \text{---------- (2.5)}$$

Eqs. (2.2), (2.3) and (2.5) are combined to give:

$$\frac{d^3M}{ds^3} + \frac{1}{R}\frac{dR}{ds}\frac{d^2M}{ds^2} + \frac{1}{R^2}\frac{dM}{ds} + \frac{bdq}{ds} + \frac{bq}{R}\frac{dR}{ds} = 0 \qquad \text{---------- (2.6)}$$

Eq. (2.6) relates the moment on the section to the external load. To know the relationship between arch displacement and external loading, let's consider Fig. 2-2, in which P is a point on the arch axis before deformation. After deformation, this point moves to $\bar{p}$. Similarly, another point Q, which is off the centroidal axis, displaces to $\bar{Q}$ in the deformed configuration. If the position vectors of P, $\bar{p}$, Q and $\bar{Q}$ are respectively represented by $\bar{r}_o$, $\bar{R}_o$, $\bar{r}$, and $\bar{R}^*$ and the assumptions in Ch. 1 are used, one has

$$\bar{r} = \bar{r}_o + \zeta\,\bar{n} \qquad \text{---------- (2.7)}$$

$$\bar{R}_o = \bar{r}_o + w\,\bar{n} + u\,\bar{a} \qquad \text{---------- (2.8)}$$

$$\bar{R}^* = \bar{r}_o + w\,\bar{n} + u\,\bar{a} + \zeta\,\bar{n} - \zeta\,\Omega\,\bar{a} \qquad \text{---------- (2.9)}$$

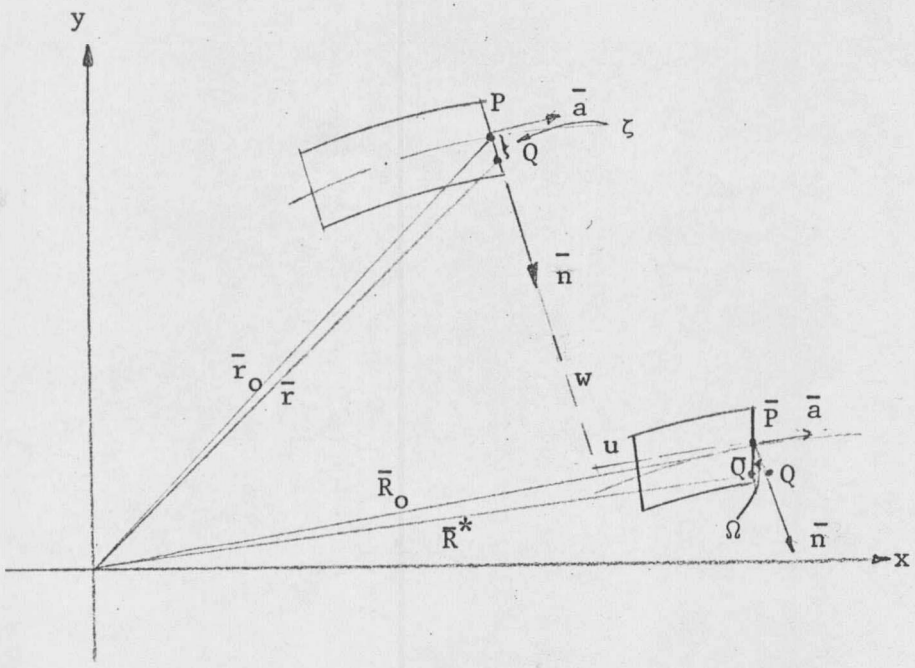


Fig. 2-2. An Arch Section Before and After Deformation

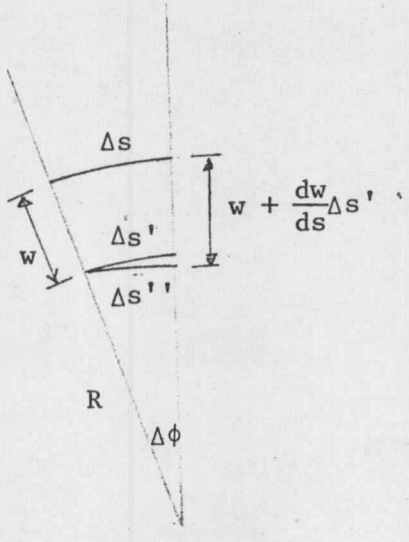


Fig. 2-3. Deformation of a Small Arch Element

in which

$\bar{n}$ = unit normal vector

$\bar{a}$ = unit tangential vector

w = radial displacement

u = tangential displacement

ζ = length of PQ

Ω = angle Q $\bar{p}$ $\bar{Q}$

From Eqs. (2.7), (2.9), and noting that

$$\frac{d\bar{r}_o}{ds} = \bar{a} \qquad \text{---------- (2.10)}$$

$$\frac{d\bar{n}}{ds} = -\frac{1}{R}\bar{a} \qquad \text{---------- (2.11)}$$

one has

$$d\bar{r} = (1 - \frac{\zeta}{R})\ \bar{a}\ ds + \bar{n}\ d\zeta \qquad \text{(2.12)}$$

and

$$d\bar{R}^{*} = (ds + \frac{du}{ds}\ ds - \frac{w}{R}\ ds - \frac{\zeta}{R}\ ds - \zeta\ \frac{d\Omega}{ds}\ ds - \Omega d\zeta)\ \bar{a}$$

$$+ (\frac{dw}{ds}\ ds + \frac{u}{R}\ ds + d\zeta - \frac{\Omega\zeta}{R}\ ds)\ \bar{n} \qquad \text{(2.13)}$$

With the strain component in the axial direction denoted by $e_{\alpha\alpha}$, in the radial direction by $e_{\zeta\zeta}$, and the shearing strain by $e_{\alpha\zeta}$, it follows:

$$2\ (e_{\alpha\alpha}\ dsds + 2\ e_{\alpha\zeta}\ ds\ d\zeta + e_{\zeta\zeta}\ d\zeta\ d\zeta) = d\bar{R}^{*} \cdot d\bar{R}^{*}$$
$$- d\bar{r} \cdot d\bar{r} \qquad \text{(2.14)}$$

Substituting Eqs. (2.12) and (2.13) into (2.14), carrying out the inner products, and equating the corresponding coefficients of (dsds), (dsdζ) and (dζ dζ) respectively, the following tensorial strain components are obtained:

$$e_{\alpha\alpha} = \frac{du}{ds} - \frac{w}{R} + \frac{1}{2}\ (\frac{du}{ds})^2 + \frac{1}{2}\ \frac{w^2}{R^2} + \frac{1}{2}\ (\frac{dw}{ds})^2$$
$$- \frac{w}{R}\ \frac{du}{ds} + \frac{dw}{ds}\ \frac{u}{R} + \frac{1}{2}\ \frac{u}{R^2}^2 - \zeta\ [\frac{\Omega u}{R^2} + \frac{d\Omega}{ds}$$
$$+ \frac{1}{R}\ \frac{du}{ds} + \frac{\Omega}{R}\ \frac{dw}{ds} + \frac{d\Omega}{ds}\ \frac{du}{ds} - \frac{w}{R^2} - \frac{w}{R}\ \frac{d\Omega}{ds}]$$
$$+ \zeta^2\ [\frac{1}{2}\ (\frac{d\Omega}{ds})^2 + \frac{1}{2}\ \frac{\Omega^2}{R^2} + \frac{1}{R}\ (\frac{d\Omega}{ds})] \qquad \text{(2.15)}$$

$$2\, e_{\alpha\zeta} = \frac{u}{R} + \frac{dw}{ds} - \Omega - \Omega \frac{du}{ds} + \Omega \frac{w}{R} + \zeta\Omega \frac{d\Omega}{ds} \quad \text{---------- (2.16)}$$

$$e_{\zeta\zeta} = \frac{1}{2} \Omega^2 \quad \text{---------- (2.17)}$$

Some of the terms in these equations are significant while others are not. To sort out the terms which are significant, recourse is made to non-dimensionalizing these terms with the following substitutions:

$$\bar{s} = s/R \quad \text{---------- (2.18a)}$$

$$\bar{w} = w/t \quad \text{---------- (2.18b)}$$

$$\bar{\zeta} = \zeta/t \quad \text{---------- (2.18c)}$$

$$\bar{\Omega} = \frac{R}{t} \Omega \quad \text{---------- (2.18d)}$$

$$\bar{u} = \frac{R}{t^2} u \quad \text{---------- (2.18e)}$$

in which t is the thickness of the arch. Eq. (2.18d) is obtained by letting the cross sectional rotation, indicated by Ω, equal $\frac{dw}{ds}$, i.e., $\Omega \doteq \frac{dw}{ds} = \frac{t}{R} \frac{d\bar{w}}{d\bar{s}}$. Eq. (2.18e) is derived from the consideration that axial displacement is due to the differential in w, the radial displacement. Consider Fig. 2-3,

$$\Delta s' = (R - w)\, \Delta\phi$$

$$\Delta s'' = [(\Delta s')^2 + (\frac{dw}{ds} \Delta s')^2]^{1/2}$$

$$= (\Delta s') \left[1 + \left(\frac{dw}{ds}\right)^2\right]^{1/2}$$

$$\doteqdot (\Delta s') \left[1 + \left(\frac{dw}{ds}\right)^2\right]$$

and

$$\frac{du}{ds} \doteqdot \frac{\Delta s'' - \Delta s'}{\Delta s'} \doteqdot \frac{1}{2} \left(\frac{dw}{ds}\right)^2 \doteqdot \frac{t^2}{R^2} \left(\frac{d\bar{w}}{ds}\right)^2$$

$$u \doteqdot \frac{t^2}{R} \left(\frac{d\bar{w}}{d\bar{s}}\right)^2 \bar{s}$$

Hence

$$\bar{u} = \frac{R}{t^2} u$$

which is Eq. (2.18e)

If each value in Eqs. (2.18) is considered to have the magnitude of order unity, and by substituting Eqs. (2.18) into Eqs. (2.15), (2.16) and (2.17), and rearranging the terms in ascending powers of t/R, one can tell the relative significance of each term in these equations. By dropping terms with higher order power than $(t/R)^2$, one has

$$e_{\alpha\alpha} = -\frac{w}{R} + \frac{du}{ds} + \frac{1}{2}\left(\frac{dw}{ds}\right)^2 - \zeta\left(\frac{d\Omega}{ds} - \frac{w}{R^2}\right) \qquad \text{---------- (2.19)}$$

$$e_{\alpha\zeta} = -\Omega + \frac{dw}{ds} \qquad \text{---------- (2.20)}$$

$$e_{\zeta\zeta} = 0 \qquad \text{---------- (2.21)}$$

Neglecting the transverse shear deformation gives

$$\Omega = \frac{dw}{ds} \qquad \text{---------- (2.22)}$$

Introducing two expressions,

$$e_c = \frac{du}{ds} - \frac{w}{R} + \frac{1}{2}\left(\frac{dw}{ds}\right)^2 \qquad \text{---------- (2.23)}$$

and

$$K_c = \frac{d^2w}{ds^2} - \frac{w}{R^2} \qquad \text{---------- (2.23a)}$$

and noting that the tensorial strain is related to the physical strain [42] by

$$\bar{e}_{\alpha\alpha} = e_{\alpha\alpha}/(\bar{g} \cdot \bar{g})^{1/2} \qquad \text{---------- (2.24)}$$

in which $\bar{g}$ is defined by

$$\bar{g} = \frac{d\bar{r}}{ds} = \frac{d\bar{r}_o}{ds} + \zeta \frac{d\bar{n}}{ds} = \left(1 - \frac{\zeta}{R}\right) \bar{a} \qquad \text{---------- (2.25)}$$

at $\zeta = 0$, $\bar{g} = \bar{a}$

it follows that

$$\bar{e}_{\alpha\alpha} = \frac{e_c}{1 - \zeta/R} - \frac{\zeta}{1 - \zeta/R} K_c \qquad \text{---------- (2.26)}$$

The axial stress is then

$$\sigma_{\alpha\alpha} = E\, \bar{e}_{\alpha\alpha} \qquad \text{----------(2.27)}$$

in which E = Young's modulus; and the axial force is

$$N = \int_A \sigma_{\alpha\alpha}\, dA = E\, e_c \int_A \frac{1}{1 - \zeta/R}\, dA - E\, K_c \int_A \frac{\zeta dA}{1 - \zeta/R} \qquad (2.28)$$

or

$$N = EAe_c + \frac{EI^*}{R^2} e_c - \frac{EI^*}{R} K_c \qquad (2.29)$$

where $$I^* = \int_A \frac{\zeta^2}{1 - \zeta/R}\, dA \qquad (2.30)$$

Similarly, the bending moment is

$$M = \int_A \sigma_{\alpha\alpha}\, \zeta\, dA = \frac{EI^*}{R} e_c - EI^* K_c \qquad (2.31)$$

or

$$M = EI^* \left[\frac{1}{R}\frac{du}{ds} + \frac{1}{2R}\left(\frac{dw}{ds}\right)^2 - \frac{d^2w}{ds^2}\right] \qquad (2.32)$$

Substitution of Eq. (2.32) into Eq. (2.6) yields

$$EI^* \left(\frac{d^3}{ds^3} + \frac{1}{R}\frac{dR}{ds}\frac{d^2}{ds^2} + \frac{1}{R^2}\frac{d}{ds}\right)\left[\frac{1}{R}\frac{du}{ds} + \frac{1}{2R}\left(\frac{dw}{ds}\right)^2 - \frac{d^2w}{ds^2}\right] + \frac{bdq}{ds} + \frac{bq}{R}\frac{dR}{ds} = 0 \qquad (2.33)$$

In this last equation, EI^* was assumed constant. As before, $\frac{1}{R}\frac{du}{ds}$ and $\frac{1}{2R}\left(\frac{dw}{ds}\right)^2$ may be neglected. Eq. (2.33) then becomes

$$EI^* \left(\frac{d^3}{ds^3} + \frac{1}{R}\frac{dR}{ds}\frac{d^2}{ds^2} + \frac{1}{R^2}\frac{d}{ds}\right)\left(\frac{d^2w}{ds^2}\right) - \frac{bdq}{ds} - \frac{bq}{R}\frac{dR}{ds} = 0 \quad (2.34)$$

Eq. (2.34) is the governing equation of general arches for small deflection under external load q. For high arch problems in which e_c in Eq. (2.23) is set to zero, Eqs. (2.33) and 2.34) need a little modification. The linearization of this process is the classical inextensional theory.

2.3 Equations for Shallow Arches

The governing differential equations for shallow arches may be derived in the same manner as the derivation of Eq. (2.34). However, some appropriate considerations must be made. It is well known that, if the arch rise is great, the inextensional theory will hold in general. In the case of shallow arches, i.e., the ratio of the arch rise vs. span is less than 0.115 which approximately corresponds to the average value 0.08 of $(\frac{dy_o}{d\alpha})^2$ for a circular arch, however, this theory fails to predict the behavior of the arch. This is because the effects due to the axial thrust can no longer be ignored in this case. In other words, the axial strain now has to be included. Furthermore, for shallow arches the axial force N is approximately constant throughout the span [41], which implies, from Eq. (2.3),

$$\frac{dN}{ds} = 0$$

or $$N = -N_o \qquad \text{----------(2.35)}$$

The curvature $\frac{1}{R}$ in this case may be approximated as

$$\frac{1}{R} \doteq \frac{d^2}{dx^2}(w - y_o) \qquad \text{----------(2.36)}$$

If the arch is also assumed thin in thickness, Eq. (2.32) gives

$$M \doteq -EI \frac{d^2w}{dx^2} \qquad \text{----------(2.37)}$$

From Eq. (2.2), Eq. (2.5), and Eq. (2.35),

$$\frac{d^2M}{ds^2} - \frac{N_o}{R} + bq = 0 \qquad \text{----------(2.38)}$$

Due to the shallowness of the arch, $ds \doteq dx$, and by substitution of Eqs. (2.36) and (2.37) into Eq. (2.38), it yields

$$\frac{d^2}{dx^2}\left(EI \frac{d^2w}{dx^2}\right) - N_o \frac{d^2}{dx^2}(y_o - w) - bq = 0 \qquad \text{----------(2.39)}$$

For constant EI, Eq. (2.39) becomes

$$EI \frac{d^4w}{dx^4} - N_o \frac{d^2}{dx^2}(y_o - w) = bq \qquad \text{----------(2.40)}$$

in which $N_o (= -N)$ is defined by Eq. (2.29), which, with the second and the third terms neglected, reduces to

$$N_o = -EA\left[\frac{du}{dx} - \frac{w}{R} + \frac{1}{2}\left(\frac{dw}{dx}\right)^2\right] \qquad \text{----------(2.41)}$$

Since $dx \doteq \bar{R}\, d\alpha$, $\varepsilon = \frac{-N_o}{EA}$, Eq. (2.41) may also be expressed in terms of the angular coordinate α, or

$$\varepsilon = \frac{1}{\bar{R}}\left(\frac{du}{d\alpha} - w\right) + \frac{1}{2\bar{R}^2}\left(\frac{dw}{d\alpha}\right)^2 \qquad \text{----------(2.41a)}$$

For an arch supported at two ends, which implies that $u(0) = u(L) = 0$, with the use of Eq. (2.36) and integrating Eq. (2.41) over the length of the arch, one has

$$N_o = -\frac{EA}{2L}\int_0^L \left[\left(\frac{dy_o}{dx}\right)^2 - \left(\frac{dy_o}{dx} - \frac{dw}{dx}\right)^2\right] dx \qquad \text{----------(2.42)}$$

It should be noted that q in Eq. (2.40) is the distributed load per unit length. If, instead, the external load is a point load P, then Eq. (2.40) has the form

$$EI\frac{d^4w}{dx^4} - N_o\frac{d^2}{dx^2}(y_o - w) = P\,\delta(x - C) \qquad \text{----------(2.43)}$$

in which $\delta(x - C)$ represents the Dirac delta function, while C is the distance between the left support and the point load. In the same manner as Eq. (2.41a) was obtained, Eq. (2.43) may be expressed in terms of coordinate α as

$$\frac{d^4w}{d\alpha^4} + N_1\frac{d^2w}{d\alpha^2} = P_1\,\delta(\alpha - \alpha_o) - N_1\bar{R} \qquad \text{----------(2.44)}$$

where $$N_1 = + \frac{N_o \bar{R}^2}{EI} = - \frac{A\varepsilon \bar{R}^2}{I} \qquad \text{----------(2.45a)}$$

$$P_1 = \frac{P\bar{R}^3}{EI} \qquad \text{----------(2.45b)}$$

In Eq. (2.44), α_o is the angular distance between the left support and the point load. Sometimes it is likely that the point load P and the uniform pressure q are acting on the arch simultaneously and q is not negligible when compared with P. In this case, Eq. (2.43) and Eq. (2.44) may be rewritten respectively as

$$EI \frac{d^4w}{dx^4} - N_o \frac{d^2}{dx^2}(y_o - w) = P \ \delta(x - C) + b\bar{\phi}P \qquad \text{----------(2.46)}$$

and

$$\frac{d^4w}{d\alpha^4} + N_1 \frac{d^2w}{d\alpha^2} = P_1 \ \delta(\alpha - \alpha_o) + b\bar{\phi}\bar{R}P_1 - N_1\bar{R} \qquad \text{----------(2.47)}$$

where $$\bar{\phi} = q/P \qquad \text{----------(2.48)}$$

Eq. (2.43) and Eq. (2.42) [or, Eq. (2.44) combined with Eq. (2.41a)] together form the governing equations for shallow arches subjected to a point load at any arbitrary position, while Eq. (2.46) along with Eq. (2.42) [or, Eqs. (2.47) and (2.41a)] is used to analyze any type of shallow arches under a point load and uniform pressure simultaneously.

2.4 Equations of Motion for Shallow Arches

The above section deals with arches under static loads only. If now, instead, any dynamic load is applied, the behavior of the arch becomes quite different from that in the static case. Any structural system involving dynamic loads, such as moving load or any type of load involving time, the mass must in general be considered. If one considers a point load P moving across the arch at a constant speed v, and if the dead weight of the arch is negligible in comparison with P, then, from Eq. (2.43), after some modifications, one has

$$EI \frac{\partial^4 w}{\partial x^4} - N_o \frac{\partial^2}{\partial x^2} (y_o - w) + m \frac{\partial^2 w}{\partial T^2} = P\delta(x - vT) \quad \text{------} \quad (2.49)$$

in which m = the mass of the unit length. In case the dead weight of the arch can't be neglected, Eq. (2.49) becomes

$$EI \frac{\partial^4 w}{\partial x^4} - N_o \frac{\partial^2}{\partial x^2} (y_o - w) + m \frac{\partial^2 w}{\partial T^2} = P\delta(x - vT) + b\bar{\phi}P \quad (2.50)$$

where $\bar{\phi}$ and N_o were defined respectively in Eq. (2.48) and Eq. (2.42).

Eq. (2.49) [or, Eq. (2.50)] and Eq. (2.42) constitute the governing equations for shallow arches under a moving load P. These equations provide the basis for investigating the behavior of the arch under this particular type of dynamic load.

CHAPTER 3

THE STATIC STABILITY OF SHALLOW ARCHES

3.1 Introduction

Just as an ordinary compressive member subjected to critical axial load would buckle, arches become unstable when lateral loading reaches its critical value. High arches in general buckle sideways, while shallow arches tend to buckle in such a way that the curvature becomes reversed. The phenomenon associated with the lateral case is known as "snap through." Investigation of this phenomenon has been quite extensive [1, 4, 5, 10, 15, 43, 44, 46, 48]. However, most investigations were limited to special cases: the external load is either of uniform pressure type or a single point load acting at the center of the span. A general case, for instance, such as the loading is the combination of a uniformly distributed pressure and a concentrated load applied at an arbitrary position, has not been examined to the knowledge of the writer. Therefore, this chapter is devoted to investigate the stability of shallow circular arches under two particular types of loading: (a) a point load acting at any position on the arch, and (b) that same load as in Case (a) plus uniform pressure.

3.2 Point Load

In this case, the critical load may be determined by solving Eq. (2.44) and Eq. (2.41a) simultaneously. Since N_1 in Eq. (2.44) is independent of the angular coordinate α as mentioned in Section 2.3,

Eq. (2.44) is a linear differential equation which can be solved directly either by using the Laplace transformation method or by any other mathematic technique. However, the solution so obtained must be subjected to the constraint condition expressed by Eq. (2.41a) which evidently is nonlinear.

Introducing

$$e = \sqrt{N_1}$$

$$\mu = e\beta$$

$$\eta = e\alpha$$

$$U = u/\bar{R}\beta^2$$

$$W = w/\bar{R}\beta^2$$

in which

N_1 defined in Eq. (2.45a)

β = the subtended angle of the arch

$\bar{R}$ = radius of the undeformed arch

u,w = the arch displacement in the tangential and radial directions respectively

Eq. (2.44) becomes

$$W'''' + W'' = \frac{\bar{P}}{\mu^3}\,\delta(\eta - \eta_o) - \frac{1}{\mu^2} \qquad \text{--- (3.2)}$$

in which $$\bar{P} = \frac{P_1\beta}{\bar{R}} = \frac{P\beta\bar{R}^2}{EI} \qquad \text{-------- (3.3)}$$

The primes in Eq. (3.2) denote differentiation with respect to η, and η_o is the value of η when $\alpha = \alpha_o$.

By using the Laplace Transformation method, the solution to Eq. (3.2) is found to be

$$W(\eta) = \eta\left(\frac{1}{2\mu} + \frac{\eta_o - \mu}{\mu^4}\overline{P}\right) - \left(\frac{1 - \cos\mu}{\mu^2 \sin\mu} + \frac{\sin(\eta_o - \mu)}{\mu^3 \sin\mu}\overline{P}\right)\sin\eta - \frac{1}{\mu^2}(-1 + \tfrac{1}{2}\eta^2 + \cos\eta) + \frac{\overline{P}}{\mu^3}(\eta - \eta_o - \sin(\eta - \eta_o))\, J(\eta - \eta_o) \quad \text{---} \quad (3.4)$$

where $J(\eta - \eta_o)$ is a unit step function defined by

$$J(\eta - \eta_o) = 1 \quad \eta > \eta_o$$
$$J(\eta - \eta_o) = 0 \quad \eta < \eta_o \qquad \text{---------(3.5)}$$

In obtaining Eq. (3.4), the following boundary conditions were used:

$$W(o) = W(\mu) = 0$$
$$W''(o) = W''(\mu) = 0 \qquad \text{--- (3.6)}$$

Using Eqs. (3.1) and noting that $U(o) = U(\mu) = o$, Eq. (2.41a) becomes

$$\frac{\mu^3}{12\lambda^2} = \int_o^\mu \left[W - \frac{\mu^2}{2}(W')^2\right] d\eta \qquad \text{--- (3.7)}$$

in which $$\lambda = \frac{4}{\sqrt{3}}\frac{H}{R^*} \qquad \text{-------- (3.8)}$$

In the last equation, H is the arch rise, and R^* is the radius of gyration of the cross section about an axis perpendicular to the arch plane.

Eqs. (3.4) and (3.7) are solved to obtain load-displacement curves as shown in Fig. 3-1. It is seen that by gradually increasing the load parameter $\overline{P}$, the displacement W also increases. After $\overline{P}cr$, or 01, is reached, a small disturbance would cause the arch to jump to point 02, which is the known "snap-through" pehnomenon. Thereafter W increases steadily with increasing $\overline{P}$. If the process is reversed, i.e., after the arch is buckled and $\overline{P}$ is steadily reduced, the arch would "snap back" as soon as the point 03 is reached. Certainly this is possible if, and only if, the material remains in the elastic range throughout the loading and unloading history.

Curves indicating the relationship between the external load and the radial displacement, such as shown in Fig. 3-1 and Fig. 3-2, are customarily plotted with $\overline{P}$ versus W ($\mu/2$). In other words, in general it is convenient to study the load-displacement relation by the plot of the load against the displacement of the crown of the arch. For symmetrical arches under symmetric loading such as the uniform pressure or the central point load, the curve as in Fig. 3-1 represents symmetric equilibrium path [4]. This is expected and is true of any other type of structural systems. It may be verified by inserting numerical values into Eqs. (3.4) and (3.7). On the other hand, if the

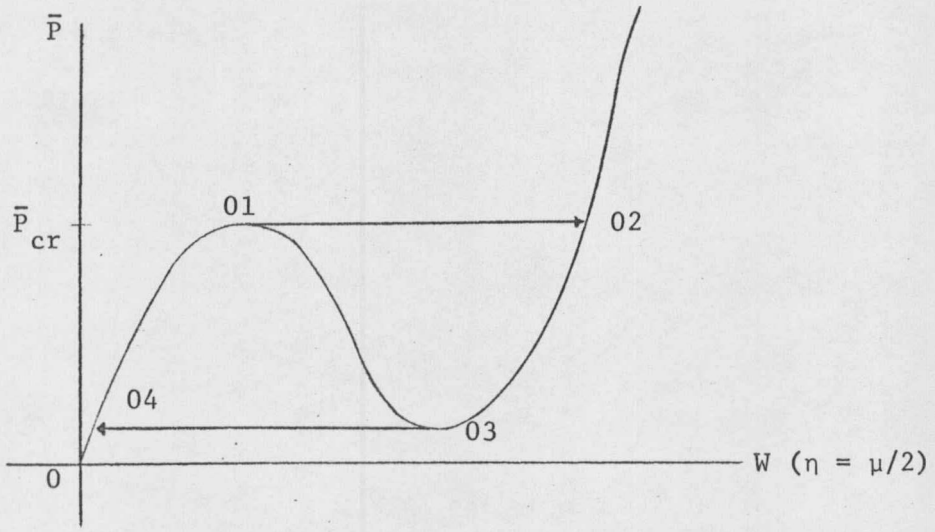


Fig. 3-1. Load-Displacement Curve (symmetric buckling)

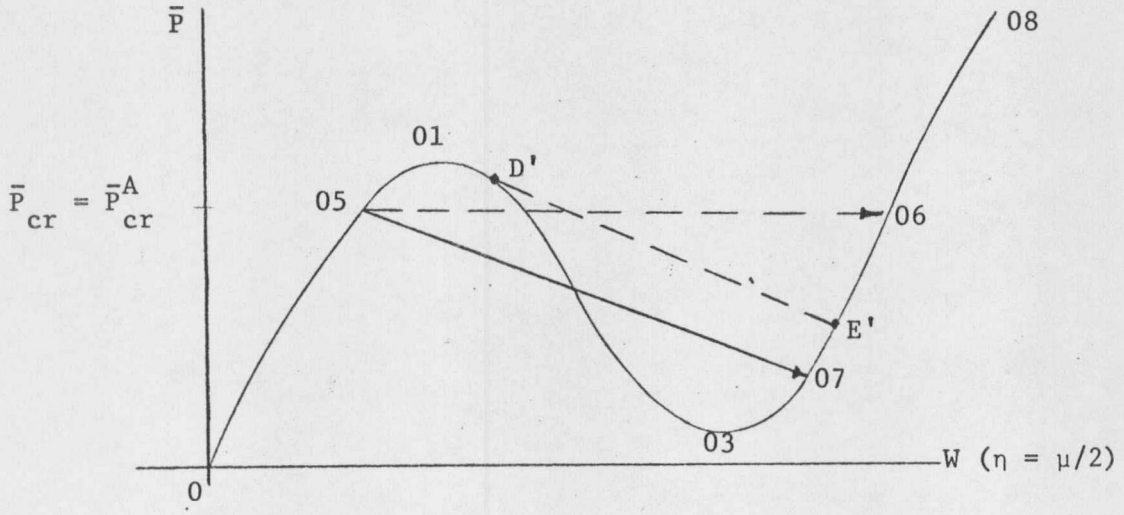


Fig. 3-2. Load-Displacement Curve (bifurcation instability)

arch geometry or the loading is nonsymmetrical with respect to the central line, one has the so-called nonsymmetrical arches. In this case, the curve, as in Fig. 3.1, does not represent symmetric equilibrium path any more. Nevertheless, a load-displacement curve such as in Fig. 3.1 which may indicate either symmetric or nonsymmetric equilibrium path may be used equally well to determine the critical load (or the snap-through buckling load) of the arch. In Fig. 3.1, as discussed above, the arch is stable so long as $\overline{P} \leq \overline{P}cr$, but it is true only when the load-displacement curve represents nonsymmetric equilibrium path. In other words, if the arch is of non-symmetric type or is under non-symmetric loading, the load corresponding to the point o1 on the load-displacement curve is the critical one. The reason behind this will be explained later. For symmetric arches subjected to symmetric loading, it is only partly true. The prebuckling deformation which is the arch displacement before snap-through, sometimes cannot reach the point 01 on the curve in this case. As this deformation reaches another point 05 on the same curve as indicated in Fig. 3-2, the arch suddenly jumps to point 07. Since in this particular case, as noted above, the deformation is symmetrical within the range 0-05 while the path 05-07 is characteristic of antisymmetry, the phenomenon of admitting both symmetric and antisymmetric solutions is referred to as bifurcation instability. The equilibrium point 05 is known as the bifurcation point. It must be noted that the admittance of the antisymmetric mode

at the point 05 on the load-displacement curve merely "triggers" the snapping-through of the arch. The final buckled configuration is still symmetrical (4). Therefore, it is evident that symmetrical arches under symmetric loading may be "triggered" to snap-through from two possible sources: one is associated with the symmetrical mode while the other is associated with the antisymmetrical mode. If one refers to the first case as the symmetric buckling, the second as the anti-symmetric buckling, then one finds that the geometric parameter λ as defined in Eq. (3.8) would decide whether the arch would buckle symmetrically or antisymmetrically. It was found by the writer that for shallow pin-pin arches under symmetric point loading the anti-symmetric buckling governs if

$$\lambda \geq 12.0 \qquad \text{--- (3.9)}$$

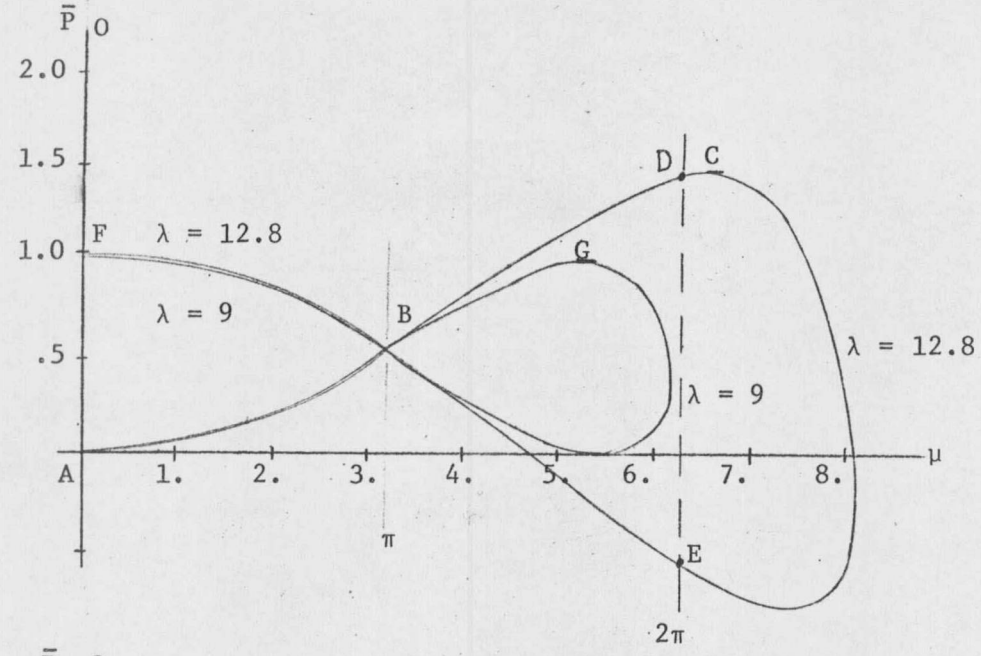
and the symmetric buckling governs if

$$4.2 \leq \lambda < 12.0 \qquad \text{--- (3.10)}$$

Inequality (3.10) indicates that for $\lambda < 4.2$ the arch can never buckle.

There is a convenient way to determine both the symmetrical critical load as well as the antisymmetric critical load. Referring to Eq. (3.4) and (3.7), as W in Eq. (3.4) is substituted into Eq. (3.7), one obtains the curve of $\overline{P}$ versus μ, as shown in Fig. 3.3. It was found that the points D and C on the curve of $\lambda = 12.8$ correspond to the points 05 and 01 in Fig. 3-2 respectively. To explain how the point D is determined, the following developments are carried out.

Fig. 3-3. Relation Between $\bar{P}$, the External Load Parameter and μ, the Axial Load Parameter



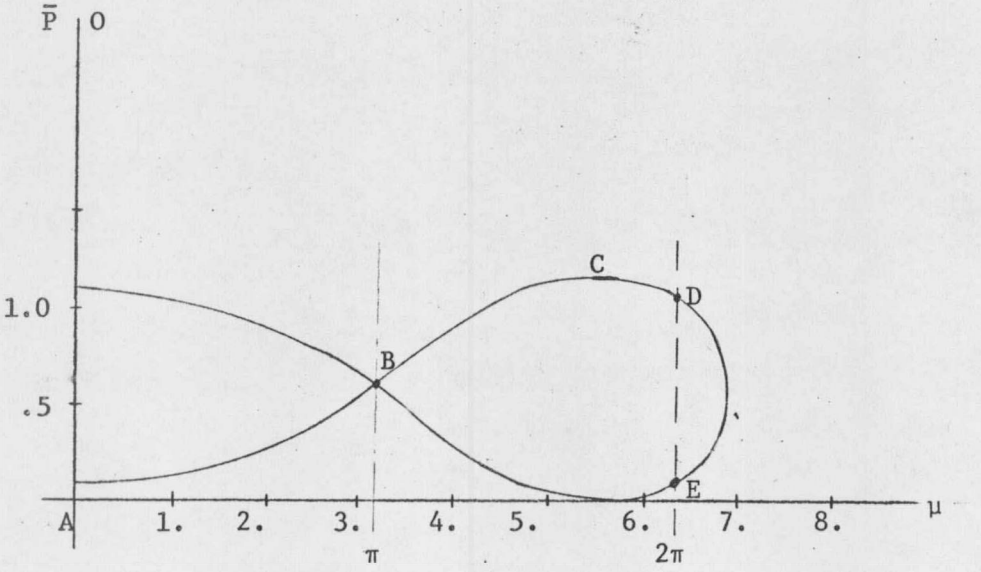


Fig. 3-4. Relation Between $\bar{P}$, the External Load Parameter and μ, the Axial Load Parameter (the bifurcation point lying in the unstable region)

It is known [5] that as the governing equations admit both a solution W and a neighboring configuration for the same value of $\overline{P}$, the external load, instability in the sense of bifurcation occurs. To determine this instability, let that neighboring configuration having an antisymmetrical form be designated w^*, and substitute $W + w^*$ for W, $\varepsilon + \varepsilon^*$ for ε in Eq. (3.7). One has

$$\frac{e^2}{\mu}(\varepsilon + \varepsilon^*) = \int_0^{\mu} \left[W + w^* - \frac{\mu^2}{2}(W' + w'^*)^2 \right] \quad d\eta \qquad \text{--- (3.11)}$$

Eq. (3.11) is obtained by rewriting the right-hand side of Eq. (3.7) as

$$\frac{\mu^3}{12\lambda^2} = \frac{\varepsilon e^2}{\mu} \qquad \text{---------- (3.12)}$$

Compare Eqs. (3.7) and (3.11) and their difference is linearized to be

$$\frac{e^2}{\mu}\varepsilon^* = \int_0^{\mu} \left[w^* - \mu^2 w'^* W' \right] \quad d\eta \qquad \text{------- (3.13)}$$

Since w^* is antisymmetric, it follows from Eq. (3.13) that

$$\varepsilon^* = 0 \qquad \text{------ (3.14)}$$

This states that at the bifurcation point, the buckling in antisymmetric mode does not require additional axial force, since the infinitesimal increment in the axial strain, i.e. ε^*, corresponds to the infinitesimal increment in the axial thrust N_1. With this in mind, using the similar substitutions as above, Eq. (3.2) gives

$$w^{*''''} + w^{*''} = 0 \qquad \text{---------- (3.15)}$$

By using the boundary conditions,

$$w^*(0) = w^*(\mu) = 0$$

$$w^{*''}(0) = w^{*''}(\mu) = 0$$

the solution to Eq. (3.15) is found to be

$$\text{Sin } \mu = 0$$

$$\Rightarrow \mu = n\pi \qquad n = 2, 3, 4, \qquad \text{------ (3.16)}$$

It was found that for non-trivial solution n = 0 must be dropped out and for consistency in the solution n = 1 is rejected. The reason behind the latter case is that, if n = 1 were employed then the critical load would be all identical for all values of λ, the geometric parameter. Now among the infinite number of n values, n = 2 is the lowest one and of practical interest. In Fig. 3-3, the straight line passing through $\mu = 2\pi$ intersects the curve of $\lambda = 12.8$ at point D and point E, which determines the antisymmetrical buckling load. As mentioned previously, D and E in Fig. 3-3 correspond to 05 and 07 in Fig. 3-2 respectively. This undoubtedly indicates that the path D E in Fig. 3-3 just as 05-07 in Fig. 3-2 is the antisymmetric equilibrium path. Furthermore, the curves on $\overline{P} - \mu$ plane may be used to determine not only the symmetric (or antisymmetric) buckling loads but also determine whether the arch would or would not buckle and whether the arch would buckle symmetrically or antisymmetrically. It was found that for

$\lambda < 4.2$ the curve can never go to the right of point B of Fig. 3-3. In the load-displacement plot as in Fig. 3-1 the curves corresponding to this range of values of λ all show a monotonic form, indicating the non-existence of the buckling phenomenon. However, if $\lambda \geq 4.2$, the curves all extend to the right of point B in the $\overline{P} - \mu$ plane. On each curve corresponding to each value of λ, there is a point at which $d\overline{P}/d\mu = 0$. This point is C for $\lambda = 12.8$ and G for $\lambda = 9$. Both points C and G correspond to the symmetric buckling loads for the two values of the geometric parameter λ. For $4.2 \leq \lambda < 12.0$, the curves either have no intersections with the straight line $\mu = 2\pi$, or the intersections are to the right of point C as shown in Fig. 3-4. This indicates that the antisymmetric mode either does not enter the picture throughout the buckling process or occurs on the unstable range. In other words, in this range of λ, the arch would buckle symmetrically. On the other hand, for $\lambda \geq 12.0$ the vertical line $\mu = 2\pi$ always stand to the left of point C as shown in Fig. 3-3, and the snap-through of the arch is always "triggered" by the anti-symmetric mode and the antisymmetric buckling load is the critical load. The above discussions clearly lead to the results of Eqs. (3.9) and (3.10).

For shallow arches under nonsymmetric loading, the problem is more complicated in the sense that the prebuckling deformation is no longer symmetrical, but a combination of symmetric and antisymmetric modes. As soon as the external load is applied, the antisymmetric

modes are present, which marks the distinguished difference from the behavior of the same arch under symmetric loading. For in the latter case for $\lambda \geq 12.0$ the antisymmetric mode is not present until the arch starts to buckle. Accordingly, in the case of nonsymmetric loading, the critical load is always the antisymmetric buckling load, and may be directly determined from the load-displacement curve.

To further clarify the difference of the behavior of an arch between symmetric loading and nonsymmetric loading, one has to go back to Fig. 3-1. In the case of non-symmetric loading, as discussed before, the load-displacement curve never represents a "symmetric" equilibrium path but a "nonsymmetric" equilibrium path, for the antisymmetric modes are present from the beginning. By increasing $\overline{P}$, the displacement increases steadily until point 01 is reached. One small disturbance, and the arch jumps to point 02. This jump is equivalent to that jump associated with the bifurcation instability of the symmetric arch under symmetric loading. As such, it is evident that for shallow arches subjected to nonsymmetric loading, the critical load is always governed by the antisymmetric mode.

By following what was mentioned in the above, it is found that the critical (buckling) load is a function of the geometric parameter λ, point of application of the point load η_o and the radius of gyration of the section R^*. If expressed in an equation, it is

$$\overline{P}cr = f(\lambda, \eta_o, R^*) \qquad \text{--- (3.17)}$$

The results expressed in numerical values are shown in Table 3-1 (Appendix A) and in Fig. 3-5. It is observed that in a particular case when η_o is taken as 0.5μ, i.e., the point load is acting at the center, the critical values agree with those obtained by Dickie and Broughton [46]. Furthermore, Fig. 3-5 clearly shows that the "weak region" associated with the point of application of the point load lies somewhere between $\eta_o = 0.3\mu$ and $\eta_o = 0.4\mu$, except for very small λ.

Fig. 3-6 shows the plot of Eq. (3.8), indicating the relationship among H, R^* and λ. This plot is useful as an aid in practical design. It is customary to express the critical loads in terms of the rise-span ratio. By letting k = H/L, the rise-span ratio, the plot essentially is one with k as the ordinate and R^*/L as the abscissa. If λ is known, the critical load may be obtained from the table. With the aid of Fig. 3-6 the section of the arch may be determined.

3.3 Point Load and Uniformly Distributed Pressure Acting Simultaneously

Similar to the foregoing section, the governing equations, Eqs. (2.41a) and (2.47), by using Eqs. (3.1), can be rewritten respectively as Eq. (3.7) and as

$$W'''' + W'' = \frac{\bar{P}}{\mu^3}\,\delta(\eta - \eta_o) + \frac{b\phi\bar{P}}{\mu^4} - \frac{1}{\mu^2} \qquad \text{----------(3.18)}$$

in which $\phi = \bar{\phi}\bar{R}\beta$ ----------(3.19)

Using the same boundary conditions and the same mathematic technique as before, the solution to Eq. (3.18) is found to be

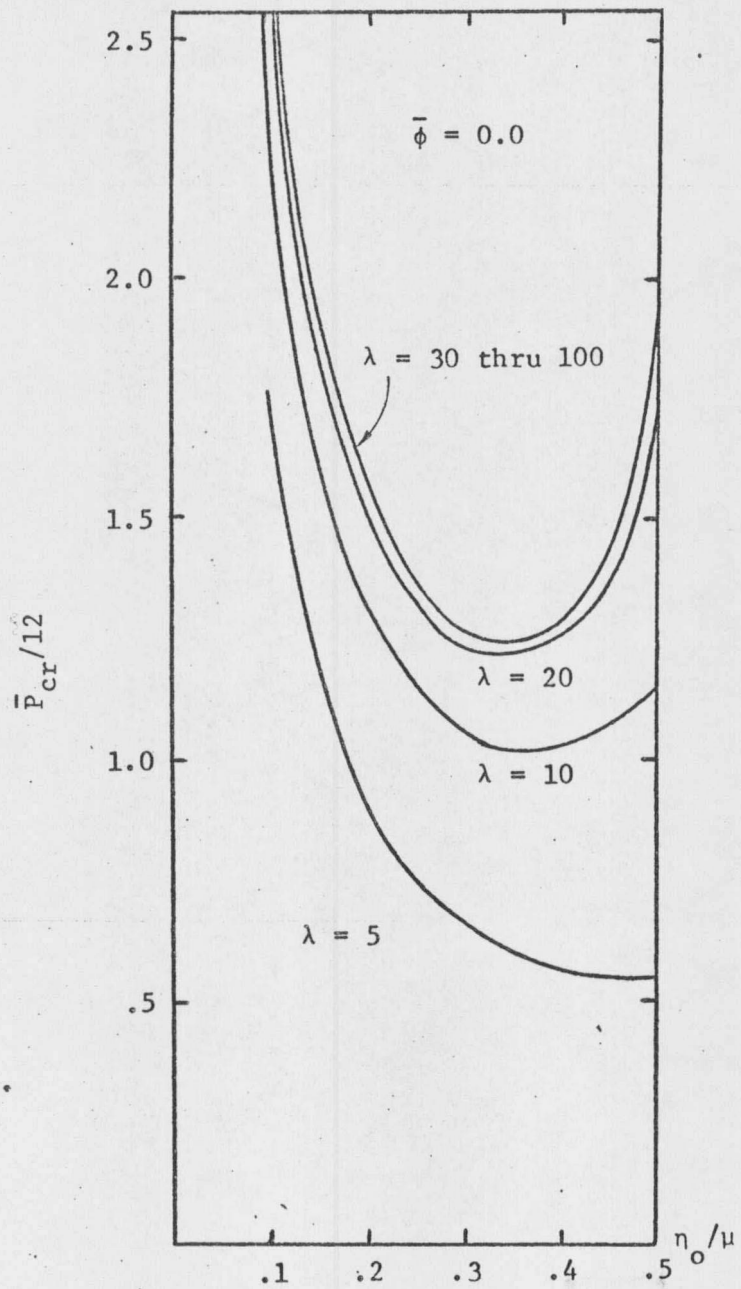


Fig. 3-5. Effect of the Load Position η_o/μ and the Geometric Parameter λ upon the Critical Loads $\bar{P}_{cr}$

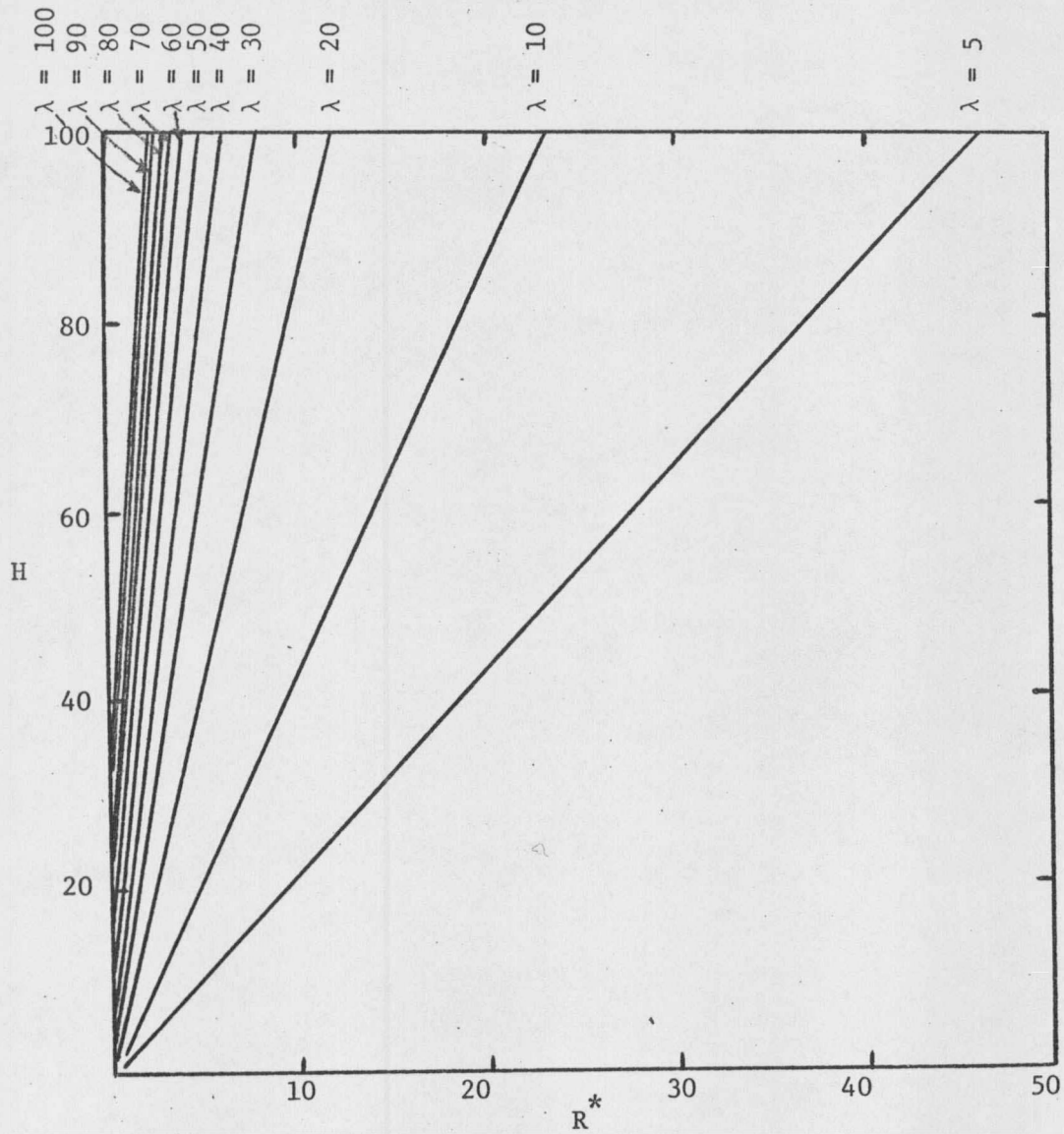
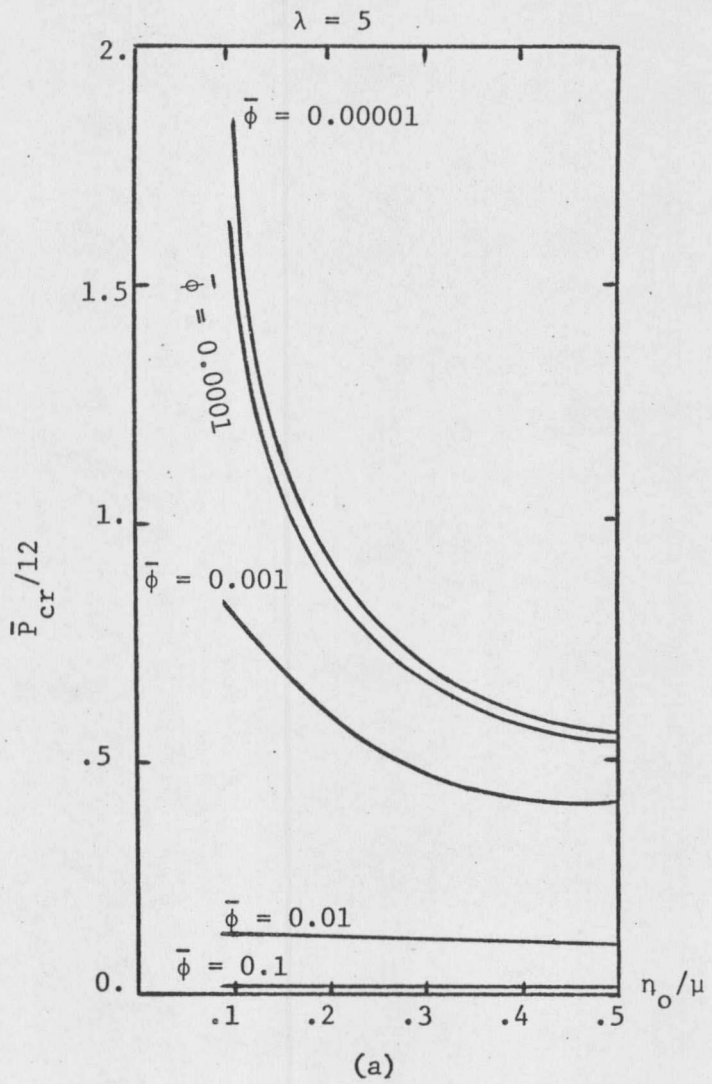


Fig. 3-6. Relation Among the Geometric Parameter λ, the Radius of Gyration R^*, and the Arch Rise H

$$W(\eta) = \left[\frac{1}{2\mu} + \frac{\eta_o - \mu}{\mu^4}\overline{P} - \frac{\phi\,\overline{P}}{2\mu^3}\right] - \left[\frac{1 - \text{Cos}\ \mu}{\mu^2\ \text{Sin}\ \mu} + \frac{\text{Sin}\ (\eta_o - \mu)}{\mu^3\ \text{Sin}\ \mu}\overline{P} + \frac{\phi\ (\text{Cos}\ \mu - 1)}{\mu^4\ \text{Sin}\ \mu}\overline{P}\right] \text{Sin}\ \eta + \left[-1 + \tfrac{1}{2}\eta^2 + \text{Cos}\ \eta\right]\left(\frac{\phi\overline{P}}{\mu^4} - \frac{1}{\mu^2}\right) + \frac{1}{\mu^3}\overline{P}\left[\eta - \eta_o - \text{Sin}\ (\eta - \eta_o)\right] J(\eta - \eta_o) \qquad \text{------ (3.20)}$$

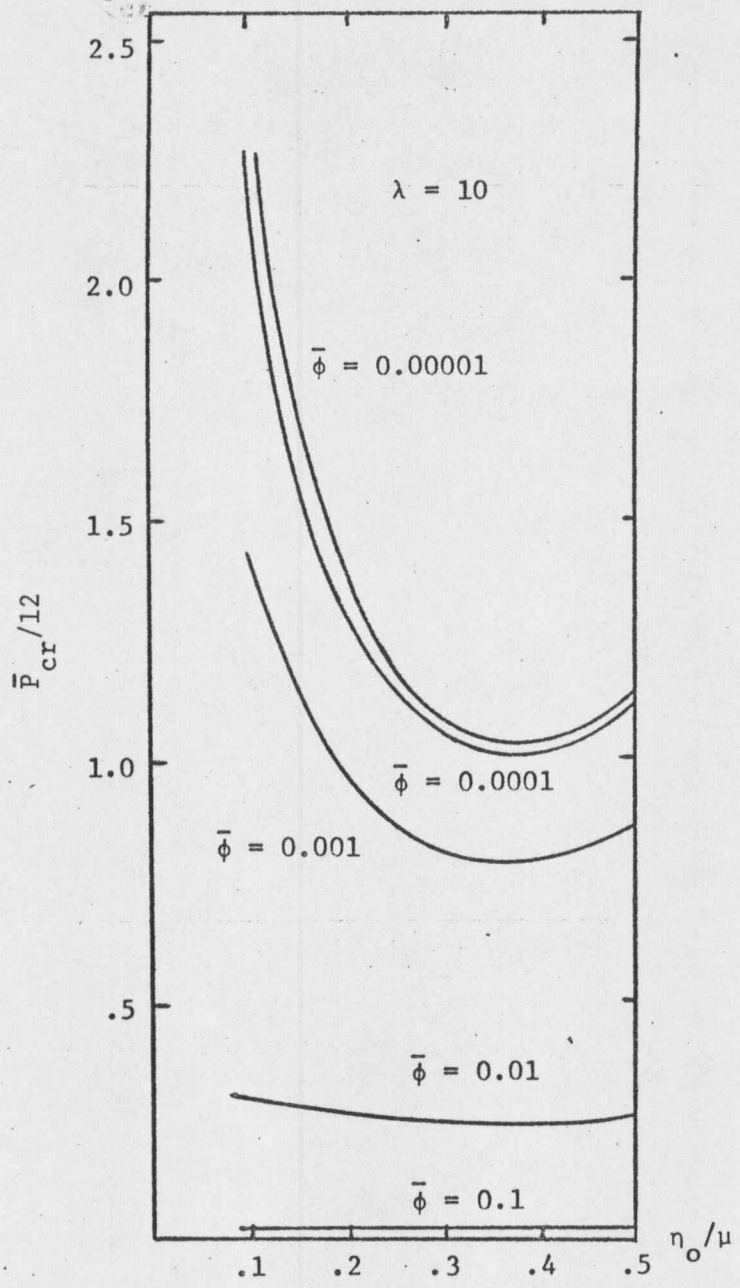
in which $J\ (\eta - \eta_o)$ is defined in Eq. (3.5).

From Eqs. (3.20) and (3.7) the critical loads may be determined. As before, the lowest buckling loads are obtained from $\overline{P}$ versus μ curves (or from $\overline{P}$ versus W curves for nonsymmetric buckling loads). Some of these values are tabulated in Table 3-2 through Table 3-8 (Appendix A) corresponding to various λ's and $\bar{\phi}$'s. For easy reference, they are also graphically shown in Fig. 3-7(a) through 3-7(f). It is seen from these tables and figures that, as in the last section, there is a "weak region" associated with the point load position. However, if $\bar{\phi}$ is large say $\bar{\phi} = 0.1$, this region all but vanishes. This is exactly as expected, since as $\bar{\phi}$ becomes greater, the uniform pressure is closer to the order of magnitude of the point load, the buckling of the arch is predominately due to the uniform pressure. Thus, the effect of the position of the point load becomes insignificant. On the other hand, as $\bar{\phi}$ becomes less and less, say $\bar{\phi} = 0.00001$, it is observed by comparing Table 3-8 and Table 3-1 that the effect of the uniform pressure upon the critical



(a)

Fig. 3-7. Effect of Uniform Pressure on the Critical Loads $\bar{P}_{cr}$



(b)

Fig. 3-7. Effect of Uniform Pressure on the Critical Loads $\bar{P}_{cr}$

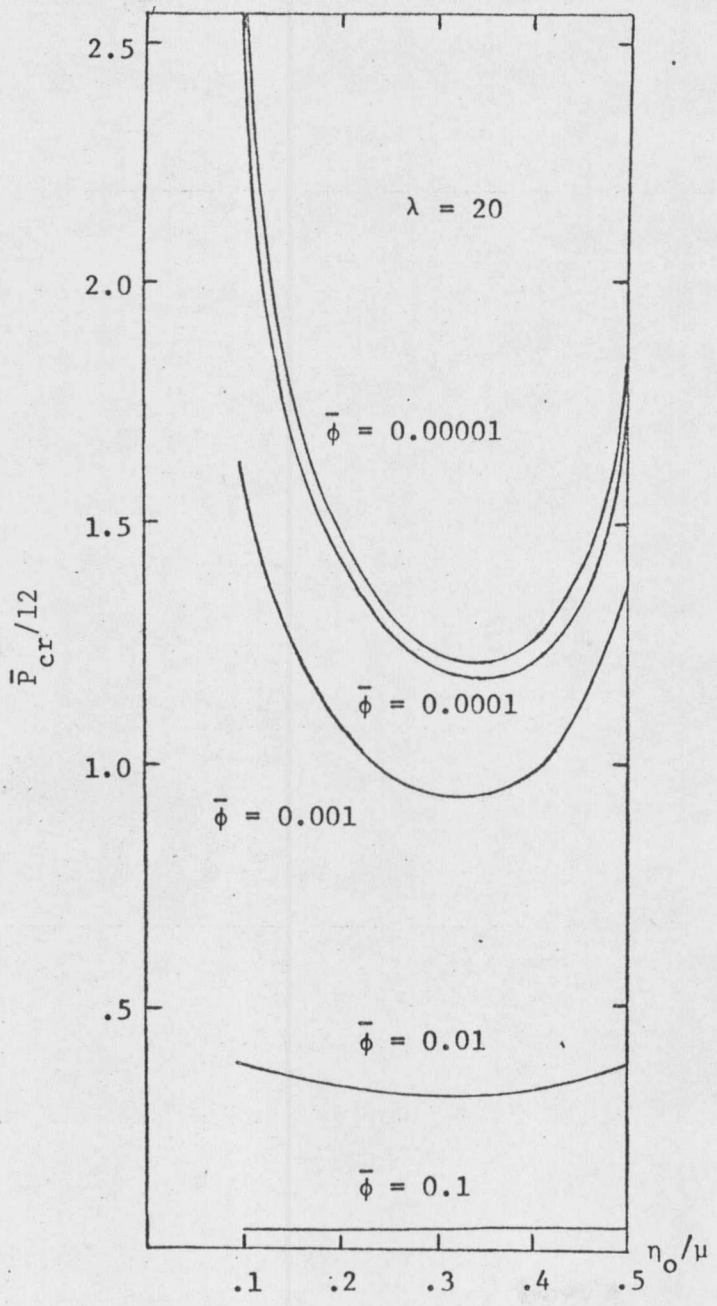


Fig. 3-7(c). Effect of Uniform Pressure on the Critical Loads $\bar{P}_{cr}$

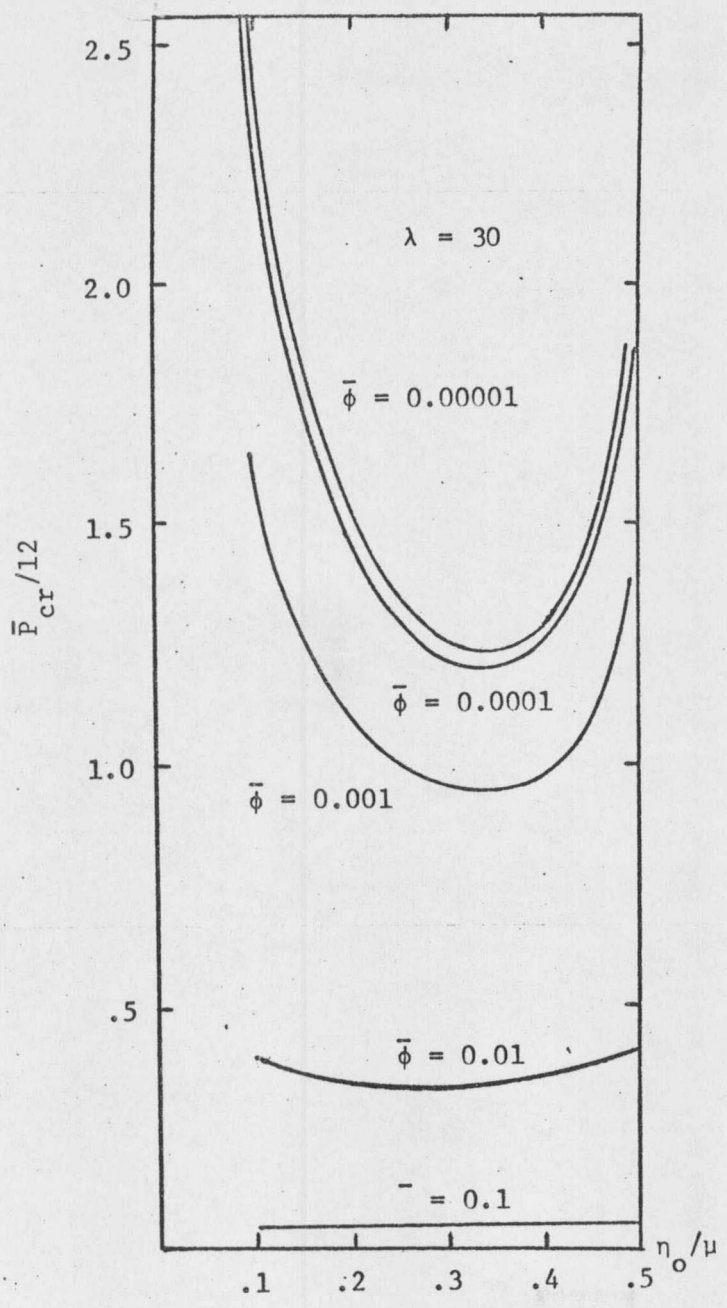


Fig. 3-7(d). Effect of Uniform Pressure on the Critical Loads $\bar{P}_{cr}$

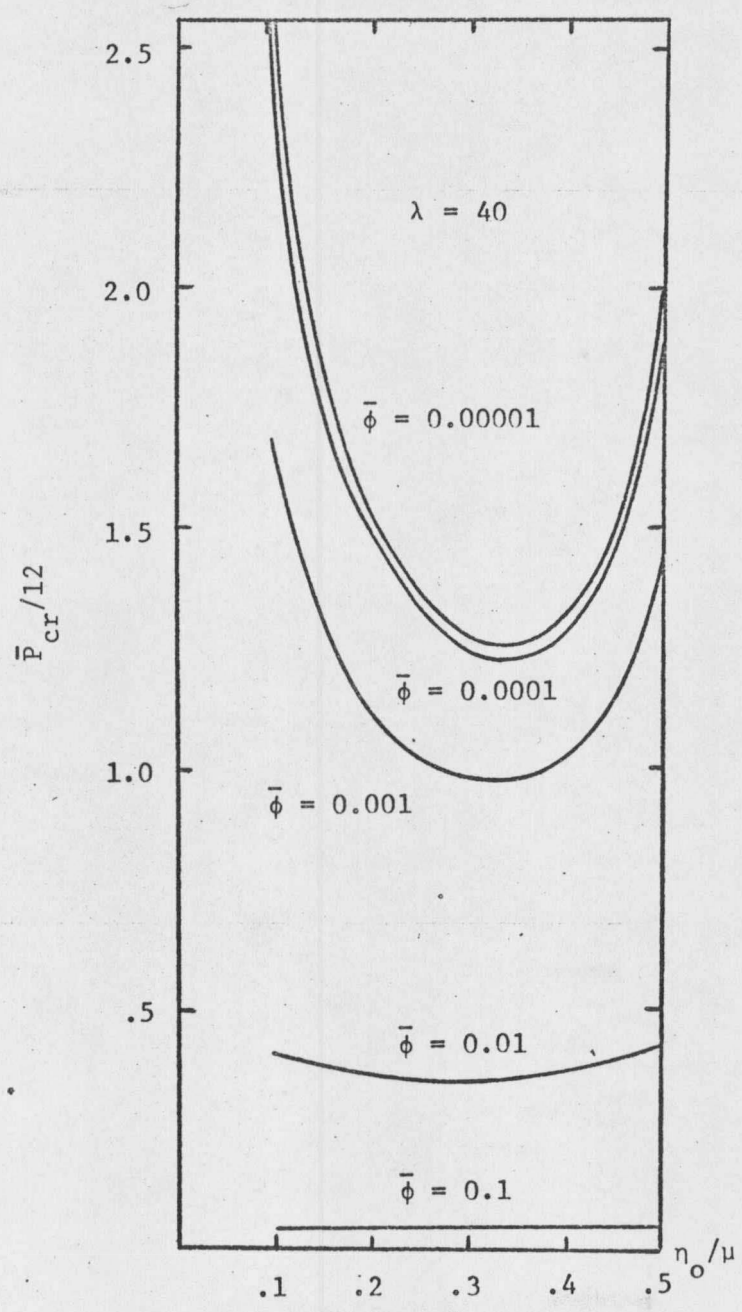


Fig. 3-7(e). Effect of Uniform Pressure on the Critical Loads $\bar{P}_{cr}$

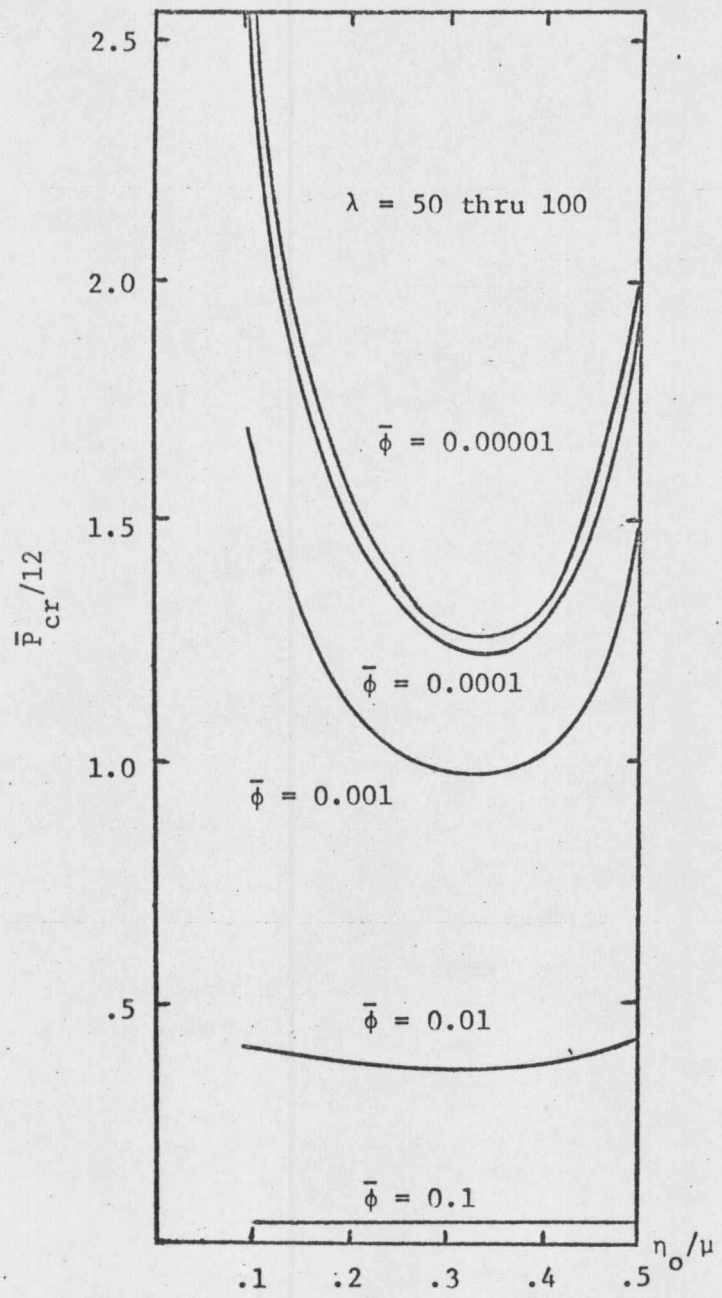


Fig. 3-7(f). Effect of Uniform Pressure on the Critical Loads $\bar{P}_{cr}$

loads is very small and may be neglected in practical considerations. This indicates that in analyzing arch stability problems, the effect of the dead weight may not be disregarded unless it is very small as compared to the critical point load.

It is noted that, if the point load is removed, and if only the uniform pressure remains acting, the problem reduces to a particular case which was solved by Dickie and Broughton (46). It can be shown that, by using Eq. (3.18) in which the first term on the right hand side is dropped and let ϕ = unity, the same results as (46) may be obtained if the same procedures as developed in the foregoing sections are followed.

CHAPTER 4

DYNAMIC STABILITY OF SHALLOW ARCHES SUBJECT TO MOVING LOAD

4.1 Introduction

Shallow elastic arches under dynamic loading have been analyzed by many investigators [9,14,15,21,22,23,26,27,47,49,50,51]. Hoff and Bruce [9] studied a sinusoidal arch under step load which is distributed sinusoidally over the arch rib. Hsu in a series of papers [14,21,23,26, 27,50] investigated arches subject to impulsive loading and obtained sufficient conditions for stability. Cheung and Babcock [15] studied clamped arches under center point load and under step load by using an energy approach. Humphreys [22] examined the dynamic stability of clamped circular arches by using the analog computer. Lock [51] investigated a sinusoidal arch by direct integration of two simultaneous equations which correspond to a two-modes approximation. Fulton and Barton [47] re-examined the same sinusoidal arch under impulsive pressure as well as step load. Smitses [49] assumed a deflection shape combining two symmetric and one antisymmetric modes in studying arches under impulsive pressure.

In the above-mentioned literature about the analysis of arches under dynamic loading, it is seen that this problem has been well examined. However, an arch subject to a moving point load, which is a problem of practical interest, has not been studied to the knowledge of this writer. Hence this chapter is devoted to the investigation of the stability of a hinged, circular, shallow arch under this particular type of loading. In

addition, the same arch under both the point moving load and its own weight (or the uniform pressure) is also studied.

4.2 Point Load

In the case that an elastic shallow arch with hinged ends is subjected only to a point load moving at a velocity v, the equation of motion is expressed by Eq. (2.49), i.e.,

$$EI\frac{\partial^4 w}{\partial x^4} - N_o\frac{\partial^2}{\partial x^2}(y_o - w) + m\frac{\partial^2 w}{\partial T^2} = P\delta(x - vT) \qquad \text{----------(4.1)}$$

The solution may be assumed to take the form

$$w(x,T) = \sum_{n=1,2,\ldots} \bar{A}_n(T)\sin\frac{n\pi x}{L} \qquad \text{----------(4.2)}$$

By substituting Eq. (4.2) into Eq. (4.1) and letting

$$\begin{aligned} A_n &= \frac{\bar{A}_n}{2R^*} \\ S &= \frac{N_o L^2}{EI\pi^2} \\ \bar{m} &= \frac{mL^4}{EI\pi^4} \\ P_2 &= \frac{PL^3}{2EI\pi^4 R^*} \end{aligned} \qquad (4.3)$$

After the whole expression is multiplied with $\sin\frac{m\pi x}{L}\,dx$ and then integrated from x = 0 to x = L, the following equation is obtained:

$$A_n(n^4 - n^2S) + \bar{m}\ddot{A}_n = 2P_2 \sin\frac{n\pi vT}{L} + \frac{SL^2}{n\pi^3\bar{R}R^*}(\cos n\pi - 1) \quad \text{----------(4.4)}$$

$$n = 1, 2, 3, \ldots$$

in which $\ddot{A}_n = \dfrac{d^2A_n}{dT^2}$

By using Eqs. (4.2), (4.3) and (2.42), one has

$$S = \sum_{n=1,2,3,\ldots} (2\lambda_n A_n - A_n^2)n^2 \quad \text{----------(4.5)}$$

in which $[\lambda_n]$ is a geometric parameter. To explain how $[\lambda_n]$ is defined, the following paragraph is presented.

The undeformed original arch shape may be expressed in the form of a series,

$$y_o = \sum_{n=1,2,3} a_n \sin\frac{n\pi x}{L} \quad \text{----------(4.6)}$$

or may be approximated as in the form

$$y_o = \frac{x}{2\bar{R}}(L - x) \quad \text{----------(4.7)}$$

From Eqs. (4.6) and (4.7), one has

$$y_o = \frac{4L^2}{\pi^3\bar{R}} \sum_{1,3,5} \frac{1}{n^3} \sin\frac{n\pi x}{L} \quad \text{----------(4.8)}$$

In other words, $[a_n]$ in Eq. (4.6) are

$$a_1 = \frac{4L^2}{\pi^3 R}$$

$$a_3 = \frac{1}{27} a_1 \qquad (4.9)$$

$$a_5 = \frac{1}{125} a_1$$

$$\vdots$$

Thus, for convenience, $[\lambda_n]$ are defined as

$$\lambda_n = \frac{a_n}{2R^*} \qquad (4.10)$$

Now one sees that the arch problem reduces to solving n simultaneous equations which must be subjected to the constraints expressed in Eq. (4.5). To investigate the instability of the problem, however, it is not necessary to consider all n modes which correspond to the n equations. It is enough just to consider the first few modes [5,22]. As a matter of fact, if Eq. (4.4) is solved numerically as shown graphically in Fig. (4-1a-e), one observes that the amplitude of A_4 and A_5 can practically be neglected, as compared with A_1, A_2 or even A_3. This is further demonstrated by the plot as shown in Fig. 4-1f. Nevertheless, all the first six modes are to be included in the present analysis.

The dynamic instability is defined as "a small increase in some load parameter results in a large increase in response" [22]. In

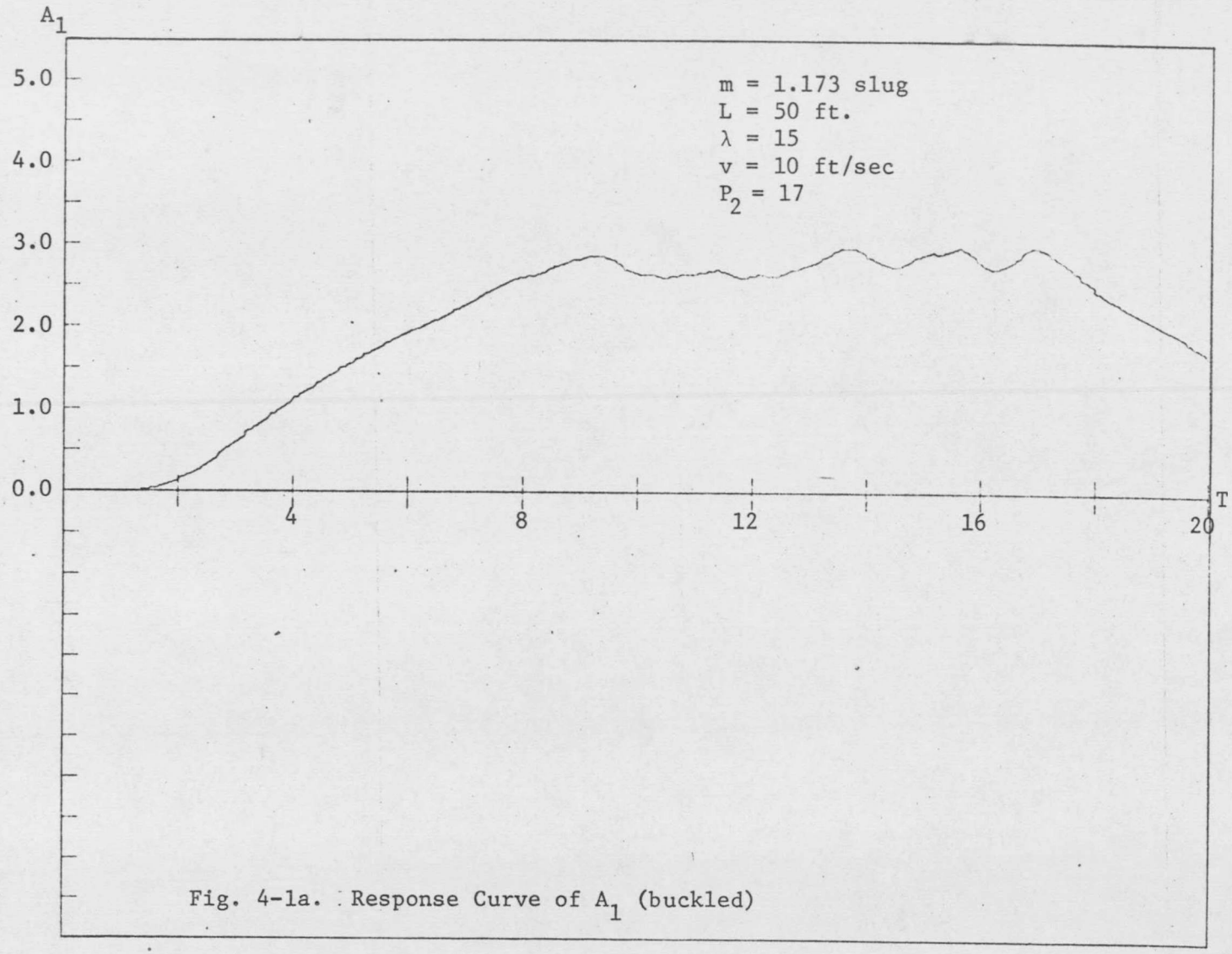


Fig. 4-1a. Response Curve of A_1 (buckled)

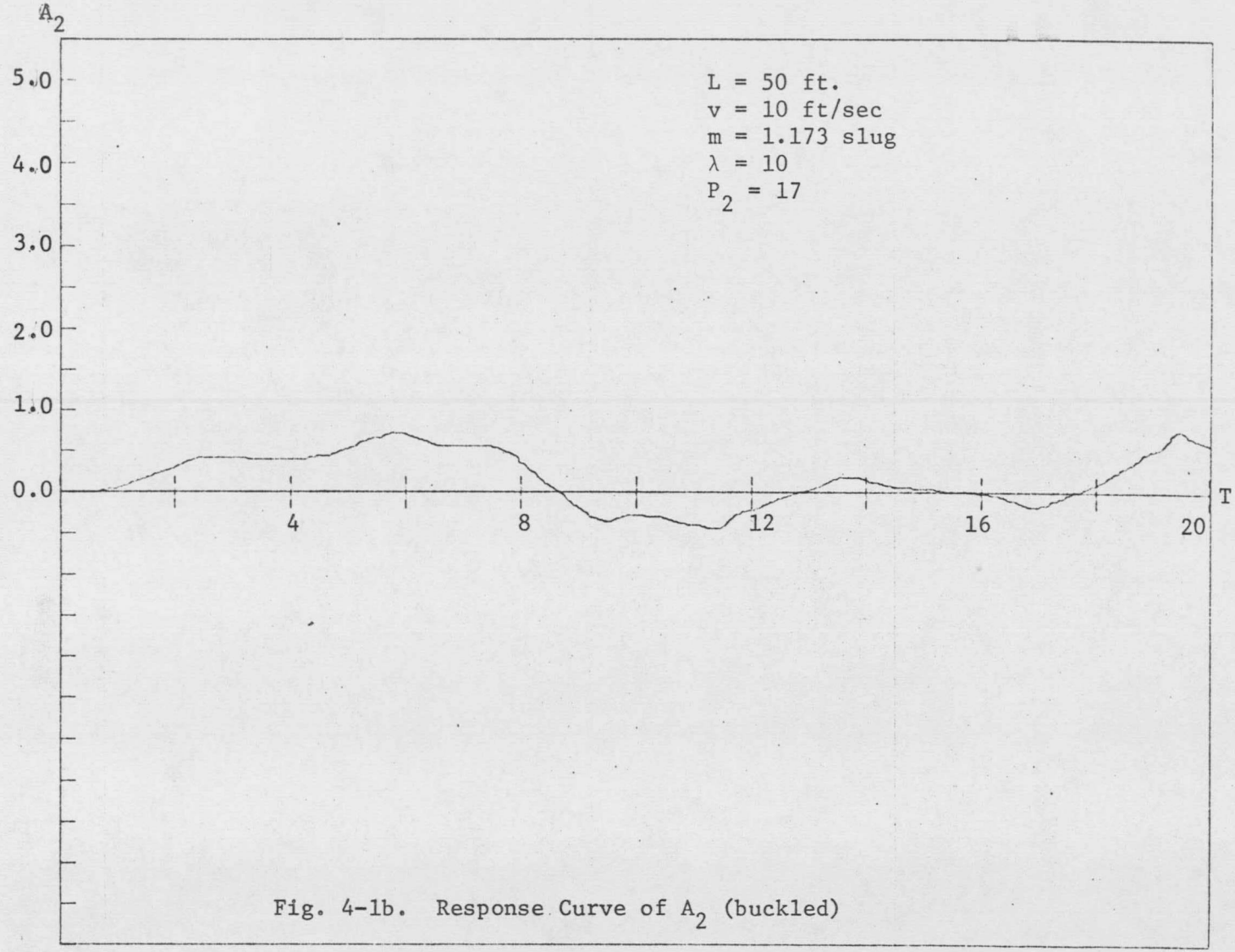


Fig. 4-1b. Response Curve of A_2 (buckled)

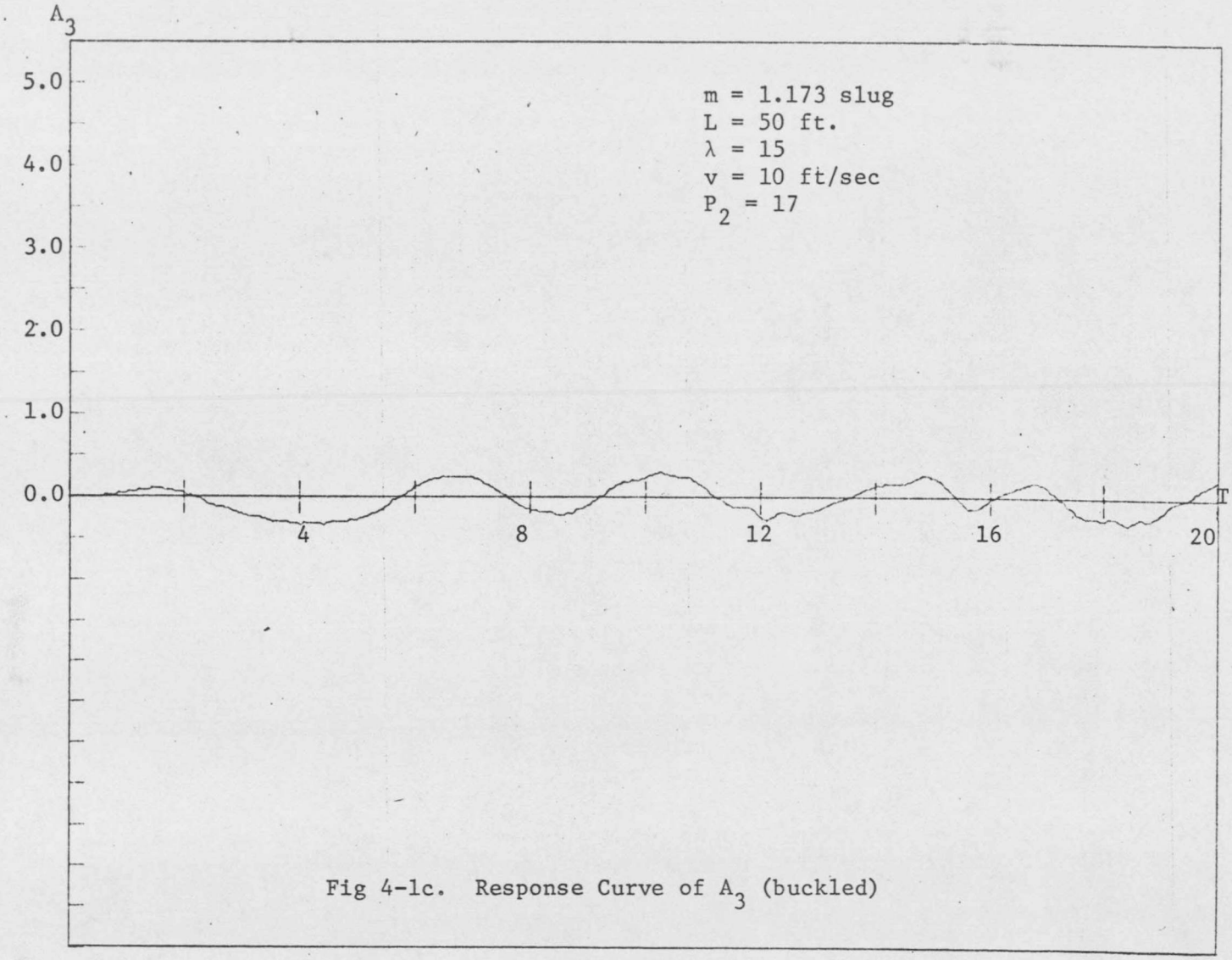


Fig 4-1c. Response Curve of A_3 (buckled)

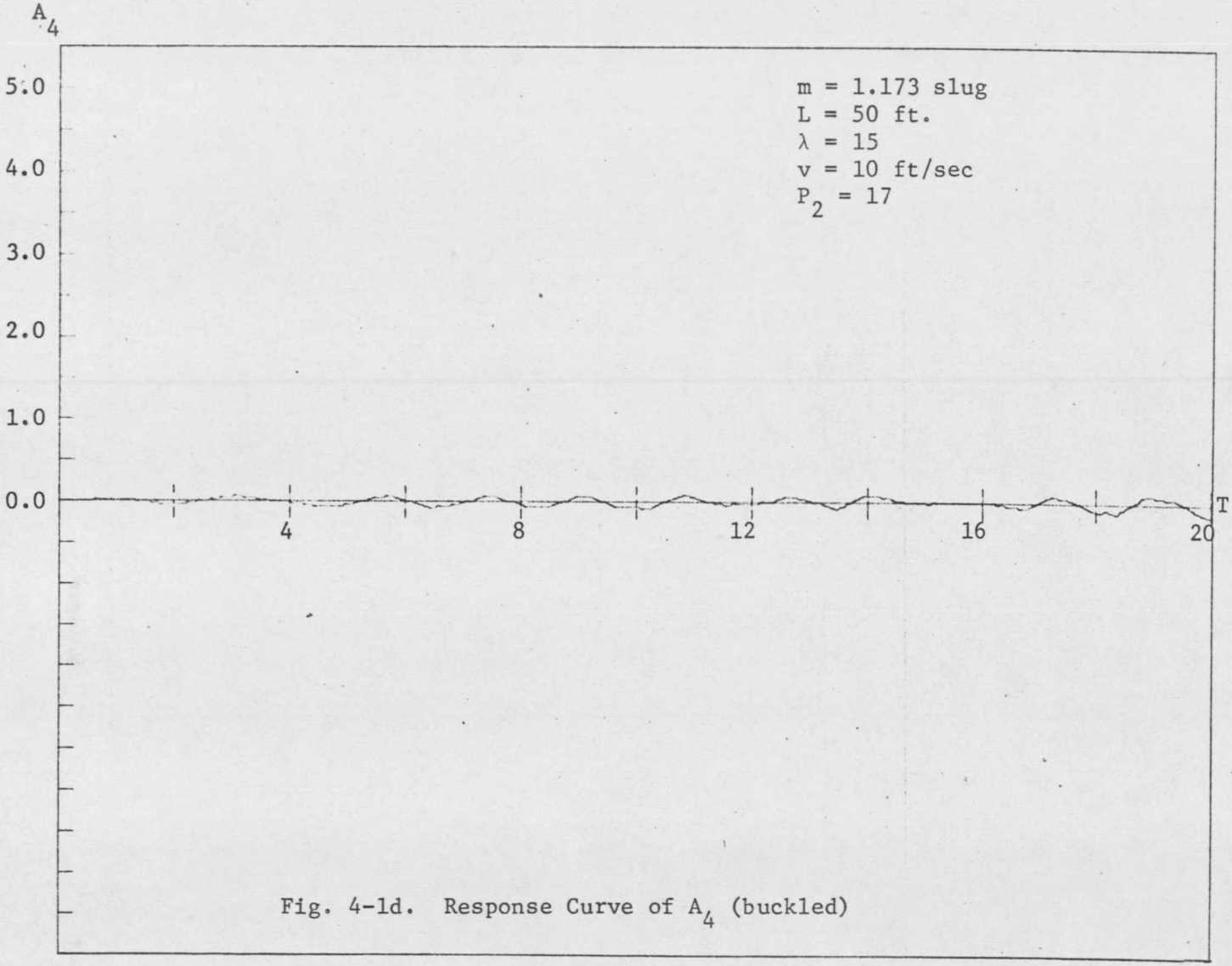


Fig. 4-1d. Response Curve of A_4 (buckled)

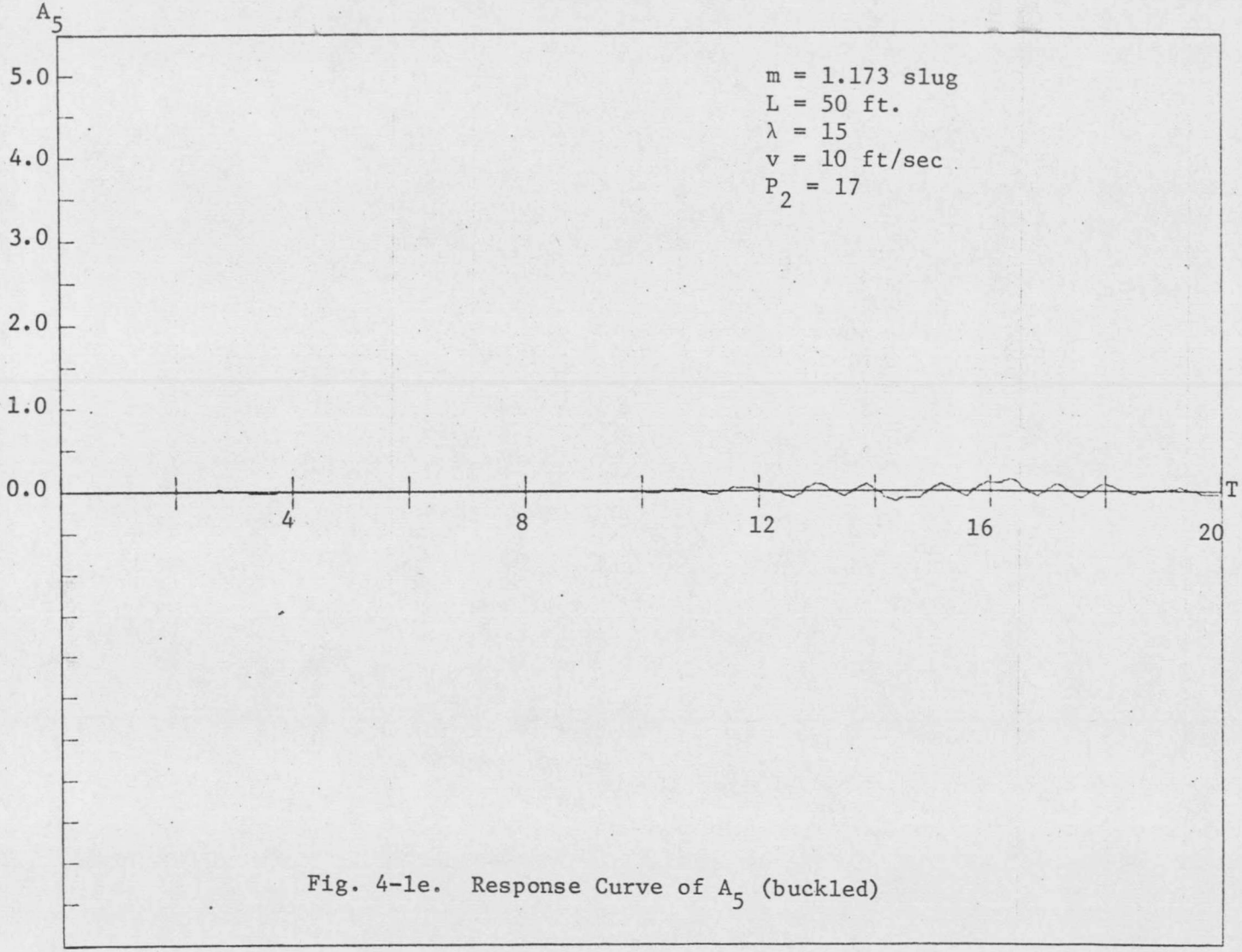


Fig. 4-1e. Response Curve of A_5 (buckled)

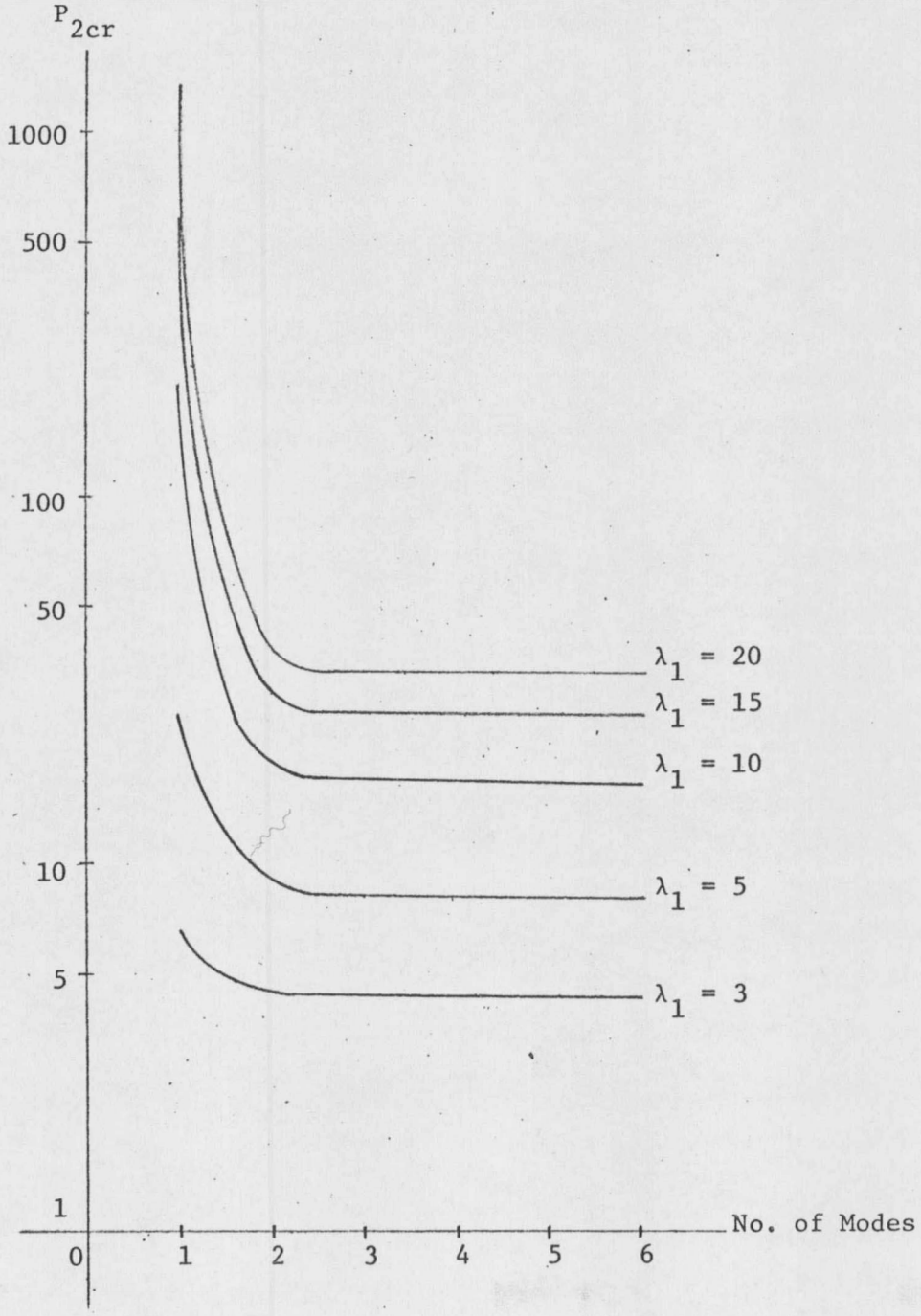


Fig. 4-1f. Effect of Number of Modes Upon Buckling Loads P_{2cr}

fact, in the current study, it is found that all the critical loads correspond to those that cause the displacement of the arch to increase very rapidly to that about two times as great as the arch rise for a small increase in the load parameter. The phenomenon of rapid increase in the arch displacement is referred to as "dynamic snapping-through" or "jump" as known in non-linear mechanics.

From Eq. (4.4) the first six equations are expanded as in the following:

$$\underline{A}_1(1 - S) + \bar{m}\ddot{A}_1 = 2P_2 \sin\frac{\pi vT}{L} - \frac{2SL^2}{\pi^3\bar{R}R^*} \qquad (4.11)$$

$$\underline{A}_2(16 - 4S) + \bar{m}\ddot{A}_2 = 2P_2 \sin\frac{2\pi vT}{L} \qquad (4.12)$$

$$A_3(81 - 9S) + \bar{m}\ddot{A}_3 = 2P_2 \sin\frac{3\pi vT}{L} - \frac{2SL^2}{3\pi^3\bar{R}R^*} \qquad (4.13)$$

$$A_4(256 - 16S) + \bar{m}\ddot{A}_4 = 2P_2 \sin\frac{4\pi vT}{L} \qquad (4.14)$$

$$A_5(625 - 25S) + \bar{m}\ddot{A}_5 = 2P_2 \sin\frac{5\pi vT}{L} - \frac{2SL^2}{5\pi^3\bar{R}R^*} \qquad (4.15)$$

$$A_6(1296 - 36S) + \bar{m}\ddot{A}_6 = 2P_2 \sin\frac{6\pi vT}{L} \qquad (4.16)$$

In the above equations, S is defined by Eq. (4.5), or

$$S = 2\lambda_1 A_1 - A_1^2 - 4A_2^2 + 18\lambda_3 A_3 - 9A_3^2 - 16A_4^2 + 50\lambda_5 A_5 - 25A_5^2 - 36A_6^2 \qquad (4.17)$$

Due to the complexities and non-linear character of the problem, the simultaneous equations cannot be solved analytically. Recourse is made of a numerical solution--by using the Runge-Kutter 4th order method. The Runge-Kutter method has been one of the standard numerical techniques in solving differential equations. With some refinements worked

out by Ralston and Wilf [53], it was reported that for some cases it agrees with the exact solution up to the eighth digit. One of the features in the refined method is that the truncation error is reduced by letting the step size be variable. In other words, as the truncation error is greater than a certain value allowed, the step size is automatically cut smaller. To account for the other source of error, i.e., the round-off error, the entire calculations are carried out with double precision.

In the investigation, these data are used: L = 50 ft, E = 475,200 psf, I = 1/96 ft^4, A = 0.5 ft^2, and m = 1.173 slug.

The results are tabulated in TABLE 4-1 (Appendix A). In the table, it is seen that the critical load increases with higher speed and also with greater geometric parameter λ_1. However, for the whole range of the speed v, the buckling loads do not necessarily increase with higher speed. To clarify this, Fig. 4-2 and Fig 4-3 are drawn. They are plotted in the non-dimensionalized form. Fig. 4-2 shows that as v/L (speed-span ratio) increases, the buckling load P_{2cr} also increases. But this is not the case for $v/L \leq 0.06$, as may be seen in Fig. 4-3. It shows that only for $v/L > 0.06$ does the buckling load increase as v becomes greater. Fig. 4-3 also shows that the minimum dynamic buckling load is less than the corresponding static buckling load about 21.9% for $\lambda_1 = 6.72$ and 17.3% for $\lambda_1 = 11.2$. Hence, it appears that as λ_1 increases, the percentage becomes smaller.

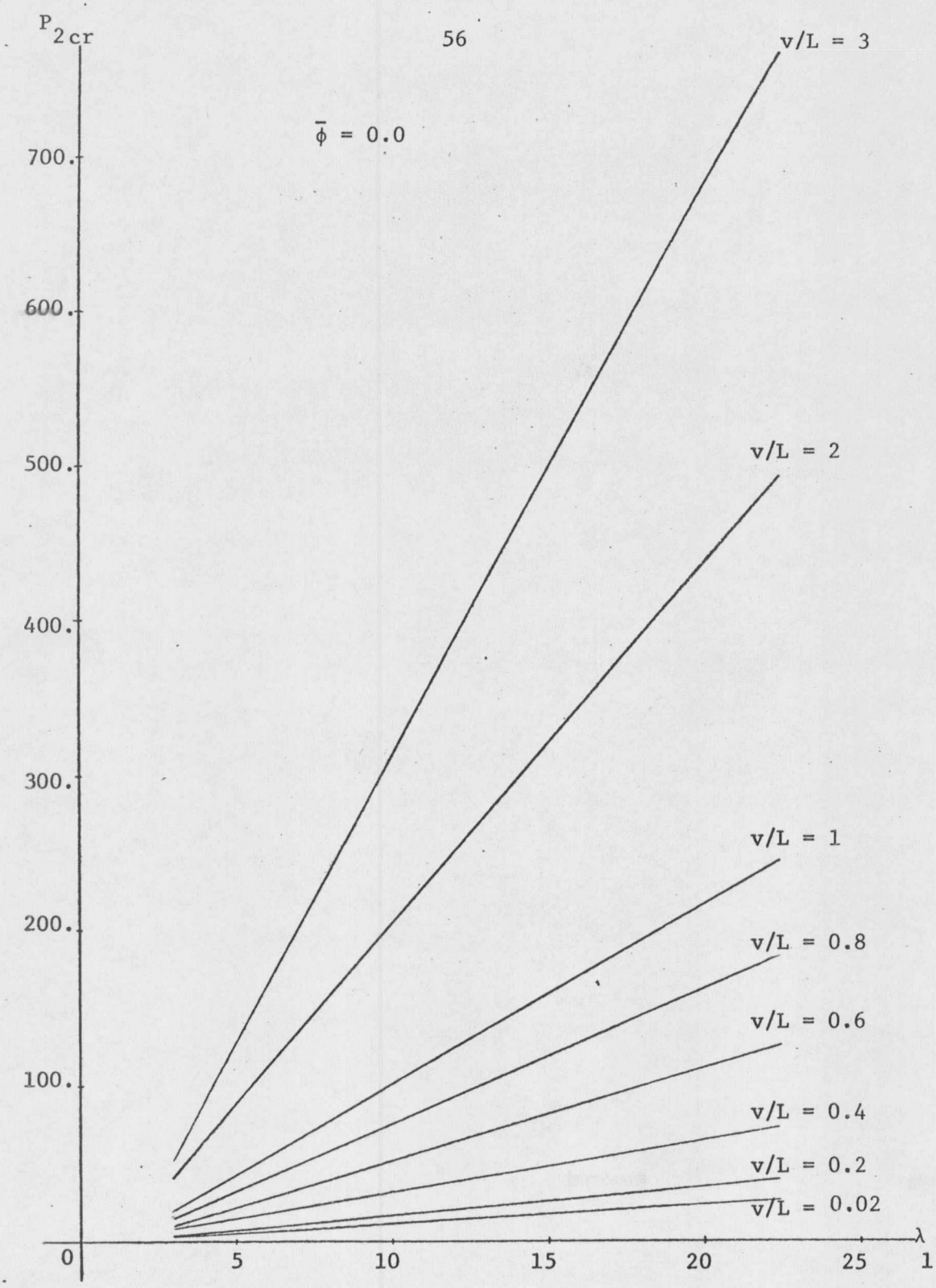


Fig. 4-2. Critical Load Parameter P_{2cr} Corresponding to Various Values of the Geometric Parameter λ_1^{2cr} and Speed-Span Ratio v/L

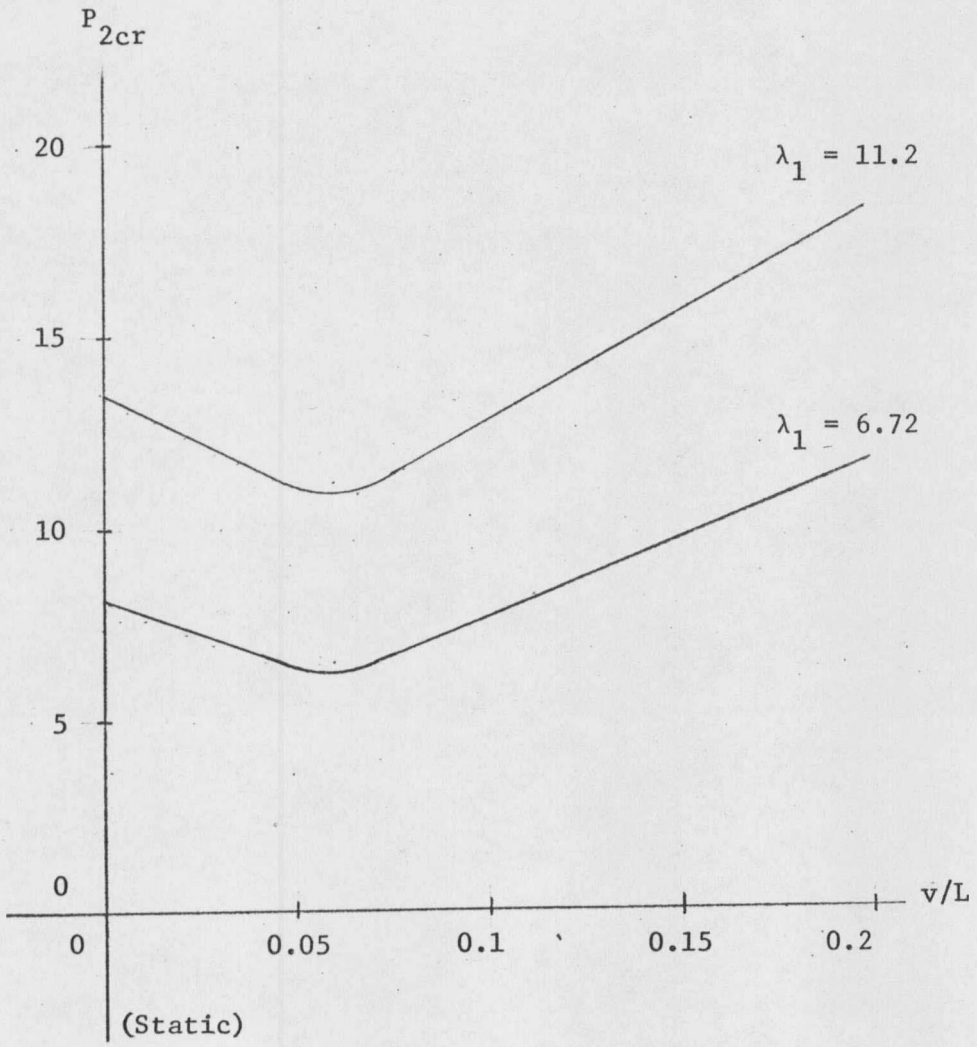


Fig. 4-3. Effect of the Speed-Span Ratio Upon the Buckling Load P_{2cr}

4.3 Point Load Plus Uniform Pressure

The governing equations for this case are Eqs. (2.50) and (2.42). With the same procedure and same substitutions as in Sec. 4.2, Eqs. (2.50) and (2.42), respectively lead to

$$A_n(n^4 - n^2S) + \bar{m}\ddot{A}_n = 2P_2 \sin\frac{n\pi vT}{L} + \frac{b\phi P_2}{n}(1 - \cos n\pi) + \frac{SL^2}{n\pi^3\bar{R}R^*}(\cos n\pi - 1) \quad \text{----------(4.18)}$$

and

$$S = \sum_{n=1,2,3}(2\lambda_n A_n - A_n^2)n^2 \quad \text{----------(4.19)}$$

in which $\phi = \frac{2L}{\pi}\bar{\phi}$ ----------(4.20)

Again the first six modes are considered. The numerical results are tabulated in TABLE 4-2 through TABLE 4-6 (Appendix A). As in the static case, if the order of magnitude of the uniform pressure is close or equal to the point load, say $\bar{\phi} = 1.0$, the critical loads are more due to the uniform pressure than due to the moving point load. This may be closely seen by observing Fig. 4-4 or comparing TABLE 4-2 and TABLE 4-6. TABLE 4-6 shows the critical values for shallow circular arches under uniform step pressure, which is a particular case and may be obtained from Eq. (4.18) by letting $\phi = 1.0$ and dropping the first term on the right-hand side. In TABLE 4-2, it is also noted that the increase in

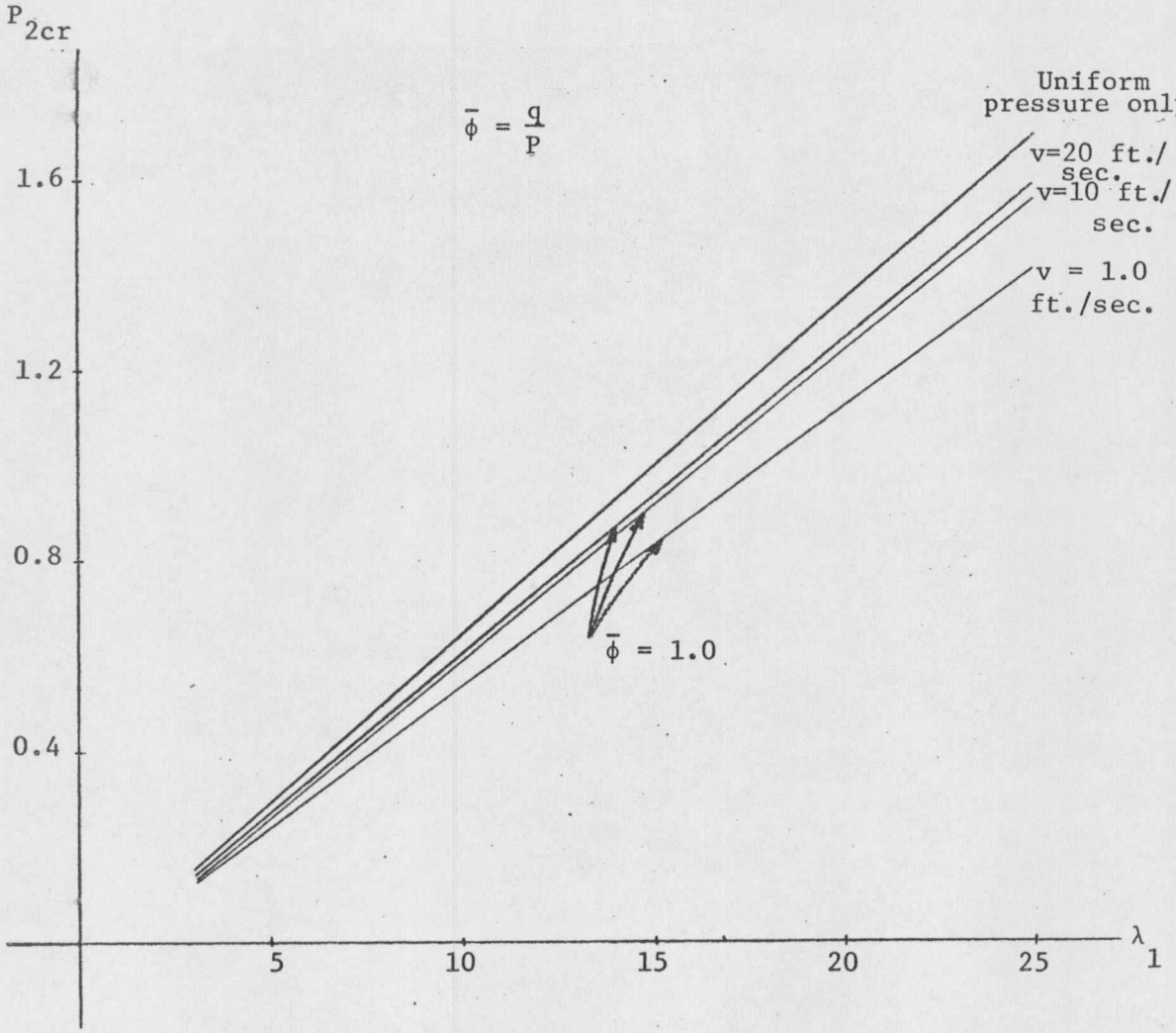
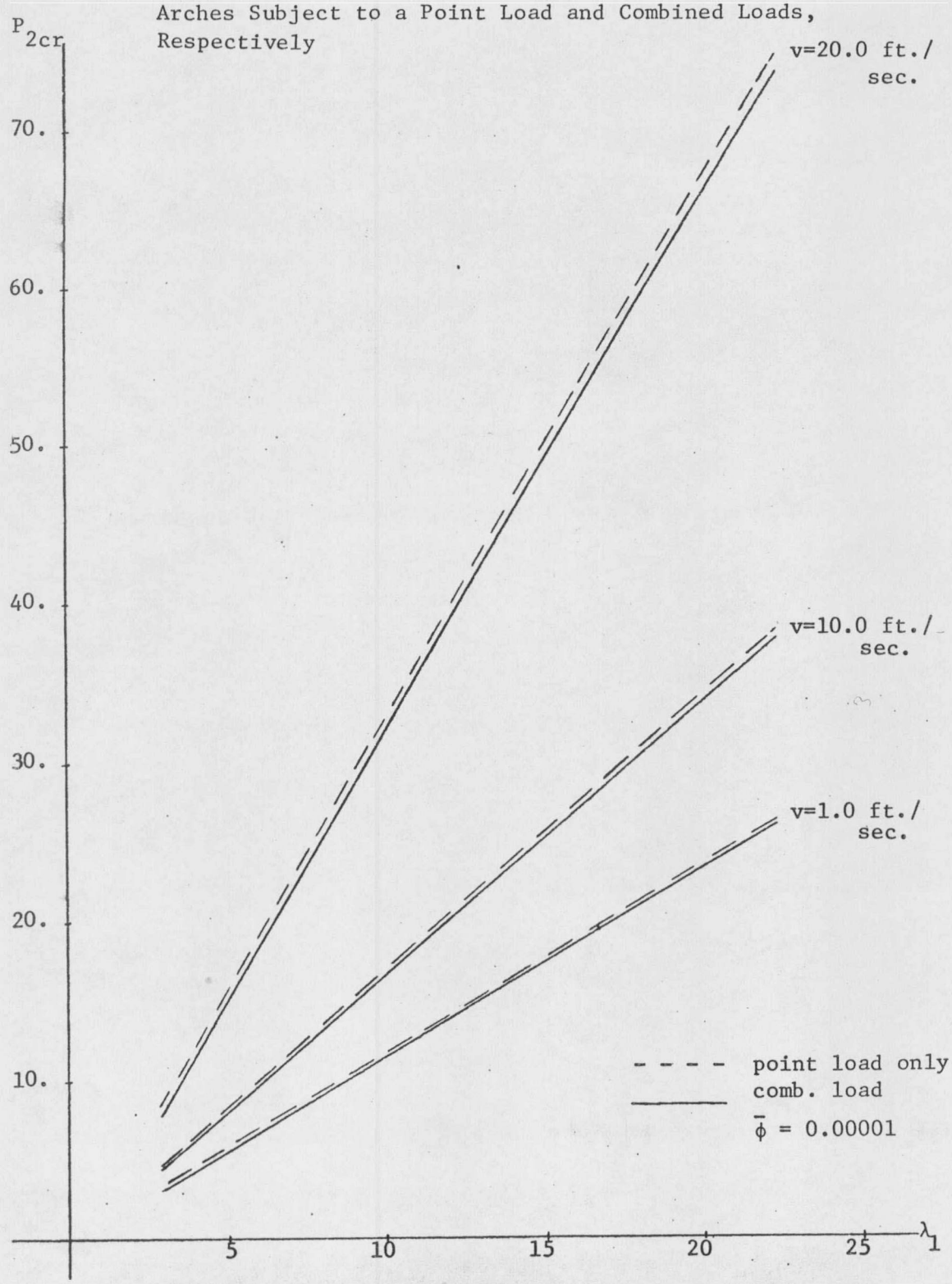


Fig. 4-4. Comparison of Critical Values for Pin-Pin Shallow Circular Arches Subject to Uniform Pressure and Combined Loading, Respectively

critical loads due to higher speed is small and insignificant. Hence, in case the dead weight of the arch is about the same order as the point moving load, the problem may be treated as a step-load problem in practical considerations.

When the uniform pressure such as the dead weight is a small fraction of the point load P, say $\bar{\phi} = 0.00001$, from TABLE 4-5 and TABLE 4-1, or more clearly from Fig. 4-5, it is seen that the effect of the uniform pressure upon the buckling loads is negligible. This is similar to the static case as mentioned in Chapter 3. Thus, in analyzing an arch problem under a point moving load, if the dead weight of the arch is small, one need not include the dead weight.

Fig. 4-5. Comparison of Critical Values for Pin-Pin Shallow Circular Arches Subject to a Point Load and Combined Loads, Respectively



4.4 Damping Effects

In any structural system, damping is always present during dynamic oscillation. But it is frequently neglected because of its small effects. In an attempt to get an insight into the actual effects of damping upon the critical loads which cause the shallow arches to snap through, it is necessary to restudy the governing equation and its solution in the case when damping is included. Assume the viscous damping is proportional to the first derivative of the displacement, then the governing equation takes the form:

$$EI\frac{\partial^4 w}{\partial x^4} - N_o\frac{\partial^2}{\partial x^2}(y_o - w) + D\frac{\partial w}{\partial T} + m\frac{\partial^2 w}{\partial T^2} = P\delta(x - vT) \qquad (4.21)$$

in which D is the damping coefficient. In Eq. (4.21) the dead weight of the arch is disregarded, since the main purpose here is to examine the relationship between the instability and the damping of the arch. If now a series solution taking the form of Eq. (4.2) is assumed, and Eqs. (4.3) are also used, as before, one has

$$A_n(n^4 - n^2S) + \bar{D}\,\dot{A}_n + \bar{m}\,\ddot{A}_n = 2P_2 \sin\frac{n\pi vT}{L} + \frac{SL^2}{n\pi^3 RR^*}(\cos n\pi - 1) \qquad (4.22)$$

in which $\dot{A}_n = \frac{dA_n}{dT}$; $\ddot{A}_n = \frac{d^2A_n}{dT^2}$

$$\bar{D} = DL^4/EI\pi^4$$

and S is defined in Eq. (4.5).

To understand how the damping affects the amplitude, we consider initially the first two modes, A_1 and A_2. Let the two equations be solved numerically and plotted. In Fig. 4-6, the plots show three response curves corresponding to D = 0.0, D = 0.1, and D = 1.0. It is seen that the presence of damping reduces the maximum amplitude of the response. It will be shown later that the arch snaps through as soon as the maximum amplitude reaches a critical value. As such, it is evident that including the damping effects the critical (buckling) loads of the shallow arches are higher than with the damping effects excluded. Accordingly, the presence of damping in the arch vibration is generally to advantage as far as the stability problem is concerned.

The results obtained from solving the six equations are tabulated in TABLE 4-7 and shown in Fig. 4-7. In Fig. 4-7, it is seen that the critical values are higher than if the damping effect is excluded. Furthermore, it is also observed that with higher speed, this effect is more pronounced.

4.5 The New Concept About Dynamic Instability

Although the definition of the dynamic instability is generally accepted as "a small increase in some load parameter results in a large increase in response" as mentioned in Sec. 4.2, many of the investigators in this field as cited in Sec. 4.1 have tried to explain why the instability of the shallow arches occurs. It can be categorized into three

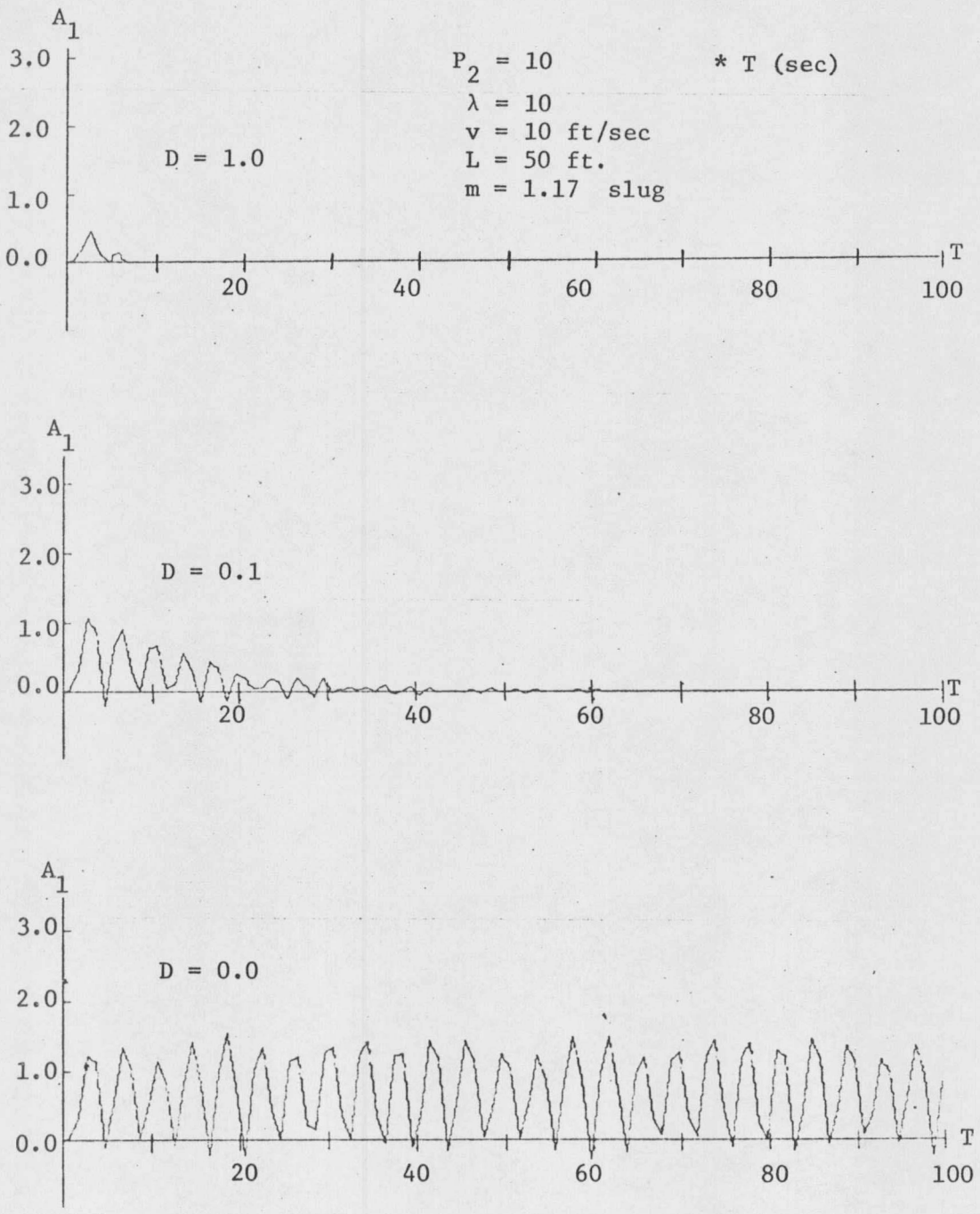


Fig. 4-6. Response Curves of A_1 Associated with D = 0.0, 0.1, and 1.0, Respectively

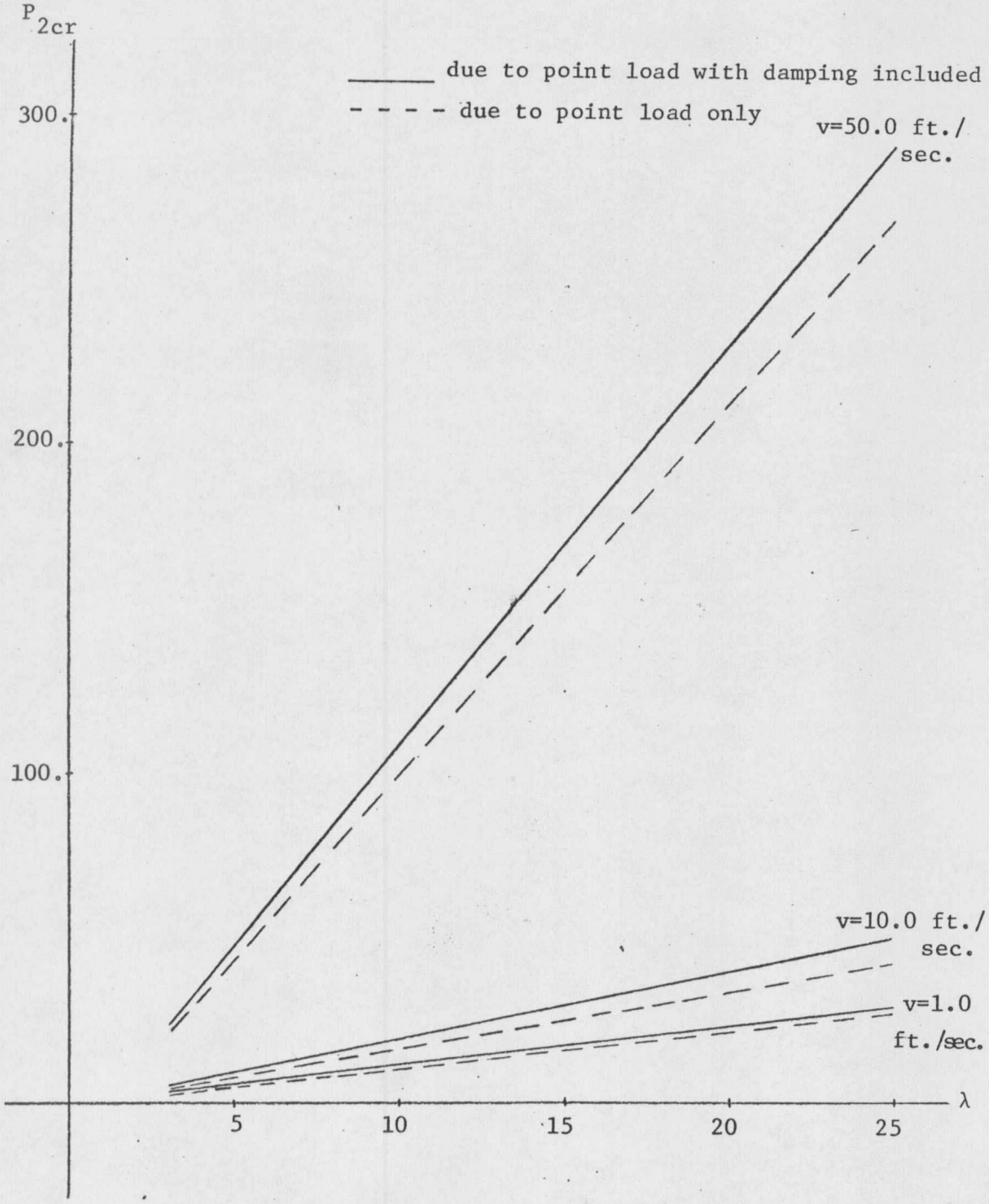


Fig. 4.7. Effect of Damping (D = 0.1)

groups. The first group including Humphreys [22] observes the load-displacement curves and the displacement response plots and finds that the arch would snap through when a load corresponding to the critical value causes the maximum amplitude of the vibration of the arch to increase very rapidly. The second group including Hoff and Bruce [9] and Hsu [26] studies the energy plane in which the local equilibrium points are examined. This idea of using the phase plane to study the stability of local equilibrium points is a great step forward in the analysis of dynamic structural systems. Unfortunately, this technique is limited to the so-called autonomous systems in which time is not explicitly involved. The third group represented by Lock [51] attempts to form a chart similar to that representing the well known Mathieu equation. Lock considered a sinusoidal arch subjected to step pressure. Due to the complexities of the problem, he used a two-modes approximation. However, to obtain the above-mentioned chart, he had to disregard some terms which are significant in general. Accordingly, the chart so obtained does not accurately predict the actual results. This may be seen by actually integrating the equations and comparing the results. Lock's chart has been extensively used as a reference [47]. Consequently, there is a great need to develop a refined concept to predict the dynamic instability of the arch system.

To help clarify some points which are to be met later, the writer wishes to express some experiences to obtain the inspiration with

which the following study is made possible. Over hundreds and hundreds of computer runnings in numerically solving the six differential equations mentioned previously, the writer found:

a) The jump phenomenon will not occur until the first mode A_1, is equal to or a little greater than the arch parameter, λ_1.

b) The maximum amplitude of A_1 would increase if the load parameter P_2 was increased.

Since the numerical technique to solve the equations is the Runge-Kutter 4^{th} order method, the initial values are generally taken to be zero for the solution. To get some insight into the behavior of the free oscillation of the system, the writer solved the first equation by first letting the amplitude of the forcing function equal to zero but giving an initial displacement. The response curve is as shown in Fig. 4-8. In this plot, the initial displacement is less than λ_1. This implies that one expects no jump but that the system would vibrate periodically. This is exactly as shown in the figure. On the other hand, if the initial amplitude is greater than some value as great as or a little greater than λ_1, one expects the system would jump or the arch would snap through. And this is exactly as shown in Fig. 4-9. It is then clear that for a certain critical initial displacement the arch snaps through. In a similar case, an initial velocity may cause the arch to buckle as may be seen from Figs. 4-10 and 4-11. This kind of loading is known as impulsive loading and has been studied by Hsu.

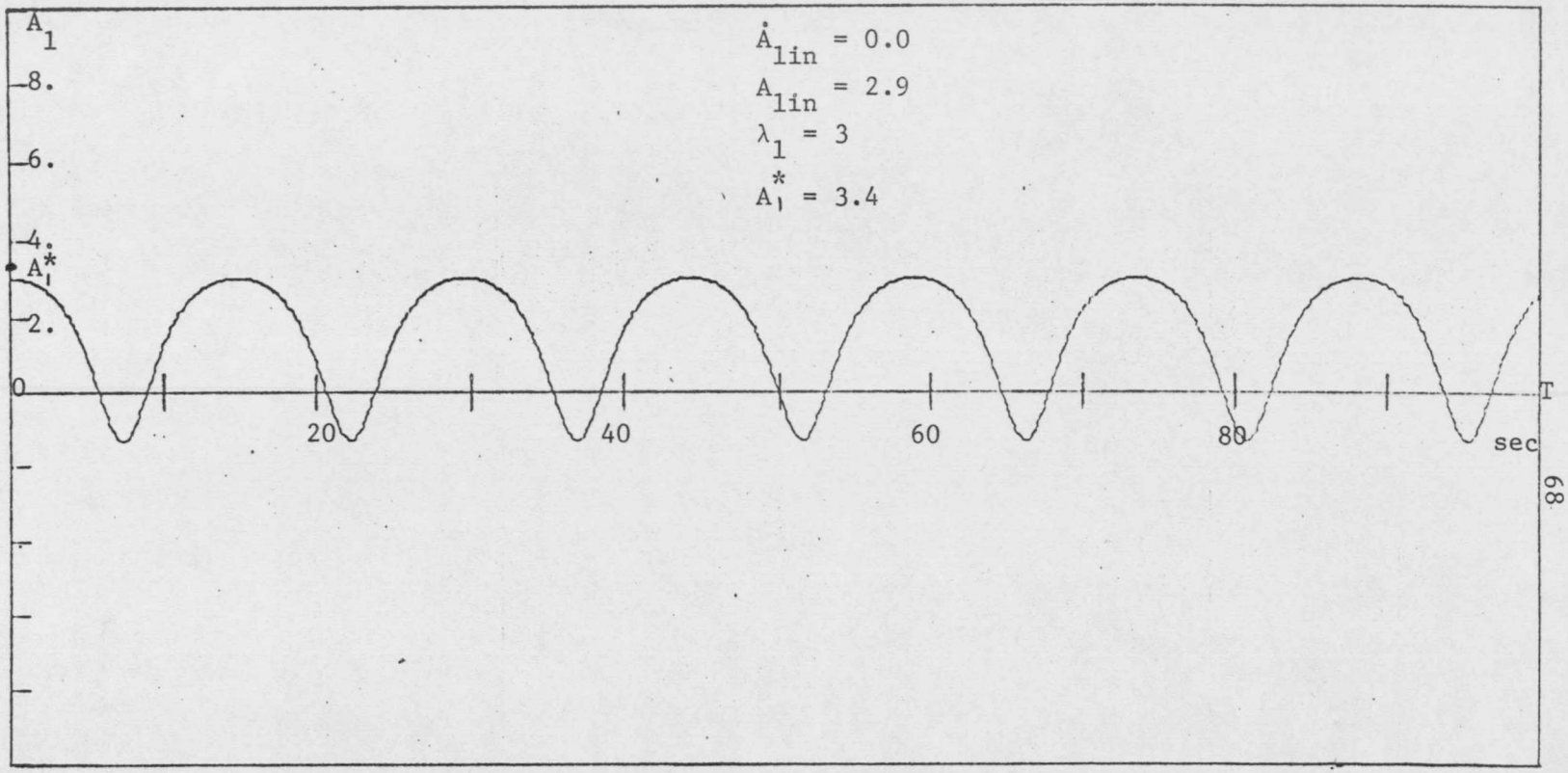


Fig. 4-8. Response Curve of A_1 (One Mode Approximation)

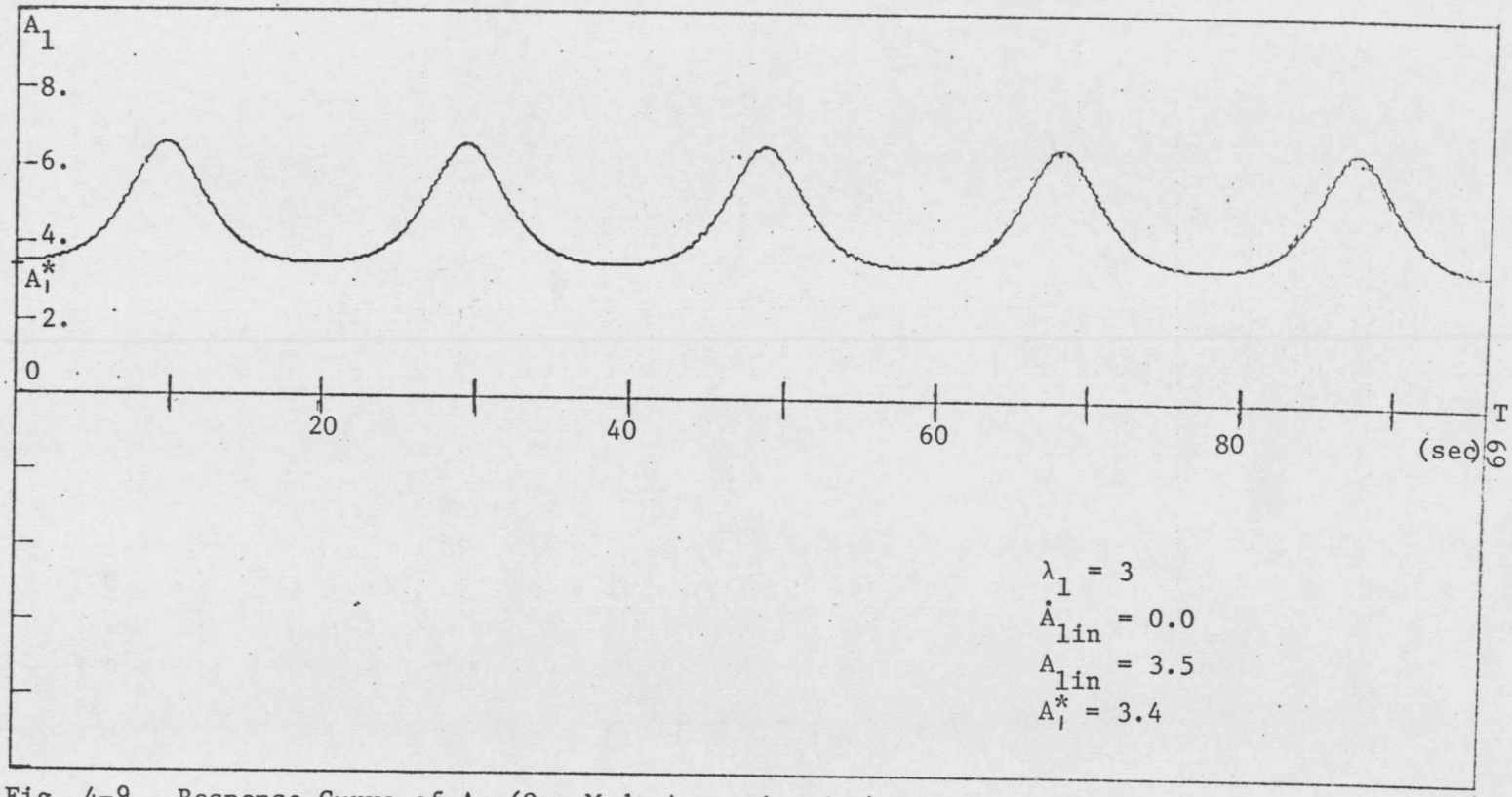


Fig. 4-9. Response Curve of A_1 (One Mode Approximation)

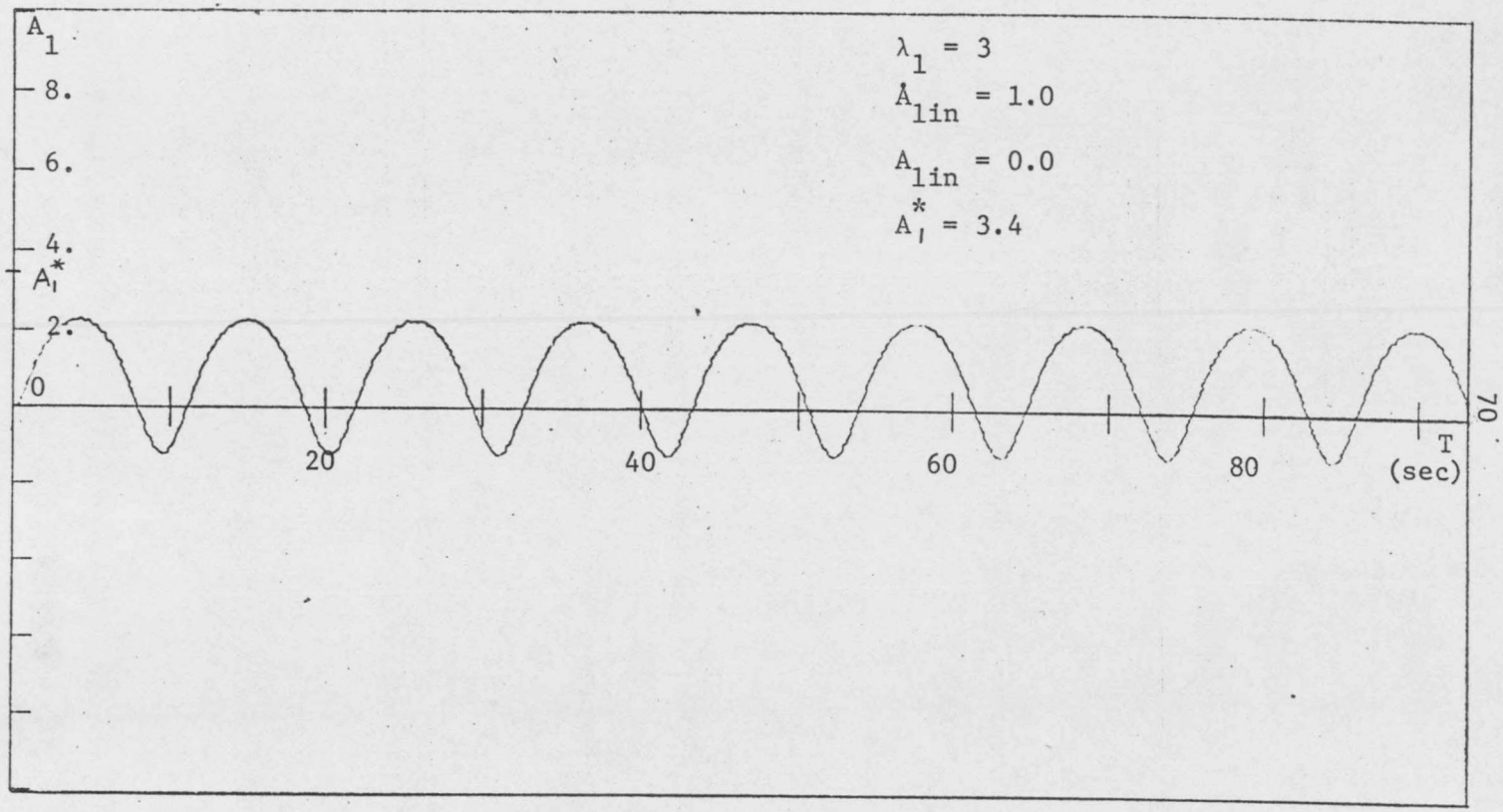


Fig. 4-10. Response Curve of A_1 (One Mode Approximation)

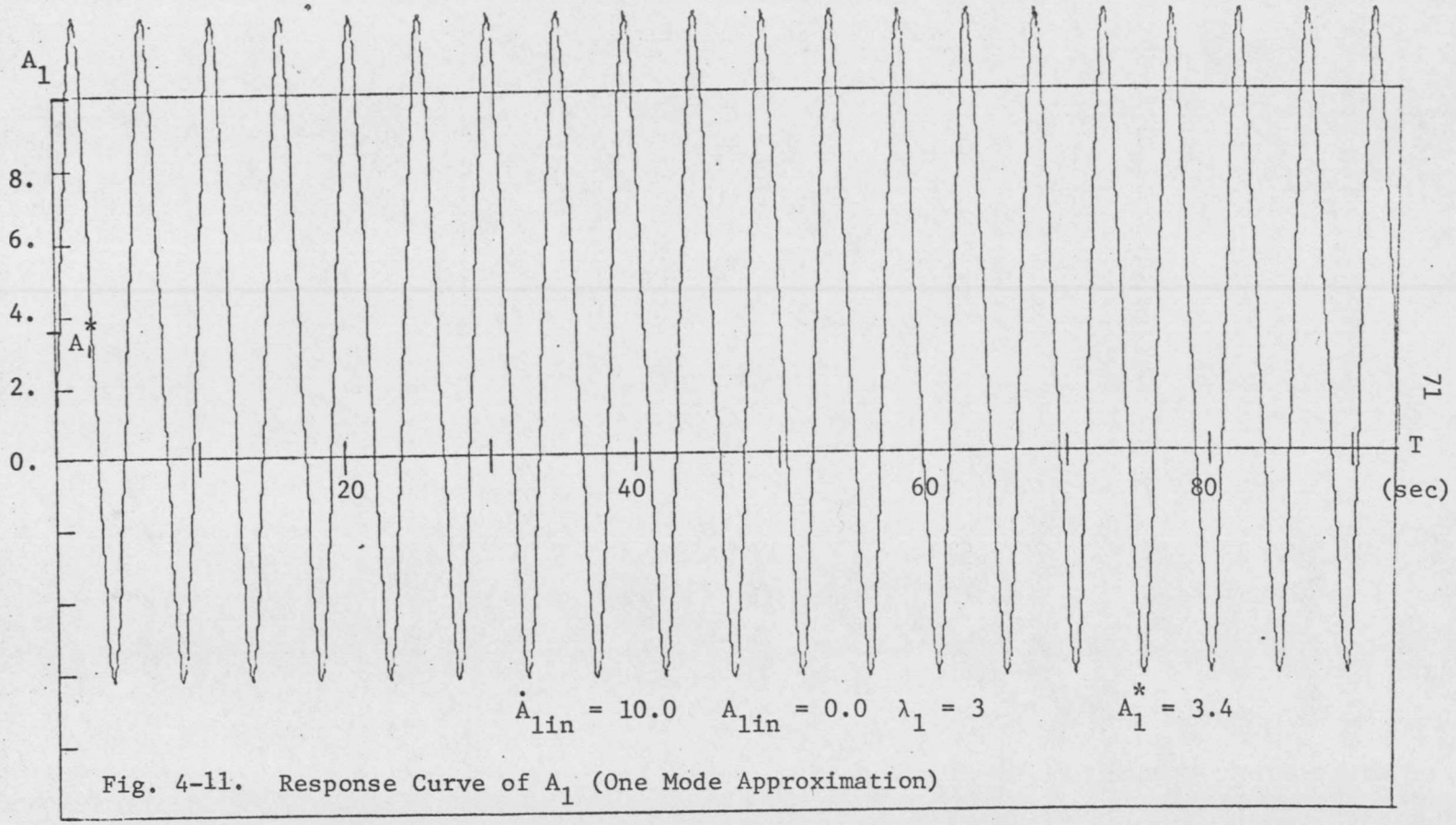


Fig. 4-11. Response Curve of A_1 (One Mode Approximation)

Thus one is aware that an arch may buckle either due to initial conditions (initial displacement or initial velocity or both) or due to the external load on the arch rib. Now the question arises as to why the arch buckles at the time when the maximum amplitude is equal to or a little greater than the arch geometric parameter λ_1 which is about equal to the arch rise in non-dimensionalized form. To answer this question let's go back to the six differential equations (Eqs. 4.11 through 4.16). But recall that among the first six modes, A_1 and A_2 are the most significant. So to understand the snapping through of the arch it may be enough just to consider the first two equations corresponding to the first two modes: A_1 and A_2. The two equations are

$$\bar{m}\ddot{A}_1 + A_1(1 + 2\lambda_1^2 - 3\lambda_1 A_1 + A_1^2 + 4A_2^2) - 4\lambda_1 A_2^2 = 2P_2 \sin\frac{\pi v T}{L} \quad \text{-----(4.23)}$$

$$\bar{m}\ddot{A}_2 + A_2(16 - 8\lambda_1 A_1 + 4A_1^2 + 16A_2^2) = 2P_2 \sin\frac{2\pi v T}{L} \quad \text{----------(4.24)}$$

When A_2 is not present, one has the "backbone" equation having the form

$$\bar{m}\ddot{A}_1 + A_1(1 + 2\lambda_1^2 - 3\lambda_1 A_1 + A_1^2) = 2P_2 \sin\frac{\pi v T}{L} \quad \text{----------(4.25)}$$

In this last equation if the third term in the bracket is dropped, one has the well known Duffing equation:

$$\ddot{A}_1 + \alpha A_1 + \beta A_1^3 = P_4 \sin\frac{\pi v T}{L} \quad \text{----------(4.26)}$$

in which $\alpha = \frac{1 + 2\lambda_1^2}{\bar{m}}$; $\beta = \frac{1}{\bar{m}}$; $P_4 = \frac{2P_2}{\bar{m}}$ ----------(4.27)

The jump phenomenon associated with the Duffing equation is well known. However, if the third term in the bracket in Eq. (4.25) is not dropped, the equation is called a non-linear equation with non-symmetric elastic force, which is generally more involved than the Duffing equation itself. But this last-mentioned equation would show a jump phenomenon also. In non-linear mechanics, standard classic techniques such as the iteration method, perturbation method, harmonic balancing method, linearization method, and so on are excellent in solving the Duffing equation, though the solution is approximate. However, these methods fail to predict the behavior of the system described by Eq. (4.25). This is because the non-linear function is non-symmetric. However, if one looks at this problem from another corner, this problem is readily solved.

Recall that the basic difference between the linear and non-linear dynamic systems lies in the fact that in linear systems the natural frequency is constant, while in non-linear systems it is not. Rewriting Eq. (4.25) as

$$\ddot{A}_1 + \omega_e^2 A_1 = \frac{2P_2}{\bar{m}} \sin \frac{\pi v T}{L} \qquad \text{----------(4.28)}$$

where $\omega_e^2 = \frac{1 + 2\lambda_1^2}{\bar{m}} - \frac{3\lambda_1}{\bar{m}} A_1 + \frac{1}{\bar{m}} A_1^2$ ----------(4.29)

Eq. (4.28) clearly shows that if $\omega_e^2 < 0$, A_1 would increase without bound. If A_1 becomes increasing unboundly, it implies that the system becomes unstable. In the case of the arch problem, this means the arch starts to snap through. Hence, what one now considers is when ω_e^2 becomes negative. By plotting Eq. (4.29), one has

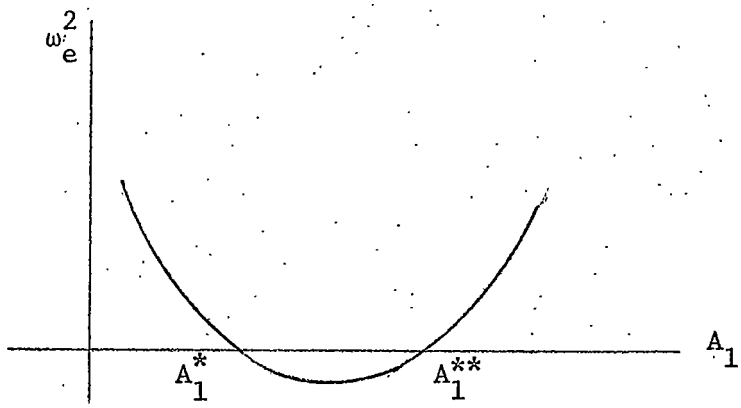


Fig. 4-12. Relation Between the Equivalent Frequency and A_1

From Fig. 4-12 it is clear that if the maximum amplitude of A_1 is equal to or greater than the critical amplitude A_1^*, the arch would jump. But A_1 cannot increase indefinitely. As soon as A_1 reaches A_1^{**}, the arch would oscillate periodically again. Thus, to know if the arch would or would not snap through, all one has to do is to check whether the critical amplitude is reached. To find the critical amplitude A_1^*, one must let $\omega_e^2 = 0$, or

$$\frac{1}{\bar{m}} A_1^2 - \frac{3\lambda_1}{\bar{m}} A_1 + \frac{1 + 2\lambda_1^2}{\bar{m}} = 0 \qquad \text{----------(4.30)}$$

From which

$$A_1^* = \frac{1}{2}[3\lambda_1 - \sqrt{\lambda_1^2 - 4}\ ] \qquad \text{----------(4.31a)}$$

$$A_1^{**} = \frac{1}{2}[3\lambda_1 + \sqrt{\lambda_1^2 - 4}\ ] \qquad \text{----------(4.31b)}$$

For $\lambda_1 = 3$, $A_1^* \doteq 3.4$. Fig. 4-8 shows the arch does not jump because $A_{1in} < A_1^*$, whereas the arch snaps through in Fig. 4-9 since $A_{1in} > A_1^*$.

When A_2 is involved, that is, Eqs. (4.23) and (4.24) are simultaneously considered, the above criterion is not valid unless some modifications are made. Let's rewrite Eq. (4.23) as

$$\ddot{A}_1 + A_1 \omega_{2e}^2 = \frac{2P_2}{\bar{m}} \sin \frac{\pi v T}{L} + \frac{4\lambda_1}{\bar{m}} A_2^2 \qquad \text{----------(4.32)}$$

$$\text{where } \omega_{2e}^2 = \frac{1 + 2\lambda_1^2}{\bar{m}} - \frac{3\lambda_1}{\bar{m}} A_1 + \frac{1}{\bar{m}} A_1^2 + \frac{4}{\bar{m}} A_2^2 \qquad \text{----------(4.33)}$$

Again setting $\omega_{2e}^2 = 0$, or

$$\frac{1 + 2\lambda_1^2}{\bar{m}} - \frac{3\lambda_1}{\bar{m}} A_1 + \frac{1}{\bar{m}} A_1^2 + \frac{4}{\bar{m}} A_2^2 = 0 \qquad \text{----------(4.34)}$$

$$\text{from which } A_1^* = \frac{1}{2}[3\lambda_1 - \sqrt{\lambda_1^2 - 4 - 16A_2^2}\ ] \qquad \text{----------(4.35)}$$

To assure A_1^* has a real value, one must have

$$A_2^* \leq \frac{1}{4}\sqrt{\lambda_1^2 - 4} \qquad (4.36)$$

If λ_1 is large,

$$A_2^* \leq \frac{\lambda_1}{4} \qquad (4.37)$$

Thus, the arch would jump if and only if Eq. (4.35) and inequality (4.36) or (4.37) are satisfied. Moreover, Eq. (4.35) indicates that A_1^* always lies in the range for the two-modes approximation:

$$\frac{3}{2}\lambda_1 \geq A_1^* \geq \frac{1}{2}(3\lambda_1 - \sqrt{\lambda_1^2 - 4}\ ) \qquad (4.38)$$

For large λ_1, $\lambda_1^2 - 4 \doteq \lambda_1^2$, then Eq. (4.38) becomes:

$$\frac{3}{2}\lambda_1 \geq A_1^* \geq \lambda_1 \qquad (4.39)$$

Eq. (4.38) was determined by considering that A_2^2 is always positive and no matter how A_2 varies the extreme possible real values for A_1^* are $\frac{3}{2}\lambda_1$ and $\frac{1}{2}(3\lambda_1 - \sqrt{\lambda_1 - 4}\ )$. In other words, the value under the square root in Eq. (4.35), that is, $(\lambda_1^2 - 4 - 16A_2^2)$ can at best be equal to zero. By examining Eq. (4.38) or Eq. (4.39), it is evident that the arch will definitely not snap through if A_{1max} is less than λ_1. The previous finding that the arch jumps when A_{1max} is equal to or a little greater than λ_1 may also be confirmed. Since it is apparent that the presence of A_2 causes A_1^* to vary approximately in between λ_1 and $1.5\lambda_1$, and

since A_2 is usually small as compared with λ_1, it follows that as A_{1max} is about equal to λ_1, the arch is on the brink of buckling.

In the above, only the jump condition of the first equation was studied although A_2 was also considered at the same time. Then one would ask: What is the jump condition of the second equation; that is, Eq. (4.24)? What is its effect upon the first equation? To answer these questions, one may go back to Eq. (4.24) and equate the equivalent frequency to zero; that is:

$$16 - 8\lambda_1 A_1 + 4A_1^2 + 16A_2^2 = 0 \quad \text{----------(4.40)}$$

from which $$4A_2^2 = -4 + 2\lambda_1 A_1 - A_1^2 \quad \text{----------(4.41)}$$

Substituting Eq. (4.41) into Eq. (4.23) leads to

$$\bar{m}\ddot{A}_1 - 3A_1 = 2P_2 \sin\frac{\pi v T}{L} - 4\lambda_1 \quad \text{----------(4.42)}$$

Apparently, Eq. (4.42) has a solution in which A_1 is unbound. This implies that long before A_2 jumps, A_1 has reached its critical value. In other words, in consideration of both Eq. (4.23) and Eq. (4.24) simultaneously, one needs to focus one's attention only on the jump condition of the first equation; that is, Eq. (4.23).

In the discussions above, the critical displacement and the jump conditions were studied. Then it seems necessary to study how A_2 affects A_{1max} during vibration, and this will be developed in the following:

It is found that A_2 is generally a small fraction of A_1 at the time when the arch starts snapping through. Accordingly, the critical amplitude expressed by Eq. (4.31a) does not differ much from that expressed by Eq. (4.35). However, inclusion of A_2 into consideration in the analysis, the amplitude of A_1 is found to increase significantly. This implies that the critical loads in this case are less than when only one mode is considered. To clarify this, let's study Fig. 4-13 through Fig. 4-17. In these figures the data are: $\lambda_1 = 3$, $v = 50$, $L = 50$, D = damping coefficient = 0. From Figs. 4-13 and 4-14, it is seen that corresponding to $P_2 = 28$, A_{1max} for the case of A_1 only is less than that for the case of A_1 plus A_2. As P_2 increases to 30 as shown in Fig. 4-15 and Fig. 4-16, A_1 jumps for the case of A_1 plus A_2 but not for the case of A_1 only. P_2 must be increased to 32 when A_1 starts to jump as shown in Fig. 4-17. Thus, it is seen that with two equations considered at the same time, the maximum amplitude of A_1 tends to increase. As a matter of fact, this fact may be proved theoretically too, as will be demonstrated.

Rearrange Eq. (4.23) in the form:

$$\bar{m}\,\ddot{A}_1 + (1 + 2\lambda_1^2)A_1 - 3\lambda_1 A_1^2 + A_1^3 + 4A_2^2(A_1 - \lambda_1) = 2P_2 \sin\frac{\pi v T}{L} \qquad \text{-----(4.43)}$$

As noted before, prior to the time when the arch starts snapping through, A_1 is generally less than λ_1. Let $\lambda_1 - A_1 = \lambda_\alpha$ which may be considered as positive throughout the following developments. It does

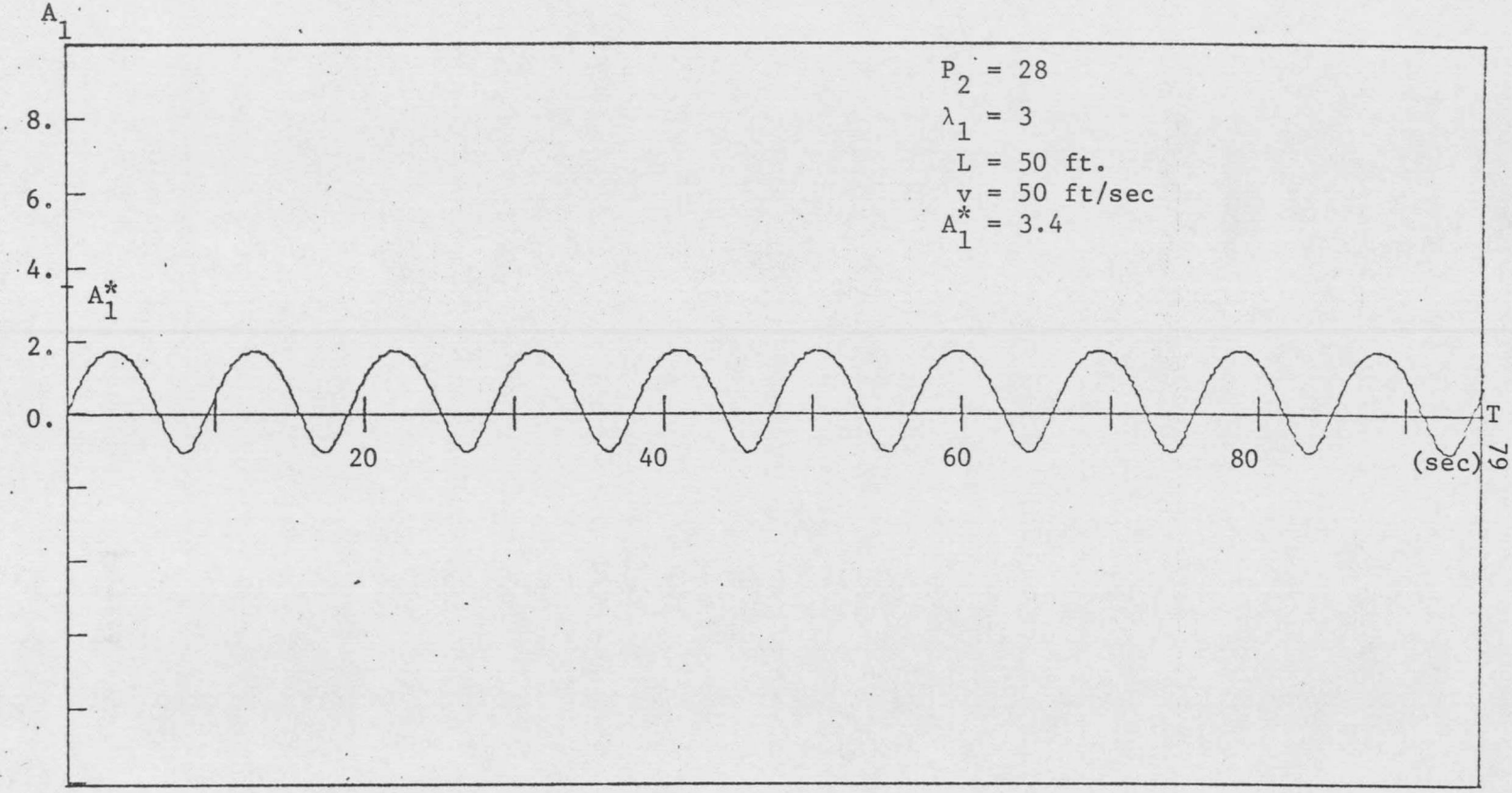


Fig. 4-13. Response History of A_1 (One Mode Approximation: A_1 Only)

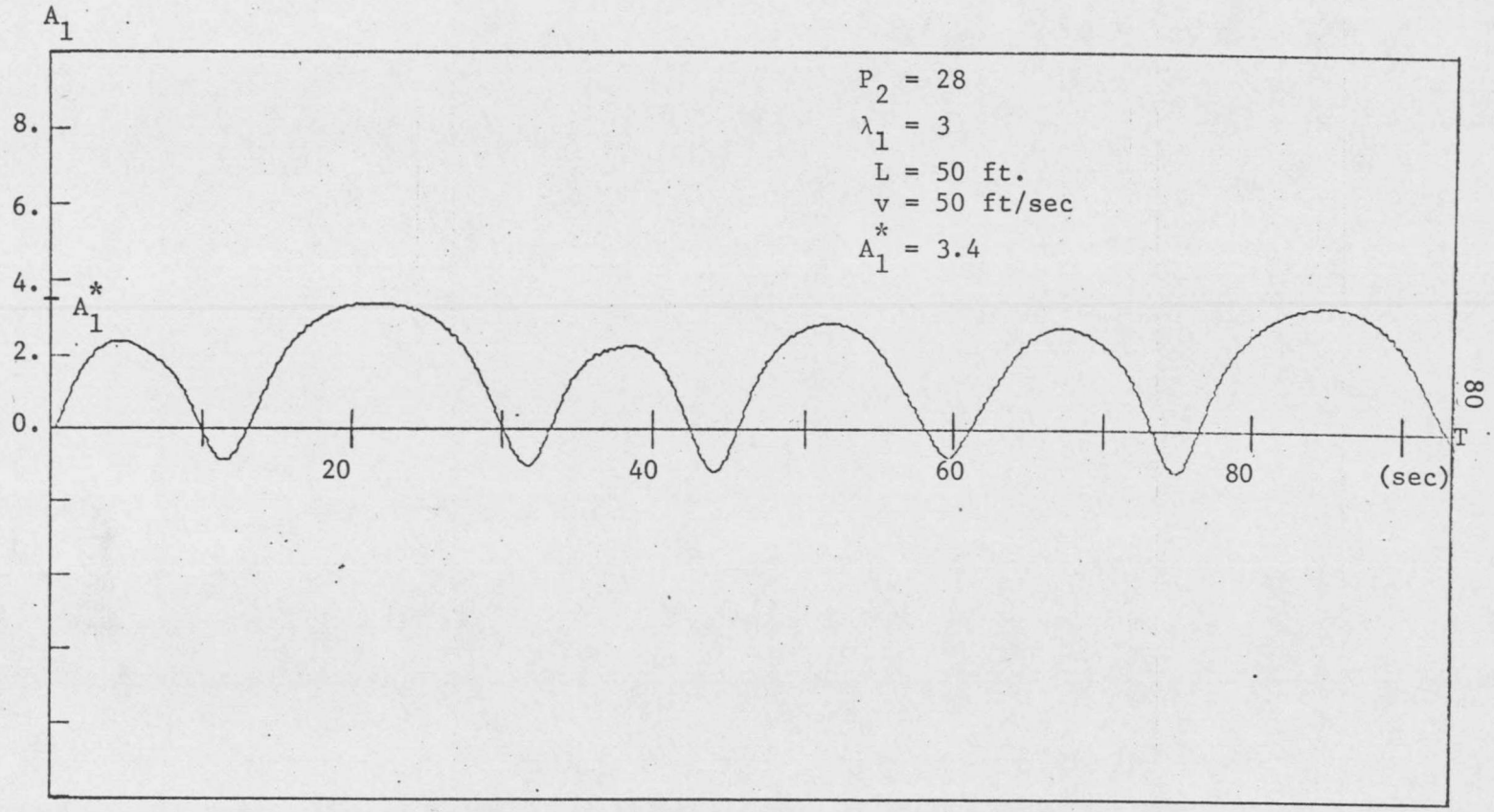


Fig. 4-14. Response History of A_1 (Two-Modes Approximation: A_1 plus A_2)

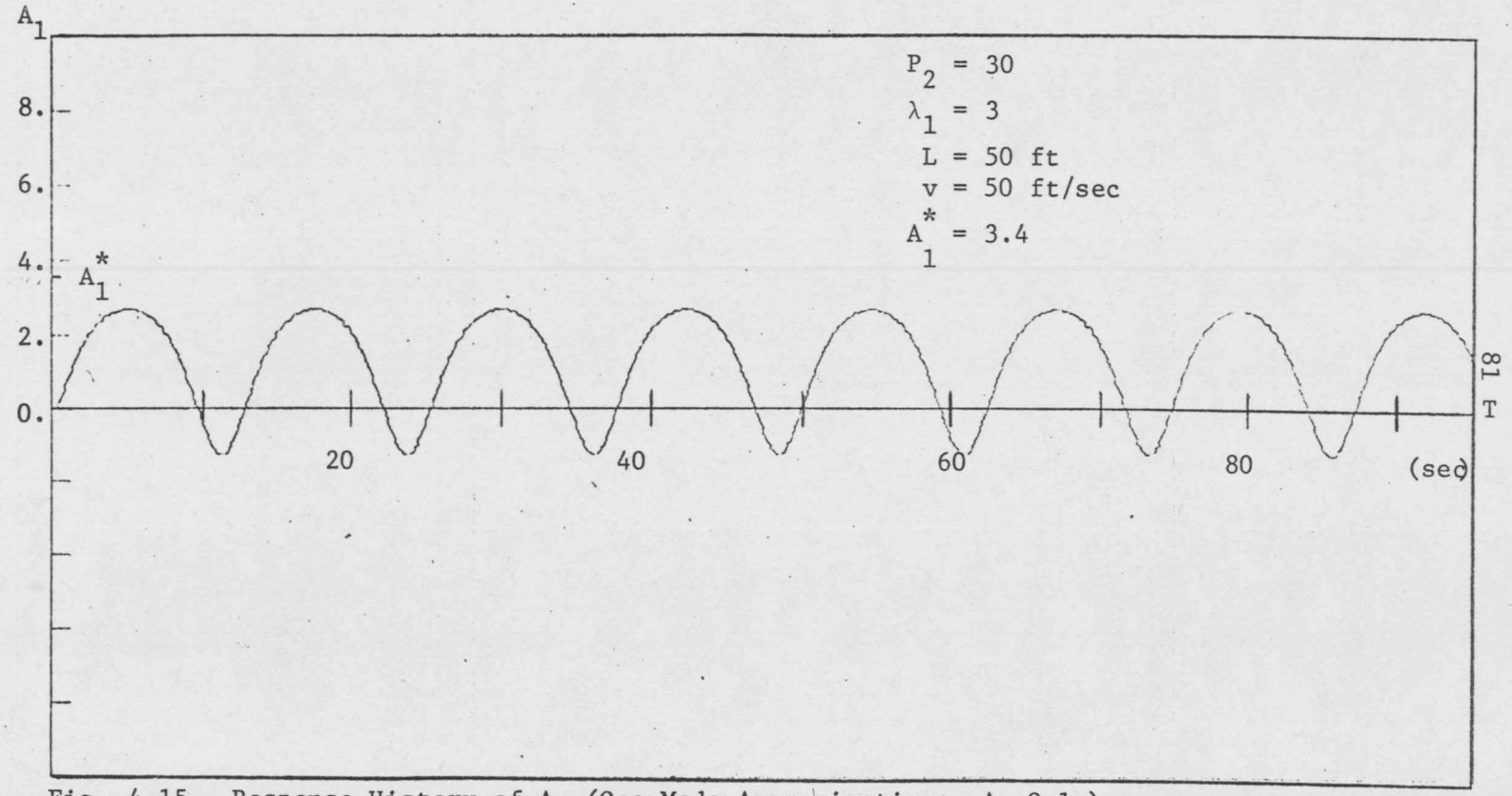


Fig. 4-15. Response History of A_1 (One Mode Approximation: A_1 Only)

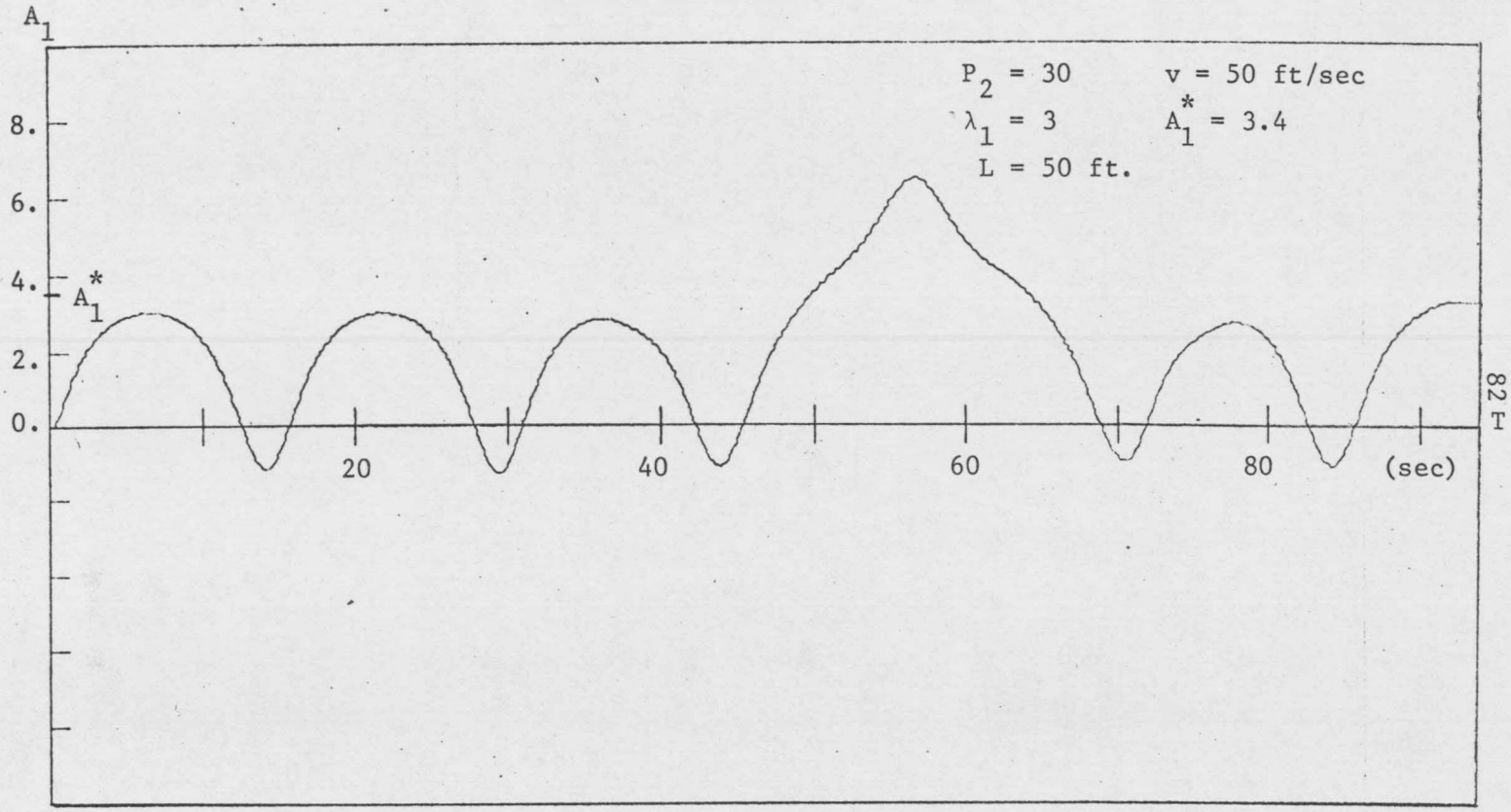


Fig. 4-16. Response History of A_1 (Two-Modes Approximation: A_1 plus A_2)

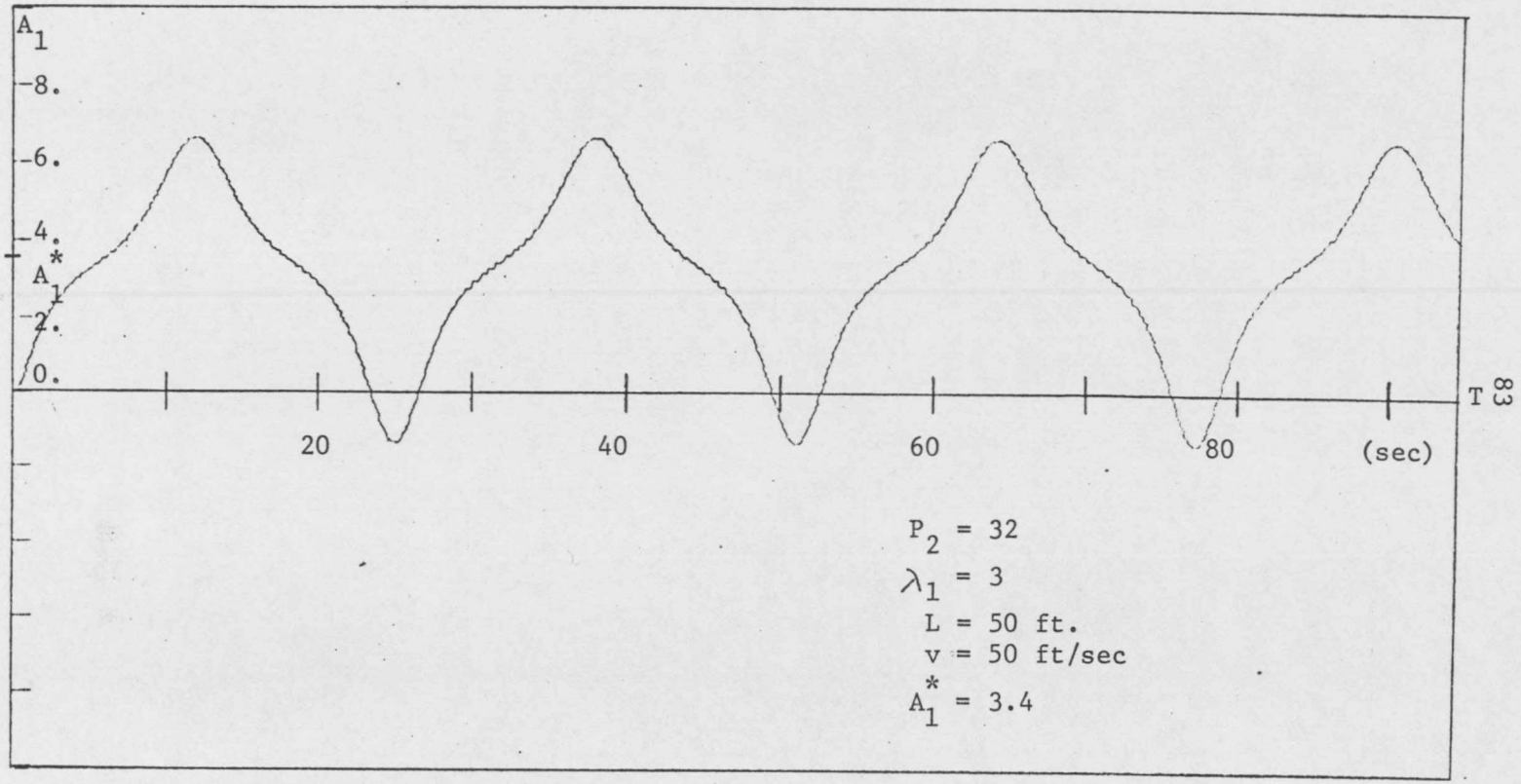


Fig. 4-17. Response History of A_1 (One Mode Approximation: A_1 Only)

not lose generality, if one just considers the homogeneous part of Eq. (4.43); that is, P_2 is taken as zero. Eq. (4.43) then becomes

$$\bar{m}\ddot{A}_1 + (1 + 2\lambda_1^2)A_1 - 3\lambda_1 A_1^2 + A_1^3 - 4A_2^2\lambda_\alpha = 0 \quad \text{----------(4.44)}$$

If one lets the initial velocity be $\bar{C}$, and integrates Eq. (4.44), one has

$$\bar{m}\frac{\dot{A}_1^2}{2} + (1 + 2\lambda_1^2)\frac{A_1^2}{2} - \lambda_1 A_1^3 + \frac{1}{4}A_1^4 - 4\int A_2^2\lambda_\alpha dA_1 = \frac{\bar{m}\bar{C}^2}{2} \quad \text{----------(4.45)}$$

It is known that as A_1 reaches its maximum, $\dot{A}_1 = 0$. It follows

$$\frac{1 + 2\lambda_1^2}{2}A_{1max}^2 - \lambda_1 A_{1max}^3 + \frac{1}{4}A_{1max}^4 = 4\int A_2^2\lambda_\alpha dA_1 + \frac{\bar{m}\bar{C}^2}{2} \quad \text{----------(4.46)}$$

The right-hand side of the last equation, denoted by K_α, is seen to be positive in general. And it is evident that it is this term that shows the net effect of A_2 upon A_{1max}. In other words, this term represents the amount with which the second equation affects the first equation.

Rearrange Eq. (4.46) to take the form

$$A_{1max}^2[2 + 4\lambda_1^2 - 4\lambda_1 A_{1max} + A_{1max}^2] = 2\bar{m}\bar{C}^2 + 4K_\alpha \quad \text{----------(4.47)}$$

It does not lose generality if the first term in the bracket of Eq. (4.47) is dropped, since the present purpose is to show how A_2 affects A_{1max}. In so doing, Eq. (4.47) reduces to

$$A_{1max}(A_{1max} - 2\lambda_1) = \pm \sqrt{2\bar{m}\bar{C}^2 + 4K_\alpha} \qquad \text{----------(4.48)}$$

or

$$A_{1max} = \lambda_1 \pm \sqrt{\lambda_1^2 \mp \sqrt{2\bar{m}\bar{C}^2 + 4K_\alpha}} \qquad \text{----------(4.49)}$$

To determine the sign in Eq. (4.49), one notes that for consistency, the sign before the outer bracket must be negative while that before the inner bracket must also be negative. To clarify this last statement, one must note these facts: (a) If $\bar{C} = 0$ and $A_2 = 0$, A_{1max} must be zero; (b) A_{1max} cannot be all negative for any value of $\bar{C}$.

Then Eq. (4.49) becomes

$$A_{1max} = \lambda_1 - \sqrt{\lambda_1^2 - \sqrt{2\bar{m}\bar{C}^2 + 4K_\alpha}} \qquad \text{----------(4.50)}$$

Eq. (4.50) clearly shows that the effect of A_2 represented by K_α upon A_{1max} is to increase it. Since A_{1max} is larger than when A_2 is excluded, the critical load is evidently less.

Thus, theoretically and graphically, we show that the presence of A_2 is to reduce the critical load. In a similar manner, it can be shown that with A_3, A_4 or higher modes included, the critical load will become less. However, as stated before, since the effect of these higher modes is negligible, in practical considerations, two-modes approximation can be justified.

In the final remark of this section, we conclude, based upon the previous findings, that:

1) A pin-pin shallow circular arch snaps through only, and if only, a critical amplitude is reached. The source of bringing the maximum amplitude of A_1 to equal to or greater than A_1^* may be:

   a) due to external load (step pressure, point load or a combination of both);

   b) due to initial displacement;

   c) due to initial velocity; and

   d) due to a combination of initial displacement and velocity.

2) In practical considerations the determination of the critical loads may be justified by using a two-modes approximation. And for the two modes, the effect of A_2 upon A_1 is merely to increase the maximum amplitude of A_1, and thus to lower the critical load.

CHAPTER 5

THE DEFLECTION AND THE STRESSES OF PINNED-END SHALLOW CIRCULAR ARCHES

5.1 Introduction

The deflection of the arch axis and the stress distributions on the arch rib are the main concerns of the structural engineers in arch design. The deformed shape of the arch axis and the stress condition on the rib are expected to be quite different for an arch subject to a static point load and subject to a moving point load. In the latter case the arch rib is subjected to distributed inertia forces in addition to the point load. The inertia forces have a significant effect on the deformed arch shape and the stress condition on the arch rib. Other factors that effect the deformation and stress conditions include the point of application of the point load, the stiffness of the arch section, the rise of the arch, etc.. In the following sections, some detailed studies about the deflection and the stresses of pin-pin shallow circular arches are presented. These studies lead to interesting results and are useful in practice.

In discussing an arch problem, the two known theories, that is, the elastic theory and the deflection theory, often come to mind. The elastic theory, also called the first order theory, is one in which the deflection of the arch axis is not considered in the stress analysis of the arch rib. The deflection theory in which the deformed shape of the

arch axis is considered has been accepted [32] as one with which the exact stress analysis of an arch can be obtained. To get an insight into the differences of the results given by the two theories respectively, a brief study is carried out in the last part of this chapter.

5.2 Static Deflection and Dynamic Deflection

The static deflection of the pinned-end shallow circular arch may be obtained by using Eqs. (3.4) and (3.7), while the dynamic deflected shape of the arch may be determined by solving Eqs. (4.11) through (4.16) simultaneously. To be convenient in doing the analysis, the external point load is taken as unity, and the following data are used:

$E = 475200$ psf $I = 1/96$ ft^4

$A = 1/2$ ft^2 $b = 1$ ft

$L = 50$ ft

In obtaining both the static deflection and the dynamic deflection, it is necessary to know the relationship among the geometric parameter λ, the span length L, the rise H, the radius of gyration R^*, the subtended angle β and the radius $\bar{R}$ of the undeformed arch. This relationship is derived in Appendix B and tabulated in TABLE 5-1 (Appendix A). To make the comparison between the static deflection and the dynamic deflection, the relationship between the two geometric parameters λ (associated with the static deflection) and λ_n (associated with the dynamic deflection) are related in the expression

$$\lambda \doteq \frac{8}{\sqrt{3}} (\lambda_1 + \lambda_3 + \lambda_5 + \lambda_7) \qquad \text{----------(5.1)}$$

and

$$\lambda_3 = \frac{1}{27} \lambda_1$$
$$\lambda_5 = \frac{1}{125} \lambda_1 \qquad \text{----------(5.2)}$$
$$\lambda_7 = \frac{1}{343} \lambda_1$$

It is noted that Eq. (5.1) is obtained by considering Eqs. (3.8), (4.8) and (4.10) together.

By following what was mentioned in the above, the numerical results of the arch deflection corresponding to various types of loading (the static load and the moving load with v = 10, 20, 30, 40 and 50 ft/sec) and various values of the geometric parameter λ are determined and tabulated as in TABLE 5-2 (Appendix A). Some representative plots of the results are shown in Figs. 5-1 through 5-3. Fig. 5-1 shows the deformed shapes of an arch with the geometric parameter $\lambda = 10$. They correspond to ten different points of application of the point load which is acting statically as well as dynamically (v = 10, 20, 30, 40 and 50 ft/sec). In this figure, one sees that the maximum static deflection is greater than the corresponding maximum dynamic deflection for some points of application of the load but smaller for other load positions. However, if one defines the absolute maximum deflection as one which is the largest of the maximum deflections corresponding to each point of application of the point load, it is seen that corresponding to a certain range of speed v the absolute maximum deflection in the static case is less than that in the dynamic case, as may be seen in Fig. 5-4c.

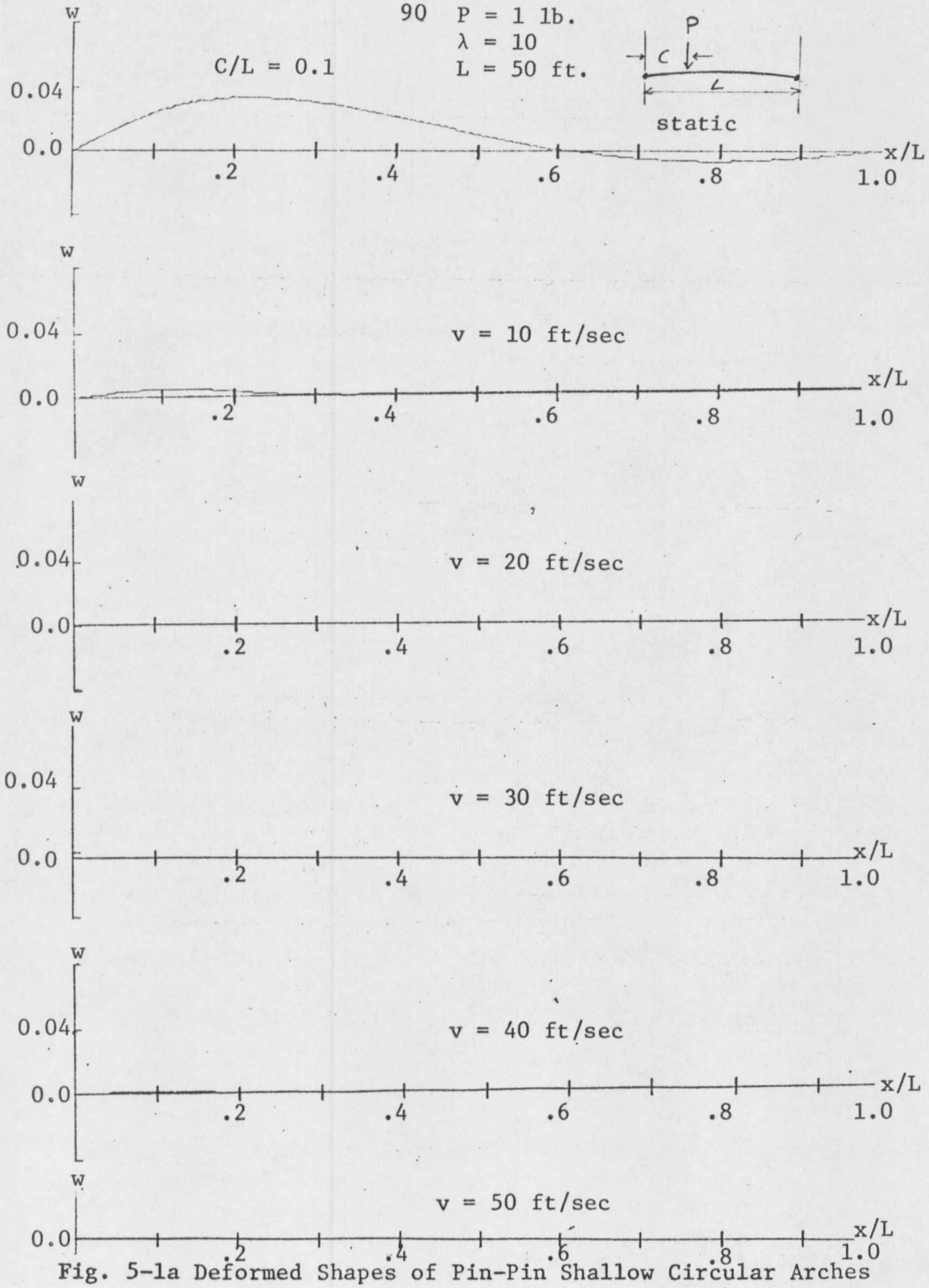


Fig. 5-1a Deformed Shapes of Pin-Pin Shallow Circular Arches

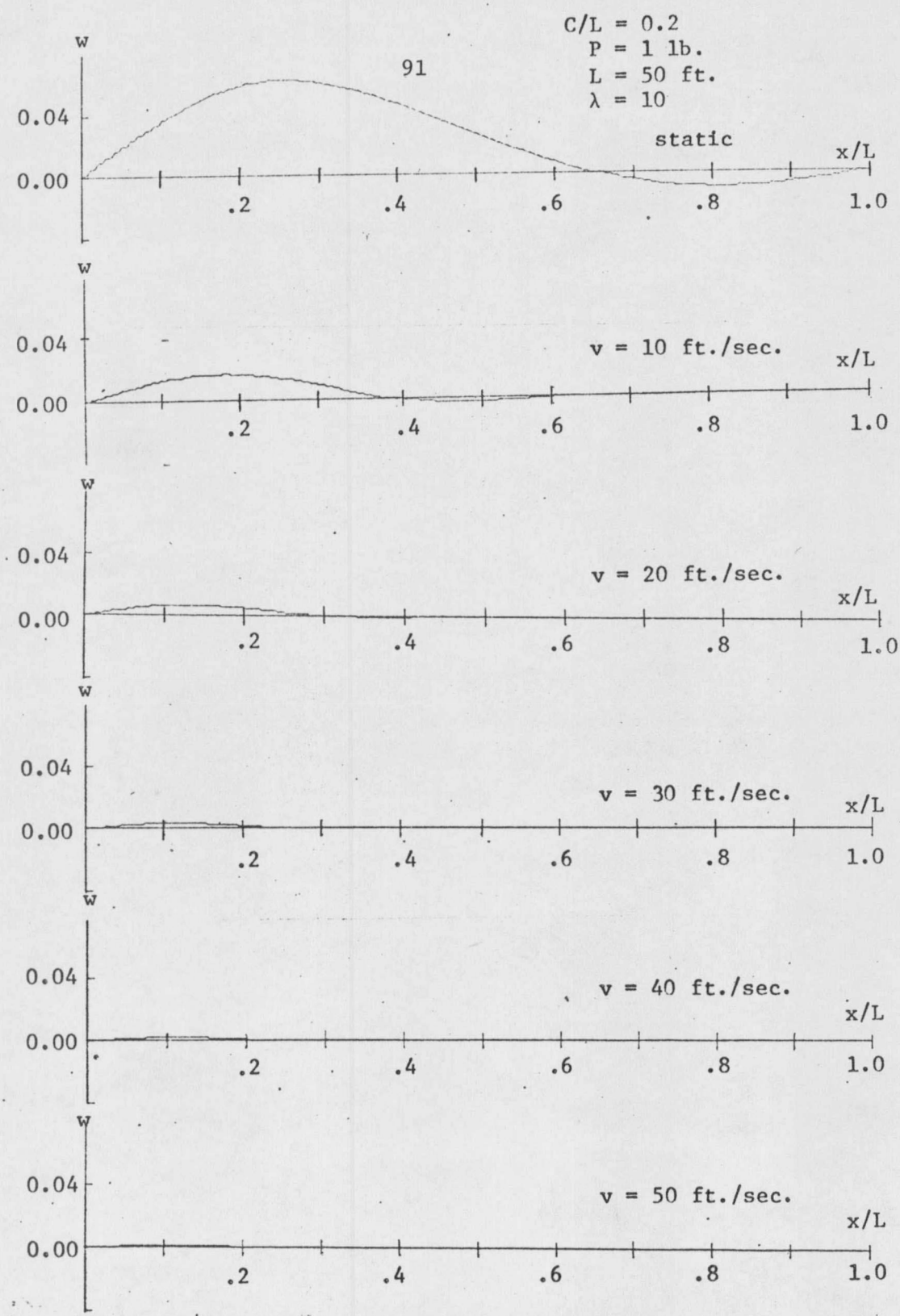


Fig. 5-1b Deformed Shapes of Pin-Pin Shallow Circular Arches

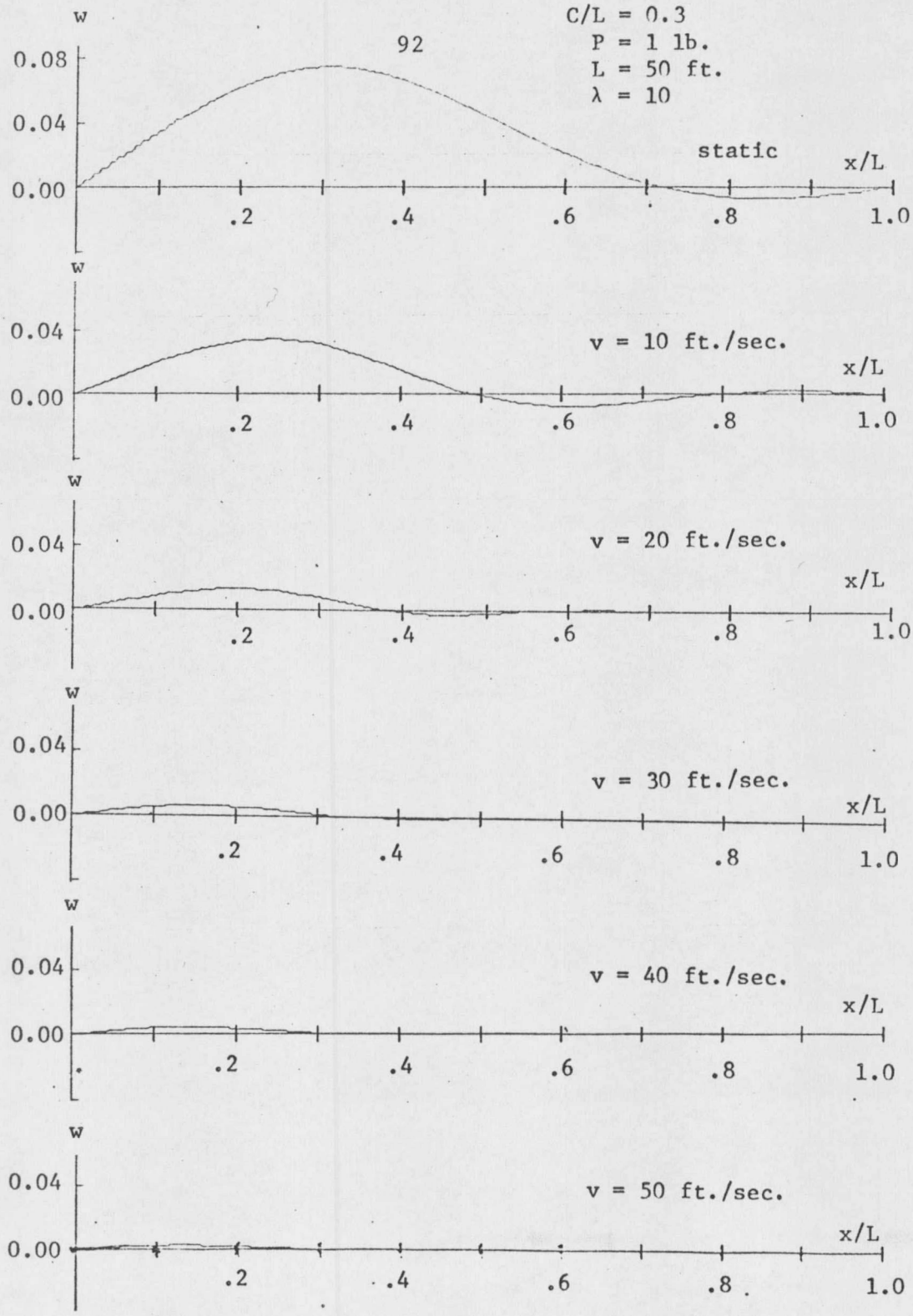


Fig. 5-1c Deformed Shapes of Pin-Pin Shallow Circular Arches

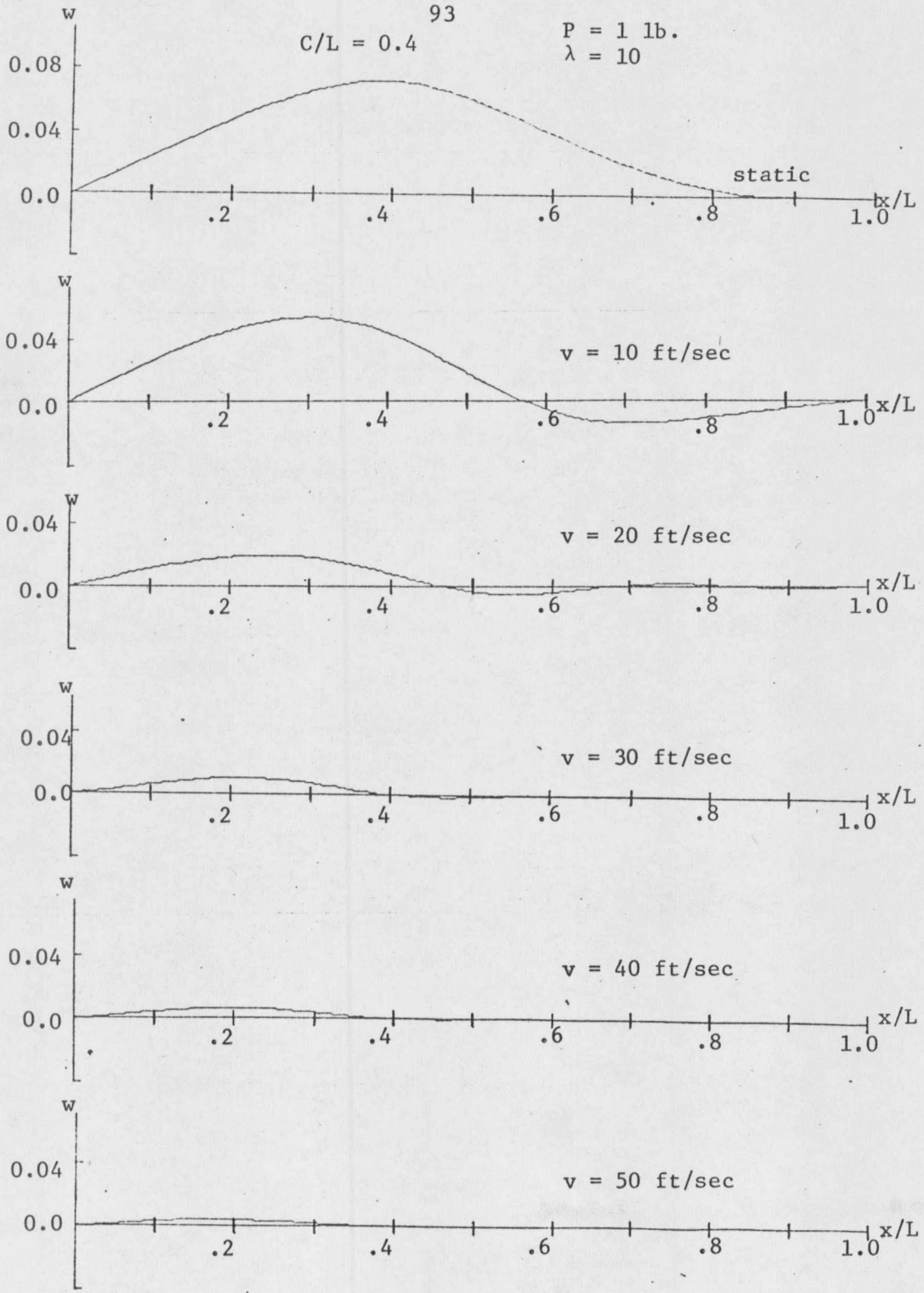


Fig. 5-1d Deformed Shapes of Pin-Pin Shallow Circular Arches

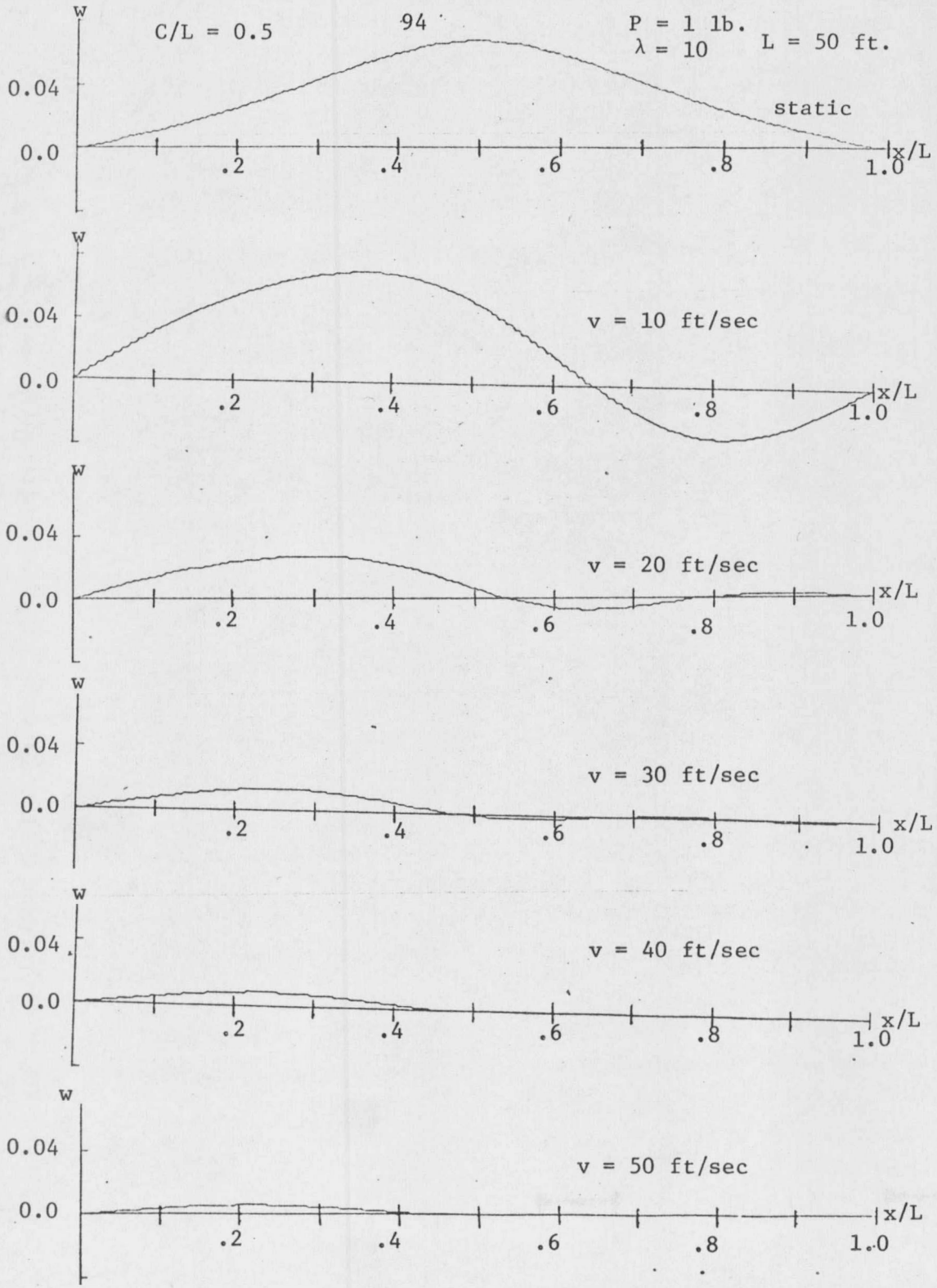


Fig. 5-1e Deformed Shapes of Pin-Pin Shallow Circular Arches

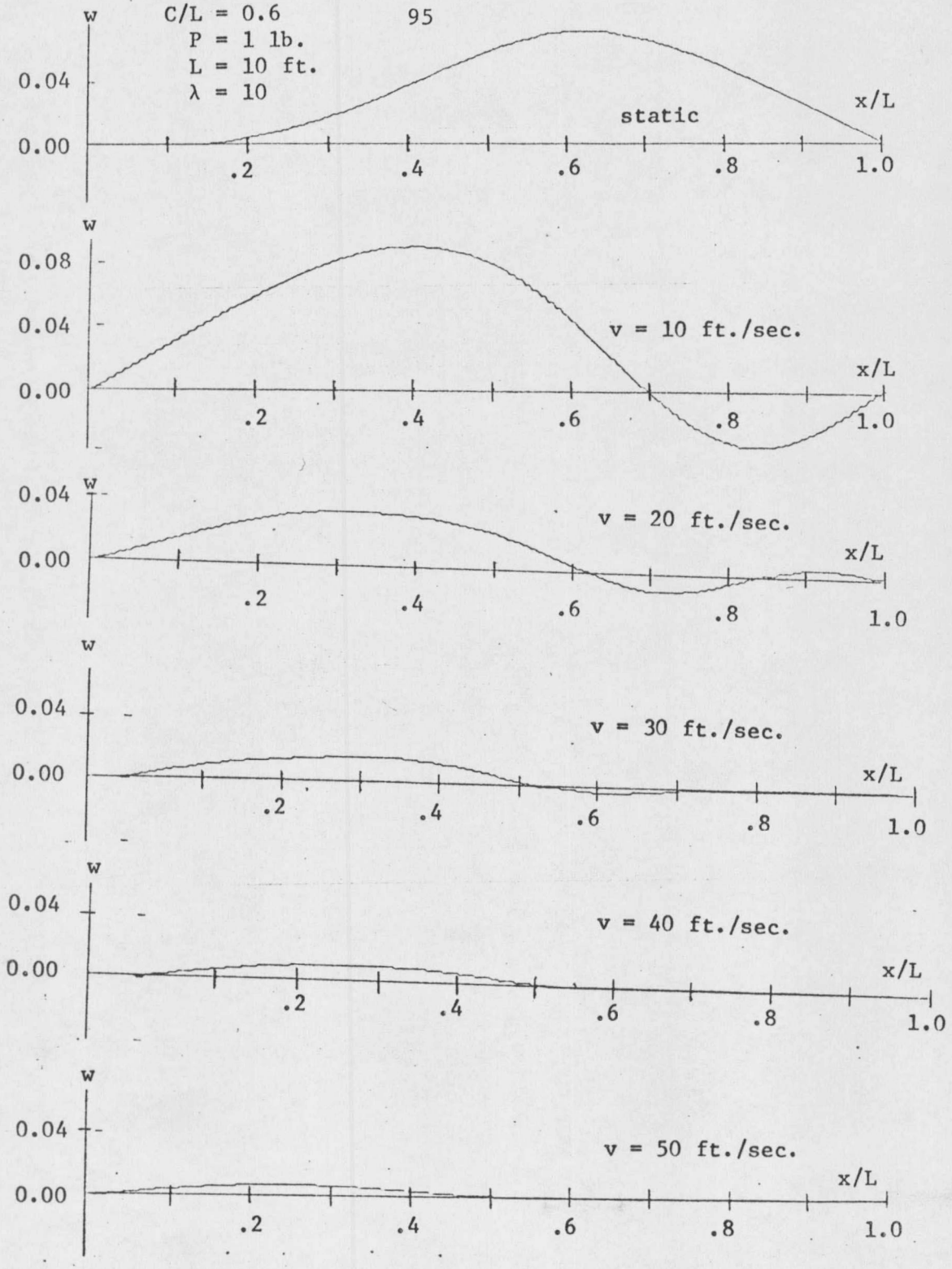


Fig. 5-1f. Deformed Shapes of Pin-Pin Shallow Circular Arches

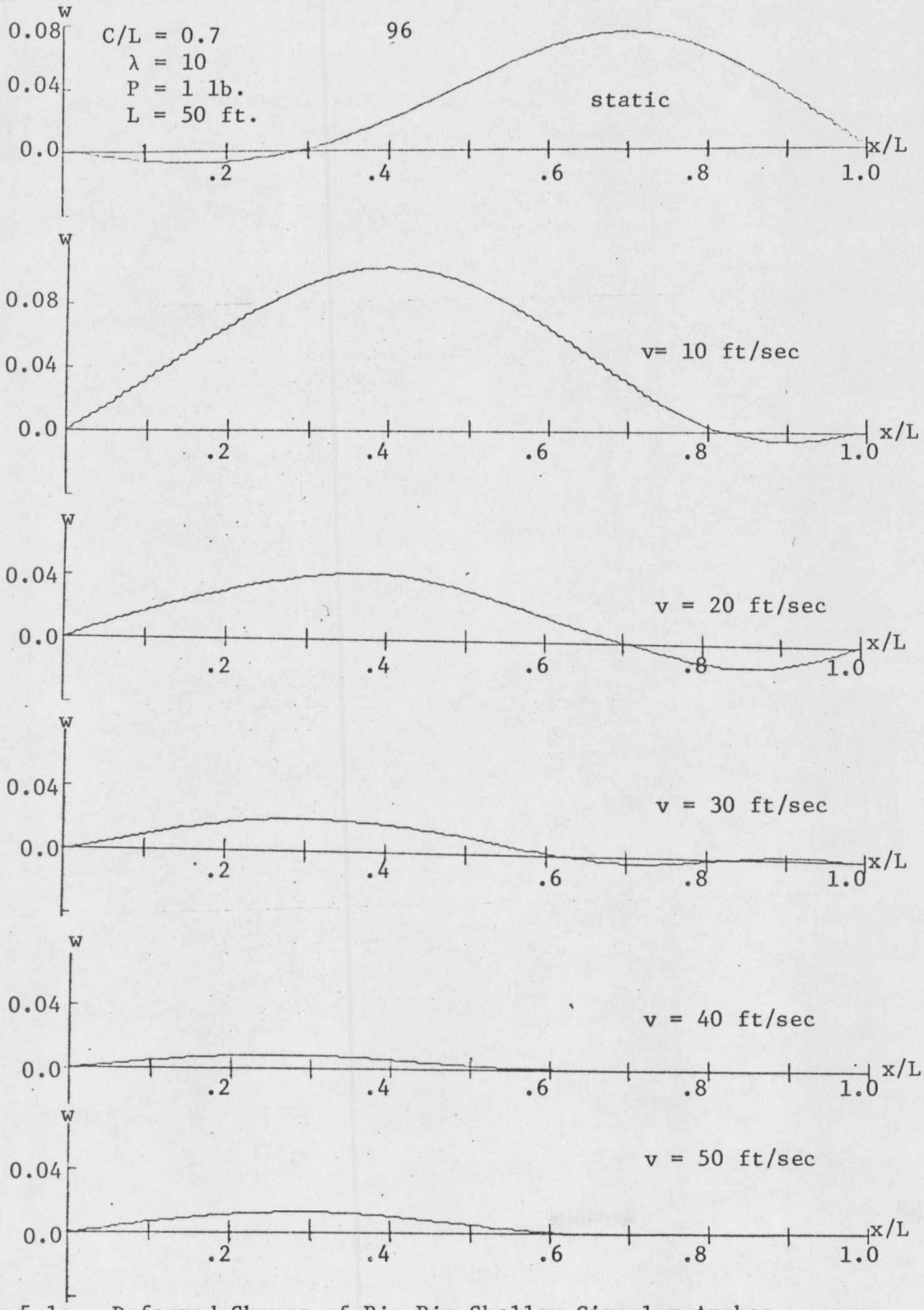


Fig. 5-1g. Deformed Shapes of Pin-Pin Shallow Circular Arches

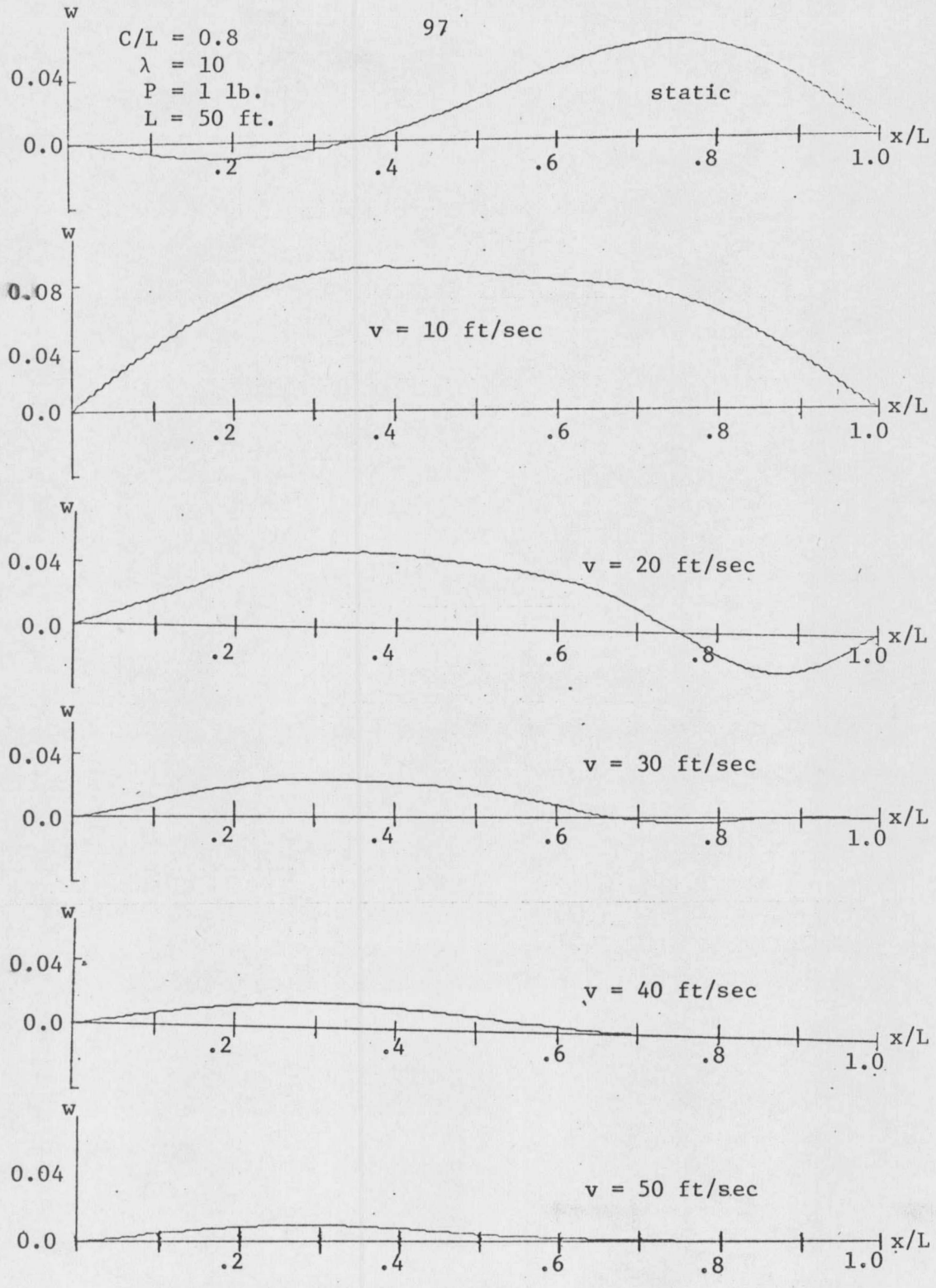


Fig. 5-1h. Deformed Shapes of Pin-Pin Shallow Circular Arches

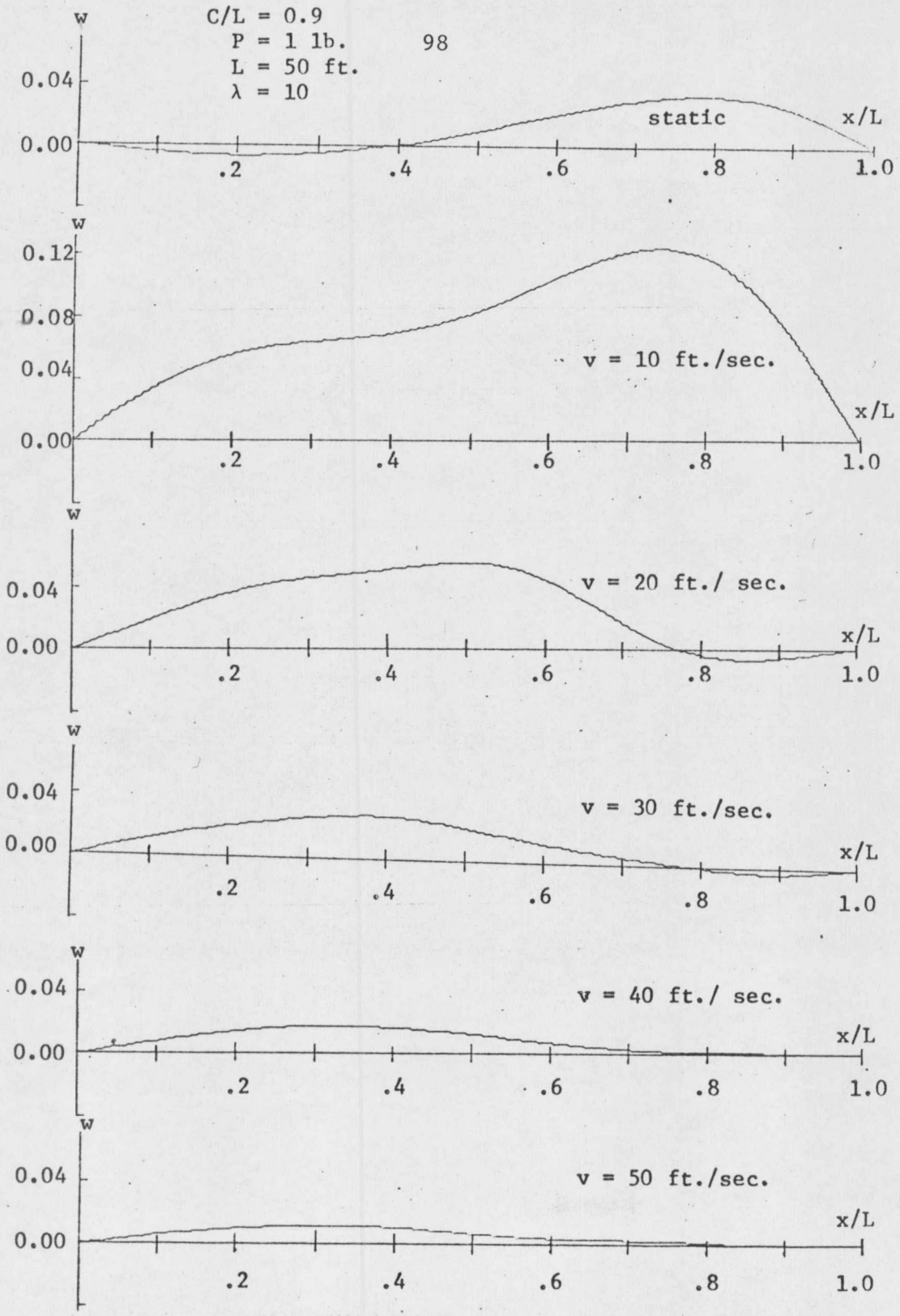


Fig. 5-1i. Deformed Shapes of Pin-Pin Shallow Circular Arches

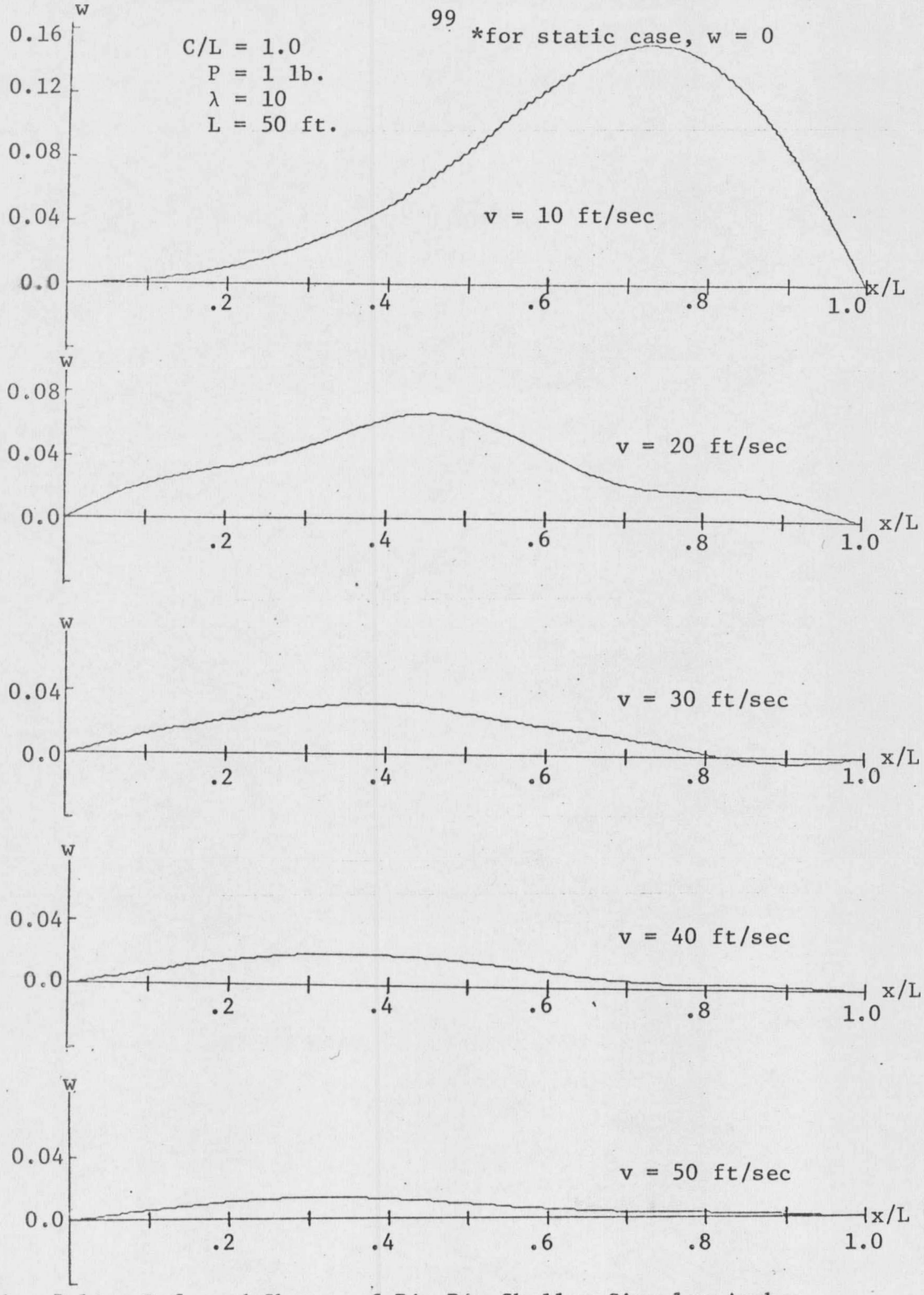


Fig. 5-1j. Deformed Shapes of Pin-Pin Shallow Circular Arches

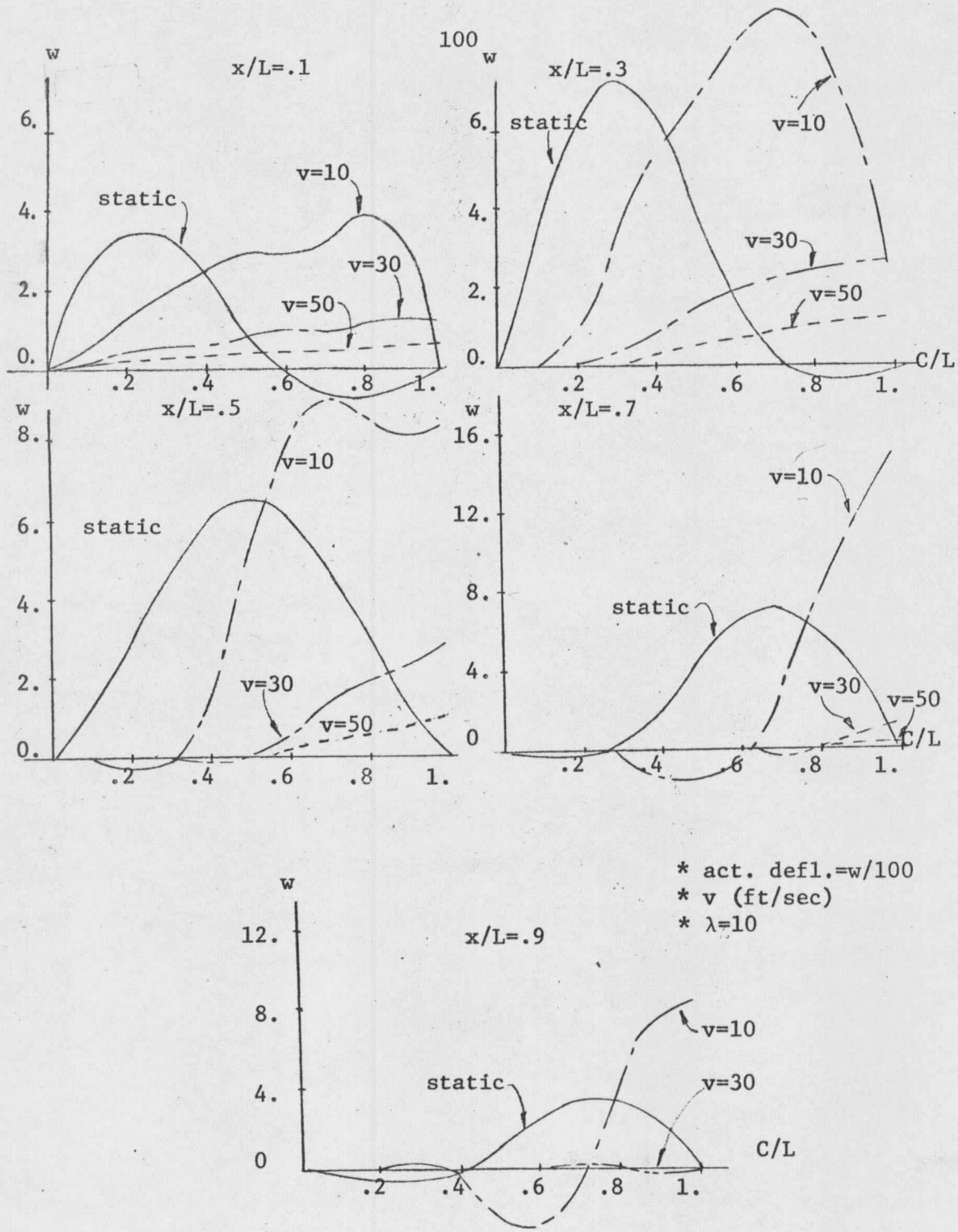


Fig. 5-2 Influence Lines for Deflection
(at x/L=.1,.3,.5,.7,.9)

In Fig. 5-2 and Fig. 5-3 the influence lines of deflection corresponding to v = 0 (static case), v = 10, 30 and 50 ft/sec for λ = 10 and λ = 30 respectively are shown. They are the influence lines at x = 0.1L, 0.3L, 0.5L, 0.7L and 0.9L respectively. One observes that the absolute maximum deflection in the dynamic case which, for example, occurs at x/L = 0.7 in Fig. 5-2, is about two times as great as the absolute maximum deflection in the static case which occurs at x/L = 0.3.

From Figs. 5-1, 5-2, or 5-3, it seems that corresponding to each point of application of the point load, the maximum deflection in the dynamic case becomes smaller as v increases. But this is not necessarily true for the whole range of speed v, as may be seen in Fig. 5-4a and Fig. 5-4b. The curves of these two figures plotted in the non-dimensionalized form indicate that there is a peak value for the abs. maximum displacement corresponding to a certain value of v/L. (This particular value is 0.12.) To the left of this peak value, the maximum displacement decreases as v becomes smaller.

Evidently the peak value shown in Figs. 5-4a and 5-4b is of practical interest. The corresponding value of v/L (= 0.12) indicates that if the span length is 1,000 ft, then corresponding to the speed v (= 120 ft/sec $\doteqdot$ 82 miles/hr.) the arch would reach its abs. maximum deflection. Also, the figures show that corresponding to λ = 10 and λ = 50, respectively, the peak value does not change its location. In other words, the critical ratio 0.12 of v/L is seen to be independent of λ, the geometric parameter of the arch.

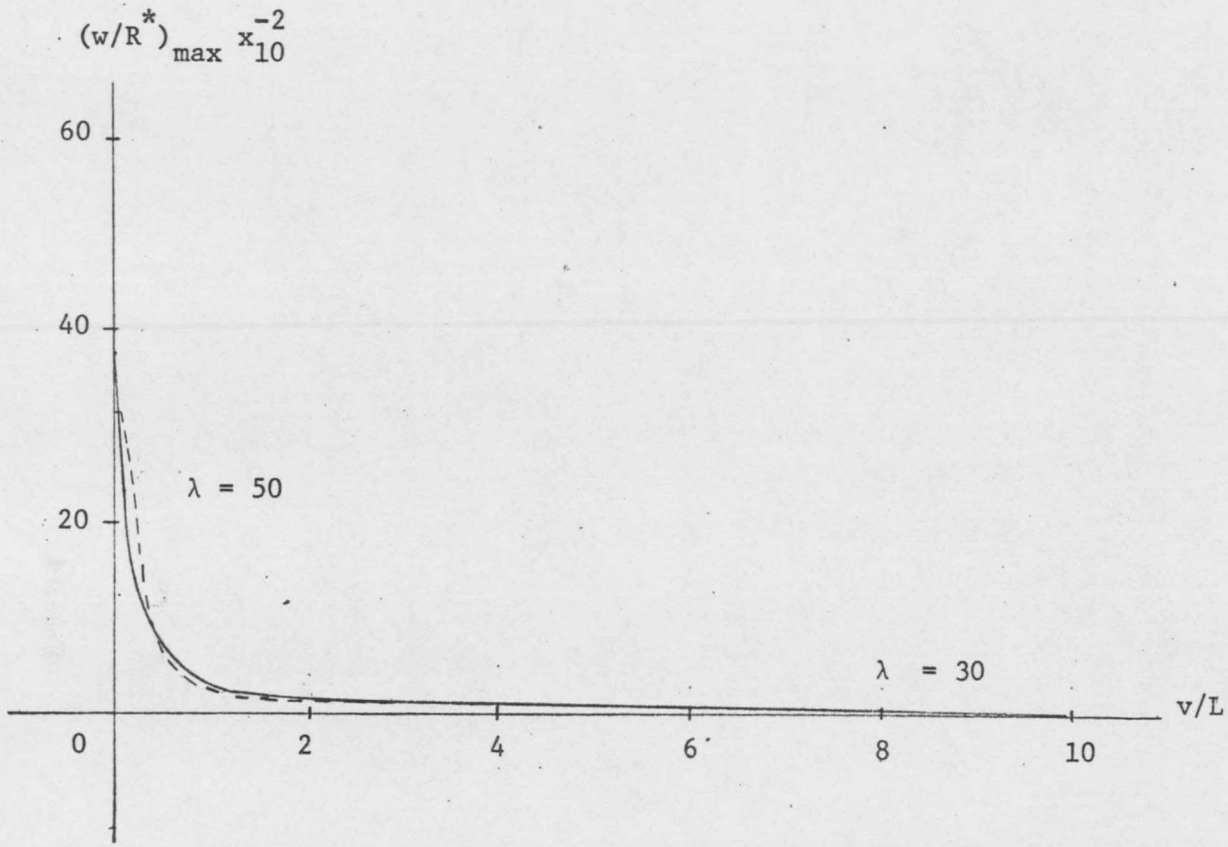


Fig. 5-4a. Effect of Speed-Span Ratio Upon the Abs. Max. Displacement

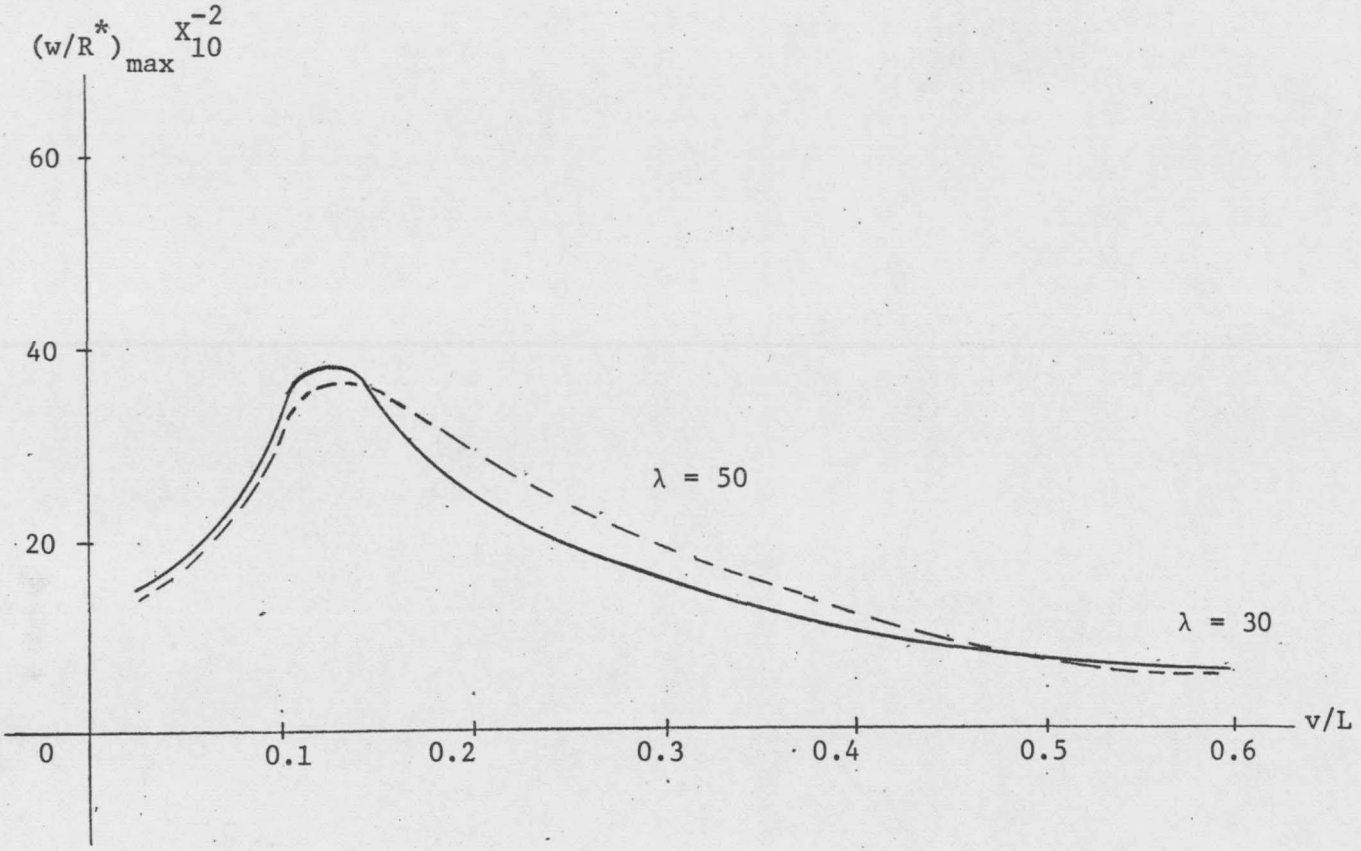


Fig. 5-4b. Enlargement of a Part of Fig. 5-4a

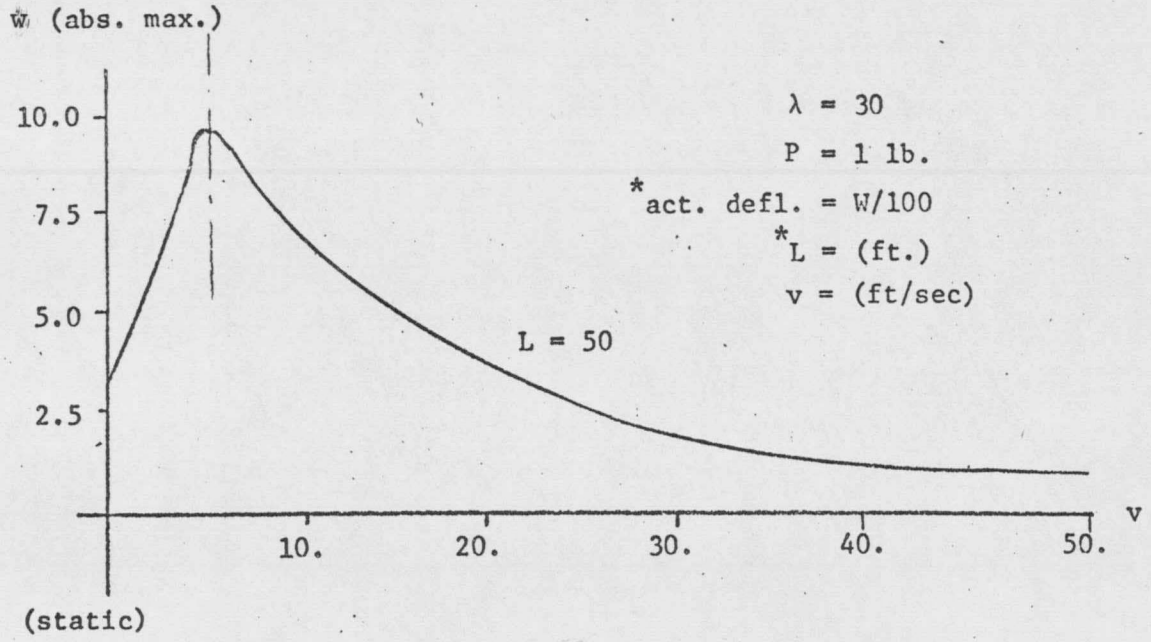


Fig. 5-4c. Effect of Speed Upon the Abs. Maximum Displacement

To get an insight into how the arch rise (represented by λ) affects the deflection, Fig. 5-5 is drawn, in which the absolute maximum deflections corresponding to various values of the geometric parameter λ for a static case and two dynamic cases (v = 10, 50 ft/sec) are shown. One observes that approximately for $\lambda > 30$ the absolute maximum deflection does not vary significantly. However, for $\lambda < 30$ the absolute maximum deflection increases significantly as λ becomes smaller, except for high values of v. This is as expected, because for relatively small λ (in this case $\lambda < 30$), the arch under consideration is close to an ordinary simple beam, which usually has greater deflection than arches.

The stiffness of the arch section is expected to effect the deflection of the arch rib. To study the relationship between the stiffness and the deflection of the arch, Fig. 5-6 showing the effect of radius of gyration (with respect to the axis perpendicular to the arch plane) on the deflection is plotted. In this figure, the deflection shapes due to a point load of unity acting at C = 0.3L and C = 0.5L, respectively, are shown. Three different values of radius of gyration R^* are taken. The figure clearly shows that the maximum deflection would decrease if the radius of gyration increases. It is seen that the stiffness effect is significant, but this effect is apparently not linear. This is different from a simple beam case in which, in general, the stiffness effect is linear.

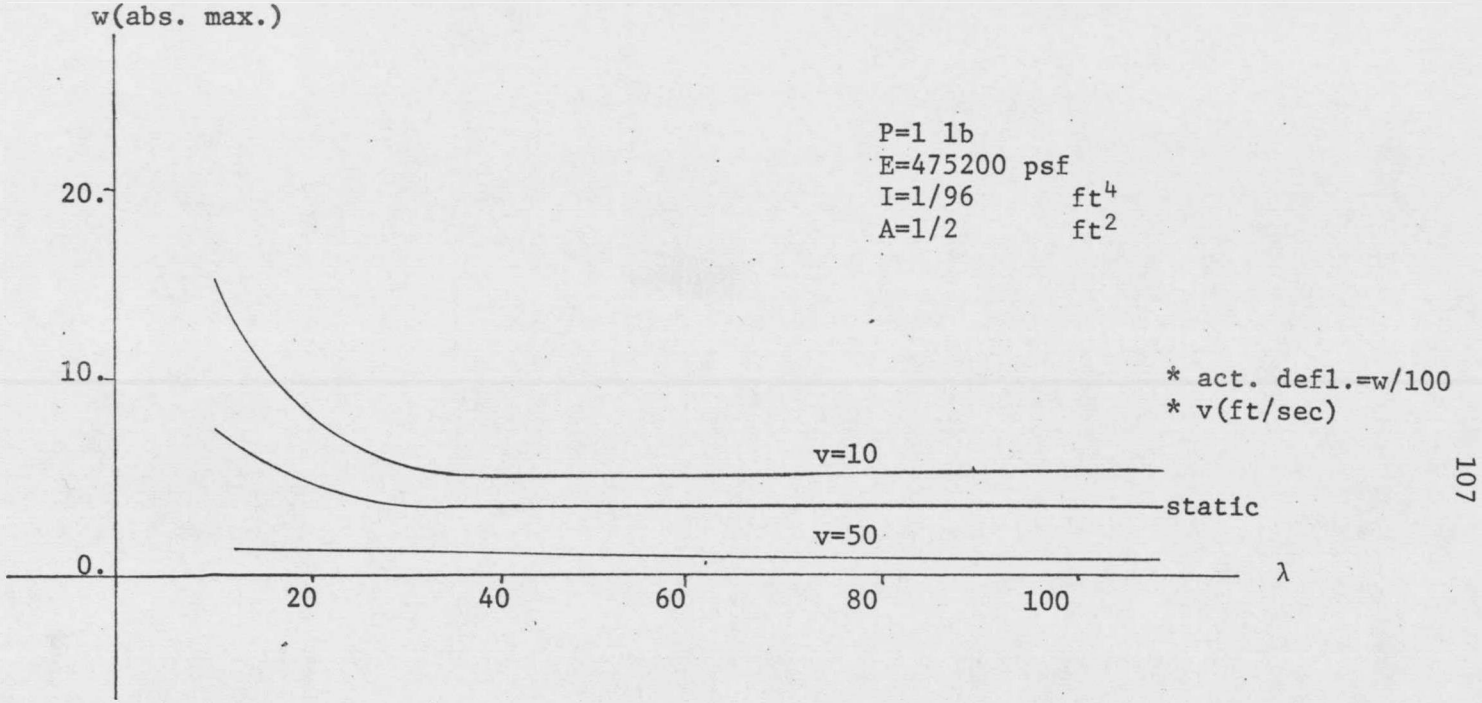
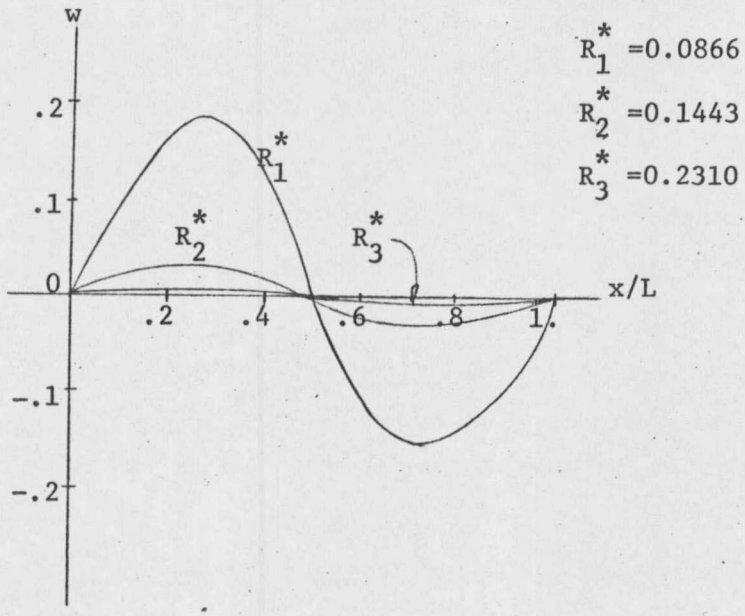
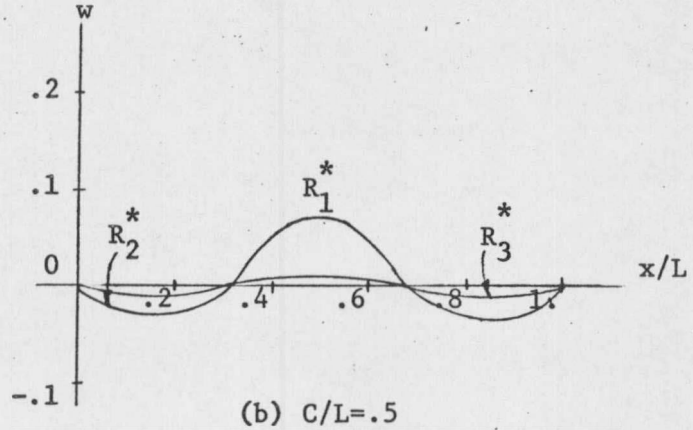


Fig. 5-5. Effect of λ upon Abs. Max. Deflection



(a) C/L=.3



(b) C/L=.5

Fig. 5-6. Effect of Radius of Gyration on Deflection
(λ=50)

It is interesting to study the deformed shape of the arch as v approaches zero. This is demonstrated in Fig. 5-7 in which the deformed shapes of the arch due to a point load of unity are shown for the static case, and the dynamic case with v = 1.0, 5.0 and 10.0 ft/sec respectively. It is seen that for a smallv (= 1.0 ft/sec in this case) the deformed shape is almost identical with that in the static case.

5.3 Static Stresses and Dynamic Stresses

The stresses on the arch rib may be easily determined if the deflection curve is known. The procedure to compute the stresses for arches under static loading are:

a) Using Eqs. (3.4) and (3.7) to find the deflection curve of the arch axis and corresponding axial thrust for each point of application of the point load.

b) The vertical support reaction components are obtained as though the arch is a simple beam.

c) Find the moment on each section and then compute the stress by the formula

$$\sigma = N/A + Mt/2I \qquad \text{----------(5.3)}$$

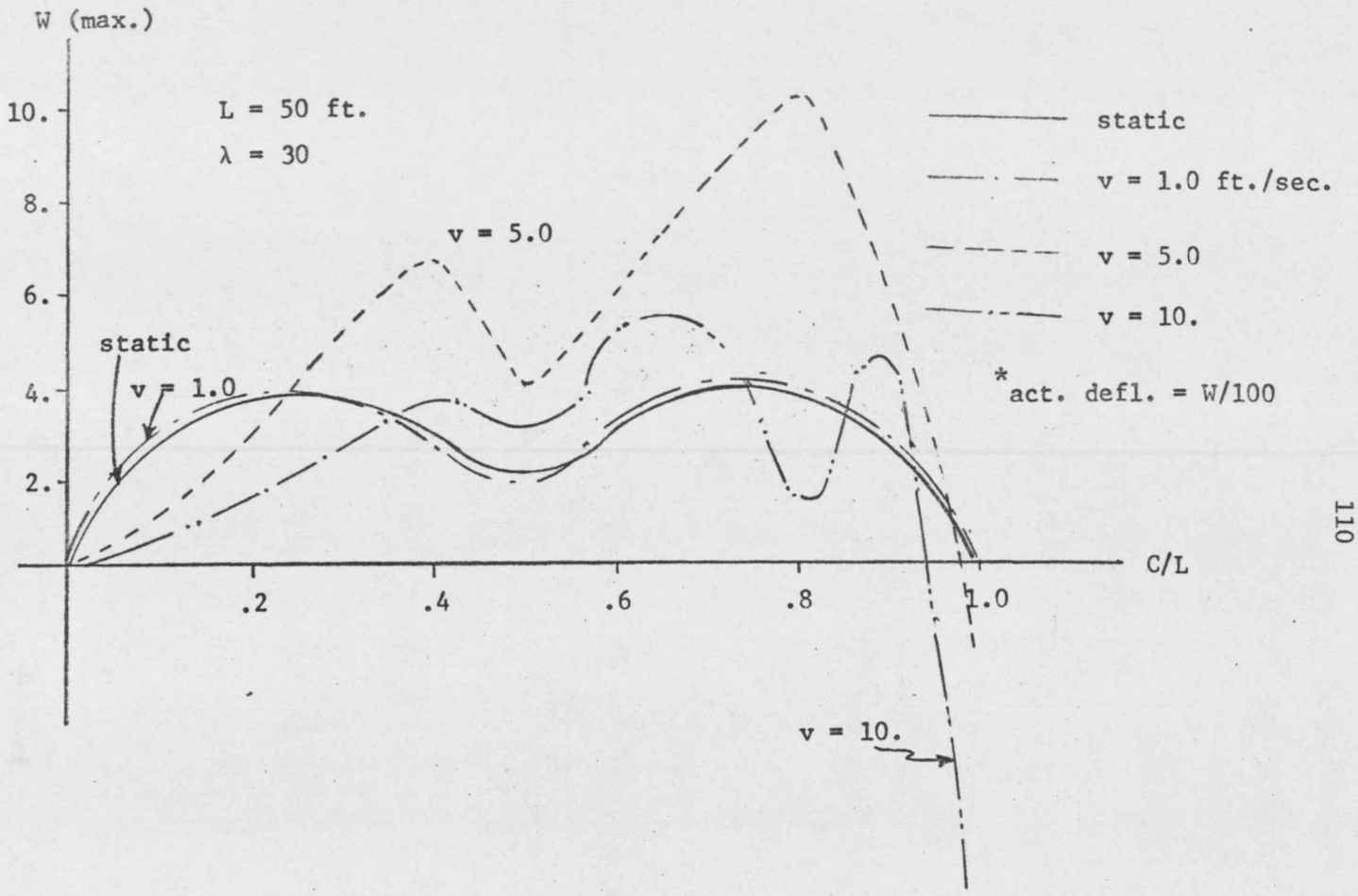


Fig. 5-7. Comparison of Maximum Defelction for a) static case, b) v = 1.0, c) v = 5.0, d) v = 10.0

in which N = normal thrust

A = sectional area

I = moment of inertia of the section

M = the moment on the section

t = the thickness of the rib

As for the stresses due to the moving load, the procedures are the same except

a) Instead of using Eqs. (3.4) and (3.7), the six dynamic equations (4.11 - 4.16) are integrated numerically.

b) Add inertia load to Eq. (5.3).

Adding the inertia load to Eq. (5.3) indicates the difference between a static problem and a dynamic problem. The inertia load is obtained by multiplying the mass of unit length with the acceleration of the arch. Since the acceleration at each section of the arch is different, the stresses due to the inertia load is obtained by using the same technique as solving a simple beam problem subject to non-uniformly distributed load.

Following these procedures, we obtain the desired results which are tabulated in TABLE 5-3. Representative plots of these results are shown in Fig. 5-8 through Fig. 5-12. It is noted that all the stresses either tabulated or shown in the figures are their extreme values, that is, the maximum value on the cross section, and the following data are used:

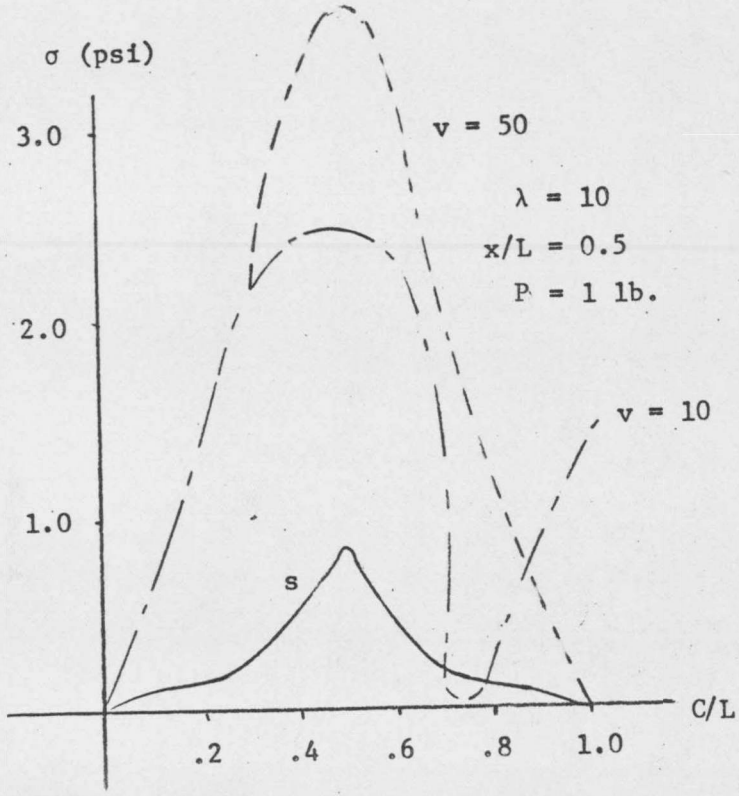


Fig. 5-8. Influence Lines for Stress σ

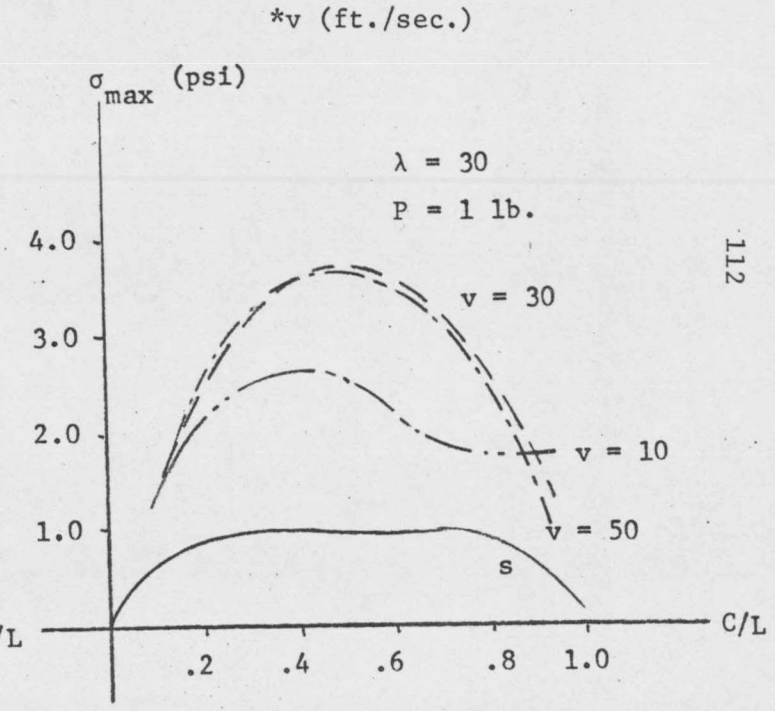


Fig. 5-9. Comparison of σ_{max}

$A = 1/2\ ft^2$ $\quad L=50\ ft$

$E = 475200\ psf$

$I = 1/96\ ft^4$

$P = 1\ lb$

These figures show that the static stress is generally much less than the dynamic stress. Let's define σ_{max} as the maximum value of the stresses corresponding to each load position (point of application of the unit load) and abs σ_{max} as the largest of these maximum stresses. Fig. 5-8 shows the influence lines for the stress σ at $x/L = 0.5$, corresponding to various load positions with V = o. (static case), 10. and 50 ft/sec respectively. It is seen that the maximum stress corresponding to V = 50 ft/sec is more than three times as great as that corresponding to the static case. Fig. 5-9 shows the comparison of σ_{max} corresponding to the static case, V = 10, 30 and 50 ft/sec respectively. It is seen that the absolute maximum stresses corresponding to V = 30 and 50 ft/sec are greater than those corresponding to the static case and V = 10 ft/sec respectively. Since the maximum displacement of the arch corresponding to V = 10 ft/sec is greater than V = 30 or 50 ft/sec as discussed in the previous section, it seems contradicting in the above statement. For it is natural to think that if the maximum displacement is greater, the maximum stress should also be greater. But it must be pointed out that this is perfectly true in the simple beam

problem but not necessarily true in the arch problem. To clarify this doubt, we must recall that an arch serves to reduce the bending moment when compared with a beam under the same conditions. It is the normal thrust that "helps" the arch to achieve this purpose. If the thrust is small in magnitude the moment due to the thrust that is to be deducted from the bending moment is negligible. If this is the case, then the arch is no more than a beam and a high stress due to the external moment is expected. With this in mind, let's study Fig. 5-13 in which the thrust corresponding to various load positions is shown with v = 10, 30 and 50 ft/sec respectively. It is seen that the thrust corresponding to v = 50 ft/sec is a small fraction of that corresponding to v = 10 ft/sec. Hence, it is evident that it is possible for the maximum stress value corresponding to v = 50 ft/sec to be greater than when v = 10 ft/sec.

The effect of the geometric parameter λ upon the abs. maximum stress is also found and shown in Fig. 5-10. One observes that the effect of the geometric parameter λ upon the abs. maximum stress is rather irregular in the dynamic case. But in the static case for greater λ, the abs. σ_{max} is less. It does not vary significantly for $\lambda > 40$.

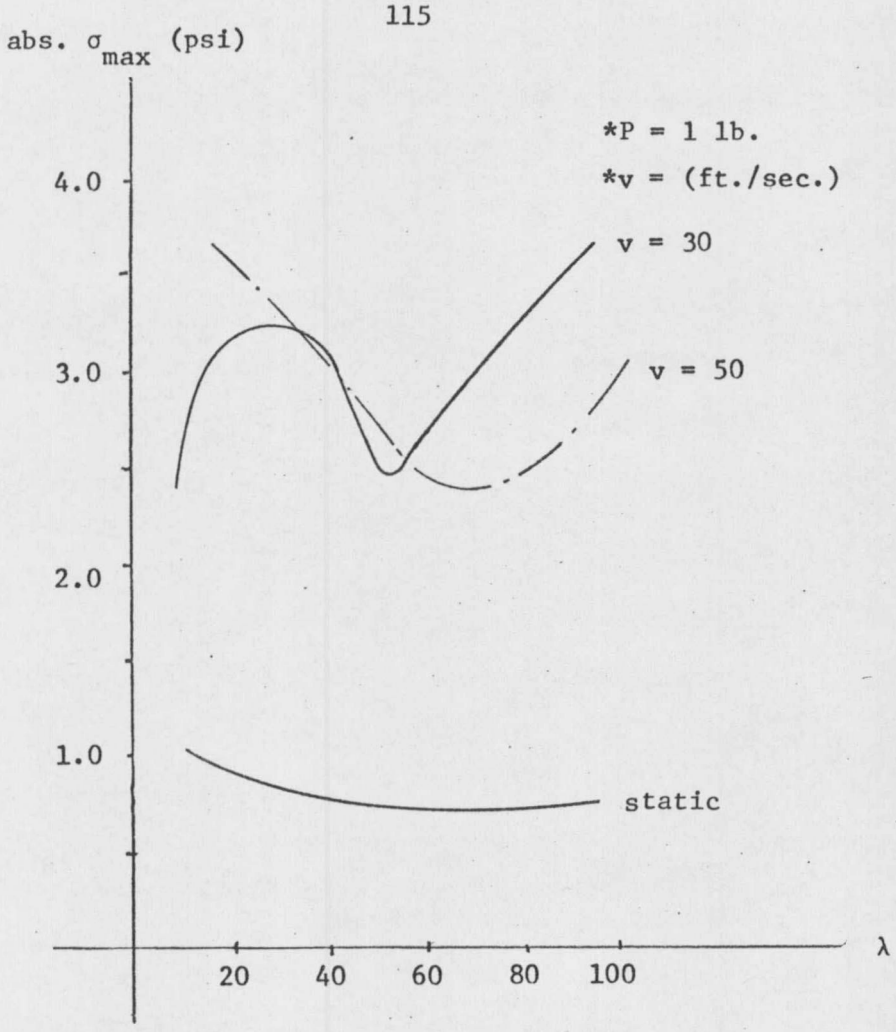


Fig. 5-10. Effect of λ upon Stresses

It is also interesting to know the effect of λ, the geometric parameter, upon the bending moment and the normal thrust in the static case in addition to the effect of λ upon the stress which has already been discussed. This is shown in Fig. 5-11. It is observed that the normal thrust N reduces as λ increases. The bending moment has the same tendency but does not vary as sharply as the normal thrust.

In Fig. 5-12 the σ_{max} corresponding to three different values of radius of gyration is calculated for various points of application of the load. The effect of a larger stiffness is to reduce the stress. It is seen this effect is not linear. This is similar to the case in which the effect of the stiffness upon the deflection is considered.

In Sec. 5-1. we mentioned the difference of the two theories: the elastic theory and the deflection theory. To get some more insight into this, we solve the problem by the two theories and use two different point loads (P = 1 lb and P = 10 lb). The procedures to find the stress by the elastic theory may be found in many textbooks, say by Maugh [54]. The stress by the deflection theory is obtained by following the procedures listed in Sec. 5.2. With the following data used:

$$A = 1/2 \text{ ft}$$

$$I = 1/96 \text{ ft}^4$$

$$E = 475200 \text{ psf}$$

$$L = 50 \text{ ft}$$

$$\lambda = 50$$

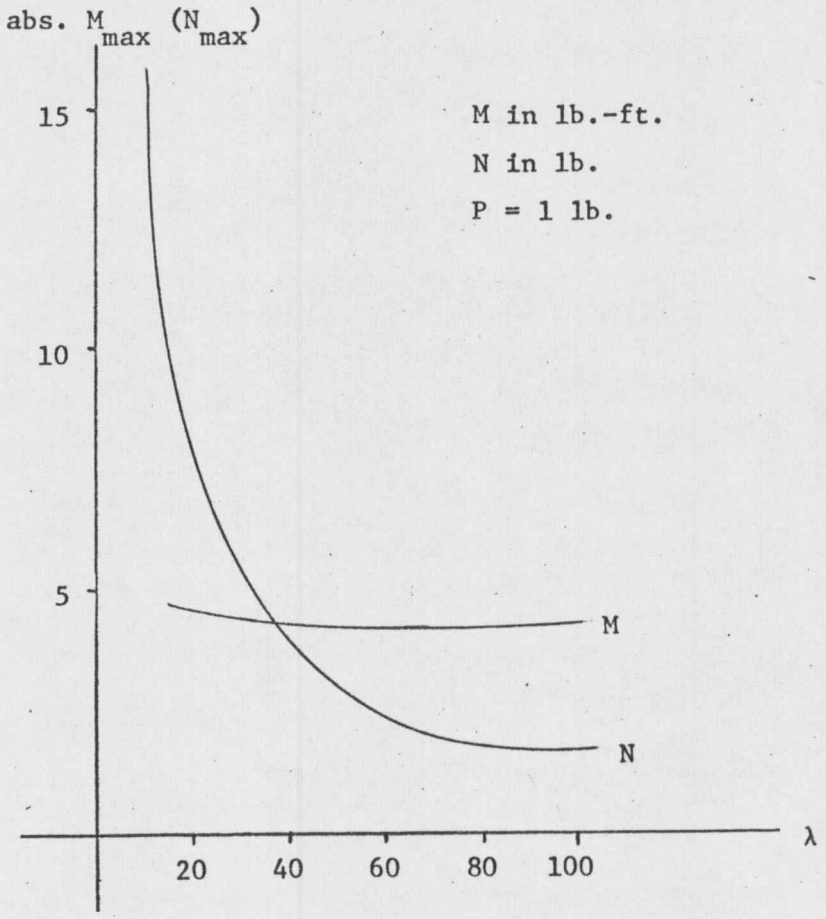


Fig. 5-11. Effect of the Geometric Parameter λ upon Abs. M_{max} and N_{max}

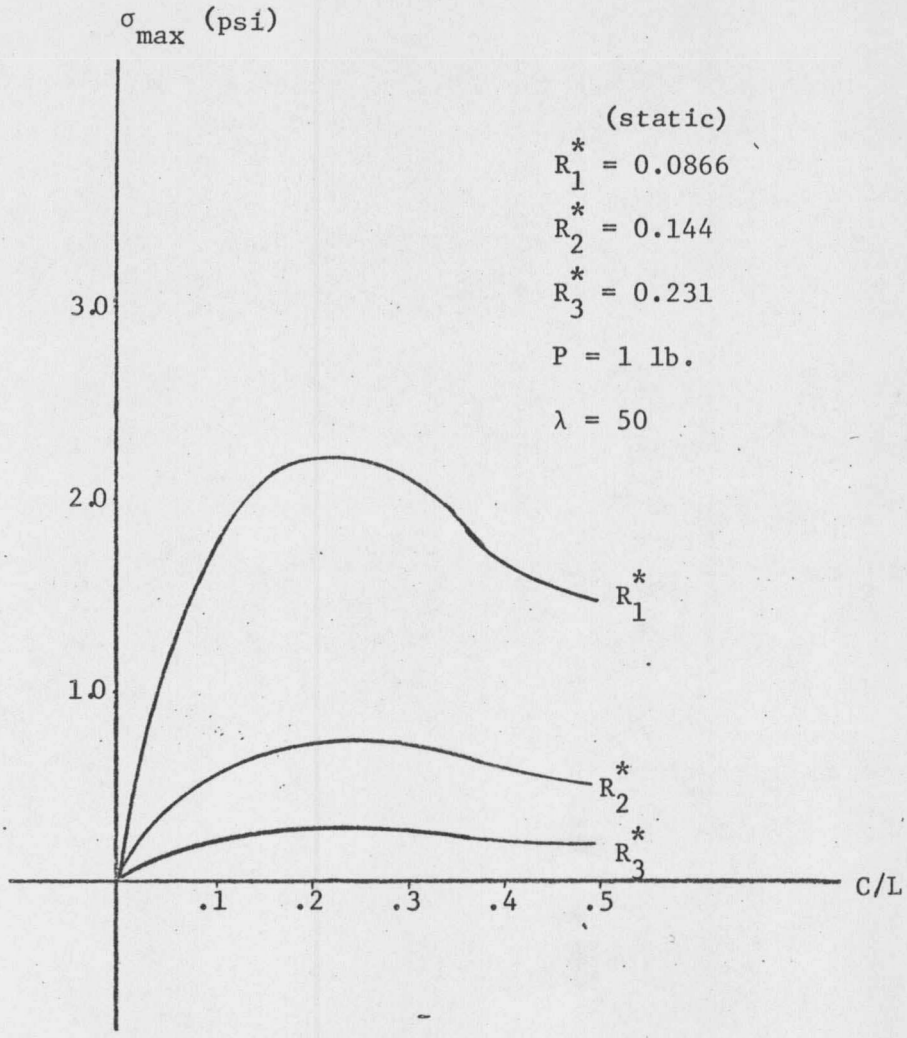


Fig. 5-12. Effect of Radius of Gyration Upon Stresses

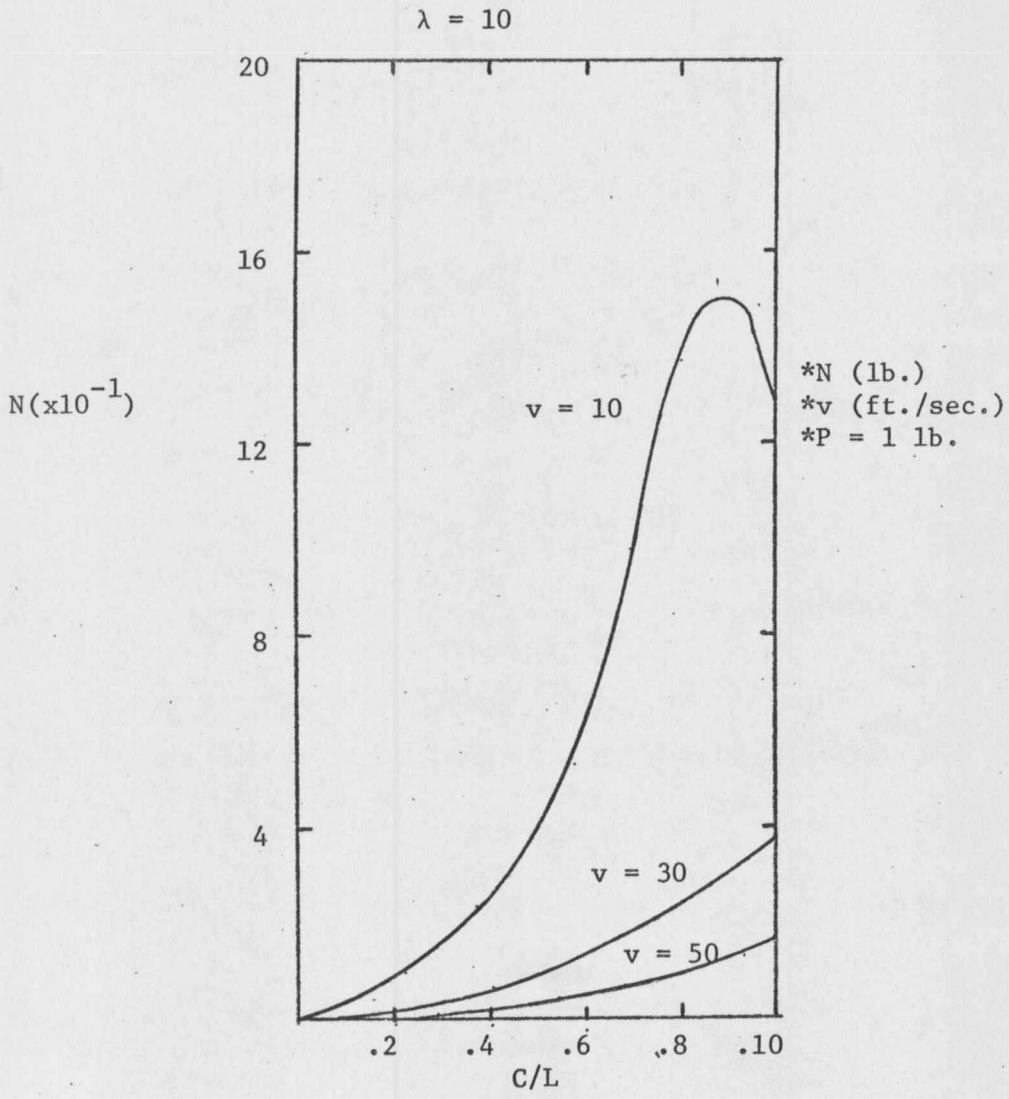


Fig. 5-13. Variation of the Axial Thrust due to v

The results are tabulated in TABLE 5-4, and is also shown in Fig. 5-14. Apparently the values computed by the first theory are much less than that by the deflection theory and, more notably, are on the unsafe side. It is noted that if P is small the difference is not too severe, but if P is large the difference is too great to be ignored.

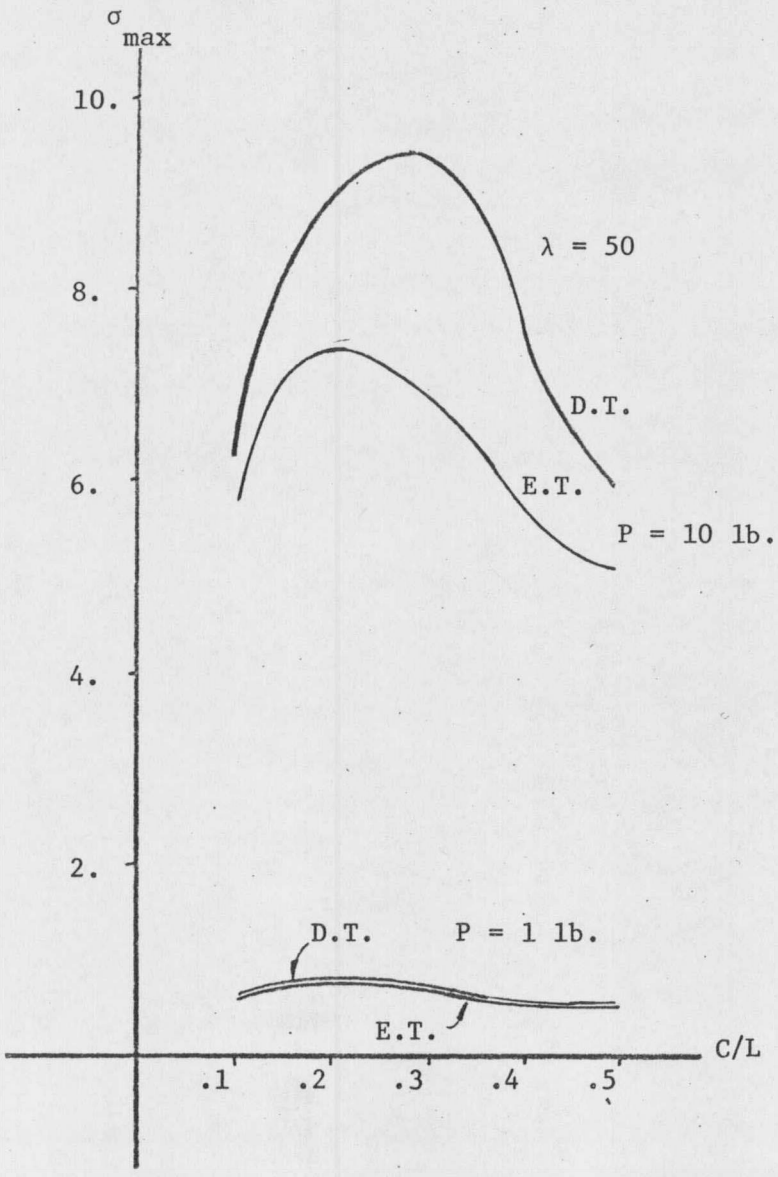


Fig. 5-14. Maximum Stresses Computed by the Elastic Theory (E.T.) and by the Deflection Theory (D.T.)

Chapter 6

DISCUSSIONS AND CONCLUSIONS

In Chapter 3 and Chapter 4, we studied the stability problem of pin-pin shallow circular arches in the static case and in the dynamic case, respectively. It was found that the stability of these arches is sensitive to the geometric parameter λ which is proportional to the arch rise if the radius of gyration of the arch section (with respect to the axis perpendicular to the arch plane) is constant. Some important conclusions in the static case may be drawn:

1) Symmetric arches under symmetric loading will not buckle if the geometric parameter $\lambda < 4.2$, will buckle symmetrically if $4.2 \leq \lambda \leq 12$, and will buckle antisymmetrically if $\lambda > 12$.

2) Symmetric arches under arbitrary loading will not buckle for the geometric parameter $\lambda < 4.2$ and will buckle antisymmetrically for $\lambda \geq 4.2$.

3) The presence of the second mode (antisymmetric mode) only "triggers" the buckling process, since the final buckled configuration is always symmetric.

4) As $\overline{\phi}$ (the ratio of the uniform pressure to the point load) is small (say, 0.00001), the dead weight of the arch may be neglected in determining the critical values.

5) The weak region is found to lie approximately between $x = .03L$ and $x = 0.4L$ from either support, in which the critical loads are

relatively less than when the point load is at other positions. However, this region disappears when the dead weight of the arch is about on the same order of magnitude as the point load.

In the dynamic case, it was found

a) In the series solution, the two modes approximation may be used to determine the critical loads in practice.

b) Except for a small range of v/L (speed-span ratio), as v/L increases, the critical load also increases.

c) Greater geometric parameter λ corresponds to higher critical loads.

d) If $\bar{\phi}$ (the ratio of the uniform pressure and the point load) is small, the dead weight of the arch may be neglected in obtaining the critical load.

e) Shallow arches will buckle if and only if the critical amplitude of the first mode A_1 is reached.

f) In two modes approximation, the presence of A_2 helps to increase the amplitude of A_1. Hence, the critical loads computed by using the first two modes are less than when only the first mode is considered.

g) For a certain range of speed-span ratio the dynamic buckling load is less than the corresponding static buckling load. And it appears that the percentage of the difference between the minimum dynamic buckling load and the corresponding static buckling load decreases as the arch geometric parameter λ_1 increases.

In studying the deflection and the stress of the arch rib in Chapter 5, it was found

a) The absolute maximum static deflection and stresses are less than the corresponding dynamic deflection and stresses.

b) The absolute maximum deflection in the static case occurs when the point load is in the weak region.

c) For the geometric parameter $\lambda > 40$, both the absolute maximum values of the deflection and the stresses approximately remain the same.

d) The effect of the geometric parameter λ upon the axial thrust is significant. For greater λ, the thrust becomes less.

e) For the geometric parameter $\lambda > 30$, the maximum bending moment does not vary significantly.

f) As in the simple beam problem, greater R^* (radius of gyration) causes less deflection and stresses.

g) The abs. maximum dynamic deflection reaches it peak value for v/L (speed-span ratio) = 0.12. It appears that this peak value is greater than the corresponding abs. maximum static deflection for all values of the geometric parameter λ_1.

h) Results computed by using the elastic theory and the deflection theory shows significant differences. As such, the elastic theory is not recommended in practical design.

In this work, our studies are limited to a rather narrow field, and many things have been idealized. In practice, the problem becomes

much more involved. An arch rib, for example, is often built with the hangers and the deck to form a complete unit of the arch bridge system. In this case, the arch bridge behaves more as a truss than as a pure arch. But, if the connections between the arch rib and the hangers are pinned, the problem may then be handled by the techniques suggested in this work. The presence of the hangers may be viewed as stiffening the arch rib and thus the critical load should be higher.

In treating the stability problem, we assumed that moment of inertia, I, is small. But if I is large, the arch will have no instability problem. It may fail because the material is overstressed. Hence, it is recommended that in practical design both the stability problem and the stress conditions should be studied.

APPENDICES

APPENDIX A

TABLE 3-1

Critical Load Parameter $\bar{P}cr$ for Pinned-end Shallow Circular Arches under Point Load Only

λ \ η_o	0.1	0.2	0.3	0.4	0.5
5	1.720	0.910	0.666	0.570	0.543
10	2.403	1.332	1.054	1.018	1.138
20	2.680	1.504	1.219	1.238	1.770
30	2.730	1.535	1.249	1.276	1.866
40	2.748	1.546	1.259	1.288	1.898
50	2.756	1.551	1.263	1.294	1.913
60	2.761	1.553	1.266	1.298	1.921
70	2.763	1.555	1.267	1.300	1.926
80	2.765	1.556	1.268	1.301	1.929
90	2.766	1.557	1.269	1.302	1.931
100	2.767	1.557	1.270	1.302	1.932

NOTE: The values in TABLES 3-1 through 3-8 are to be multiplied by 12.

TABLE 3-2

Critical Load Parameter $\bar{P}cr$ for Pinned-end Shallow Circular Arches Under Point Load and Uniform Pressure

$(\bar{\phi} = \frac{\text{uniform pressure}}{\text{point load}} = 1.0)$

λ \ $\frac{\eta_o}{\mu}$	0.1	0.2	0.3	0.4	0.5
5	0.143×10^{-2}	0.143×10^{-2}	0.143×10^{-2}	0.143×10^{-2}	0.143×10^{-2}
10	0.323	0.323	0.322	0.322	0.322
20	0.500	0.495	0.495	0.497	0.505
30	0.525	0.520	0.520	0.524	0.527
40	0.534	0.528	0.528	0.533	0.536
50	0.538	0.532	0.531	0.537	0.540
60	0.539	0.534	0.534	0.539	0.542
70	0.541	0.535	0.535	0.540	0.543
80	0.541	0.536	0.536	0.540	0.544
90	0.542	0.537	0.536	0.541	0.544
100	0.542	0.537	0.537	0.541	0.545

TABLE 3-3

Critical Load Parameter $\bar{P}_{cr}$ for Pinned-end Shallow Circular Arches Under Point Load and Uniform Pressure

$$(\bar{\phi} = \frac{\text{uniform pressure}}{\text{point load}} = 0.1)$$

λ \ $\frac{\eta_o}{\mu}$	0.1	0.2	0.3	0.4	0.5
5	1.418×10^{-2}	1.407×10^{-2}	1.399×10^{-2}	1.394×10^{-2}	1.392×10^{-2}
10	3.201	3.170	3.149	3.143	3.144
20	4.770	4.654	4.626	4.589	4.907
30	4.995	4.869	4.841	4.911	5.150
40	5.070	4.942	4.913	4.982	5.231
50	5.105	4.975	4.946	5.020	5.269
60	5.124	4.993	4.964	5.038	5.287
70	5.135	5.004	4.975	5.049	5.301
80	5.142	5.011	4.982	5.056	5.308
90	5.147	5.016	4.986	5.061	5.314
100	5.151	5.019	4.990	5.064	5.318

TABLE 3-4

Critical Load Parameter $\overline{P}cr$ for Pinned-end Shallow Circular Arches Under Point Load and Uniform Pressure

$(\overline{\phi} = \frac{\text{uniform pressure}}{\text{point load}} = 0.05)$

λ \ $\frac{\eta_o}{\mu}$	0.1	0.2	0.3	0.4	0.5
5	0.281×10^{-1}	0.277×10^{-1}	0.274×10^{-1}	0.272×10^{-1}	0.272×10^{-1}
10	0.633	0.619	0.612	0.611	0.612
20	0.922	0.885	0.875	0.892	0.956
30	0.964	0.924	0.914	0.933	1.000
40	0.978	0.938	0.927	0.947	1.020
50	0.984	0.944	0.933	0.953	1.020
60	0.988	0.947	0.936	0.956	1.031
70	0.990	0.949	0.938	0.958	1.033
80	0.991	0.950	0.940	0.960	1.034
90	0.992	0.951	0.941	0.961	1.036
100	0.993	0.952	0.941	0.961	1.036

TABLE 3-5

Critical Load Parameter $\overline{P}cr$ for Pinned-end Shallow Circular Arches Under Point Load and Uniform Pressure

$(\overline{\phi} = \frac{\text{uniform pressure}}{\text{point load}} = 0.01)$

λ \ $\frac{\eta_o}{\mu}$	0.1	0.2	0.3	0.4	0.5
5	0.132	0.124	0.118	0.114	0.113
10	0.285	0.258	0.246	0.246	0.253
20	0.383	0.338	0.324	0.335	0.396
30	0.398	0.351	0.336	0.349	0.416
40	0.403	0.356	0.340	0.353	0.422
50	0.406	0.358	0.342	0.355	0.425
60	0.407	0.359	0.343	0.356	0.427
70	0.408	0.359	0.344	0.357	0.429
80	0.408	0.360	0.344	0.358	0.429
90	0.409	0.360	0.345	0.358	0.429
100	0.409	0.360	0.345	0.358	0.429

TABLE 3-6

Critical Load Parameter $\overline{P}cr$ for Pinned-end Shallow Circular Arches Under Point Load and Uniform Pressure

$(\overline{\phi} = \frac{\text{uniform pressure}}{\text{point load}} = 0.001)$

λ \ $\frac{\eta_o}{\mu}$	0.1	0.2	0.3	0.4	0.5
5	0.786	0.559	0.455	0.408	0.394
10	1.346	0.926	0.786	0.772	0.845
20	1.592	1.085	0.936	0.963	1.324
30	1.635	1.113	0.962	0.995	1.393
40	1.650	1.122	0.971	1.006	1.416
50	1.656	1.127	0.975	1.011	1.427
60	1.660	1.129	0.977	1.013	1.433
70	1.662	1.131	0.979	1.015	1.436
80	1.664	1.132	0.980	1.016	1.438
90	1.665	1.132	0.980	1.017	1.440
100	1.665	1.133	0.981	1.017	1.441

TABLE 3-7

Critical Load Parameter $\bar{P}_{cr}$ for Pinned-end Shallow Circular Arches Under Point Load and Uniform Pressure

$$(\bar{\phi} = \frac{\text{uniform pressure}}{\text{point load}} = 0.0001)$$

λ \ $\frac{\eta_o}{\bar{\mu}}$	0.1	0.2	0.3	0.4	0.5
5	1.538	1.856	0.637	0.548	0.523
10	2.221	1.275	1.019	0.986	1.100
20	2.497	1.446	1.182	1.200	1.714
30	2.548	1.477	1.212	1.240	1.806
40	2.565	1.487	1.222	1.253	1.837
50	2.573	1.492	1.226	1.259	1.851
60	2.578	1.495	1.229	1.262	1.858
70	2.580	1.496	1.230	1.264	1.863
80	2.582	1.498	1.231	1.265	1.866
90	2.583	1.498	1.232	1.266	1.868
100	2.584	1.499	1.232	1.266	1.869

TABLE 3-8

Critical Load Parameter $\overline{P}cr$ for Pinned-end Shallow Circular Arches Under Point Load and Uniform Pressure

$(\overline{\phi} = \frac{\text{uniform pressure}}{\text{point load}} = 0.00001)$

λ \ $\frac{\eta_o}{\mu}$	0.1	0.2	0.3	0.4	0.5
5	1.700	0.904	0.663	0.568	0.541
10	2.384	1.326	1.050	1.014	1.134
20	2.660	1.498	1.215	1.234	1.765
30	2.711	1.529	1.245	1.272	1.860
40	2.728	1.540	1.255	1.285	1.892
50	2.737	1.545	1.260	1.291	1.907
60	2.741	1.547	1.262	1.294	1.915
70	2.744	1.549	1.265	1.297	1.919
80	2.745	1.550	1.265	1.297	1.922
90	2.747	1.551	1.265	1.298	1.924
100	2.747	1.551	1.266	1.297	1.926

TABLE 4-1

Critical Load Parameter P2cr for Pinned-end Shallow Circular Arches Under Point Load Only

V ft/sec \ λ1	3.	5.	10.	15.	20.	25.
1.0	3.3	5.6	11.5	17.3	23.0	28.9
10.0	4.4	8.8	17.0	26.0	34.0	42.0
20.0	7.9	15.5	32.0	50.0	67.0	80.0
30.0	12.0	24.0	54.0	83.0	112.0	135.0
40.0	16.0	33.0	78.0	119.0	159.0	205.0
50.0	20.0	45.0	101.0	154.0	217.0	272.0
100.0	39.0	95.0	195.0	326.0	430.0	550.0
150.0	60.0	140.0	390.0	474.0	663.0	872.0

TABLE 4-2

Critical Load Parameter P2cr for Pinned-end Shallow Circular Arches Under Point Load and Uniform Pressure

$(\bar{\phi} = \frac{\text{uniform pressure}}{\text{point load}} = 1.0)$

V ft/sec \ λl	3	5	10	15	20	25
1.0	0.12	0.30	0.57	0.84	1.12	1.40
10.0	0.12	0.35	0.64	0.96	1.26	1.57
20.0	0.12	0.36	0.65	0.97	0.127	1.58

TABLE 4-3

Critical Load Parameter P2cr for Pinned-end Shallow Circular Arches Under Point Load and Uniform Pressure

$(\bar{\phi} = \frac{\text{uniform pressure}}{\text{point load}} = 0.1)$

V ft/sec \ λl	3	5	10	15	20	25
1.0	1.0	2.0	4.0	6.0	7.5	9.5
10.0	1.0	2.5	5.0	8.0	10.5	13.0
20.0	1.1	3.0	6.5	9.5	12.5	15.5

TABLE 4-4

Critical Load Parameter P2cr for Pinned-end Shallow Circular Arches Under Point Load and Uniform Pressure

$(\bar{\phi} = \frac{\text{uniform pressure}}{\text{point load}} = 0.001)$

V ft/sec \ λ1	3	5	10	15	20	25
1.0	3.2	5.5	11.2	16.9	22.6	28.3
10.0	4.1	8.4	15.8	24.0	31.5	38.0
20.0	7.4	14.6	30.2	47.5	64.0	74.0

TABLE 4-5

Critical Load Parameter P2cr for Pinned-end Shallow Circular Arches Under Point Load and Uniform Pressure

$(\bar{\phi} = \frac{\text{uniform pressure}}{\text{point load}} = 0.00001)$

V ft/sec \ λ1	3	5	10	15	20	25
1.0	3.3	5.6	11.4	17.1	22.8	28.7
10.0	4.4	8.8	16.8	25.8	33.7	41.6
20.0	7.7	15.3	31.7	49.7	66.6	79.5

TABLE 4-6

Critical Load Parameter P2cr for Pinned-end Shallow Circular Arches Under Uniform Pressure Only

V ft/sec \ λ1	3	5	10	15	20	25
0.	0.15	0.40	0.65	1.05	1.3	1.7

TABLE 4-7

Critical Load Parameter P2cr for Pinned-end
Shallow Circular Arches
(Damping Effects Included)

$V_{ft/sec}$	λ_1 / D	3	5	10	15	20	25
1.0	0.001	3.3	5.6	11.5	17.3	23.0	28.9
	0.1	3.3	5.7	11.7	17.7	23.6	29.5
10.0	0.001	4.4	8.8	18.0	27.0	35.8	44.8
	0.1	5.0	9.6	19.8	29.6	39.2	49.2
50.0	0.001	22.5	48.5	105.0	160.0	224.0	281.0
	0.1	24.0	51.0	110.0	168.0	232.0	292.0

TABLE 5-1

Relationship Among λ, L, H/L, H, β and $\overline{R}$
(E = 475200 PSf, I = 1/96 ft^4, A = $\frac{1}{2}$ ft^2)

λ	L ft	H ft	H/L	β rad.	$\overline{R}$ ft
10	50	0.6250	0.0125	0.1000	500.3
20	50	1.2500	0.0250	0.1998	250.6
30	50	1.8750	0.0375	0.2994	167.6
40	50	2.5000	0.0500	0.3987	126.3
50	50	3.1250	0.0625	0.4974	101.6
60	50	3.7500	0.0750	0.5956	85.2
70	50	4.3750	0.0875	0.6930	73.6
80	50	5.0000	0.1000	0.7896	65.0
90	50	5.6250	0.1125	0.8853	58.4
100	50	6.2500	0.1250	0.9799	53.1

TABLE 5-2

Deflection of Pinned-end Shallow Circular Arches
(E = 475200 PSf, I = 1/96 ft^4, A = ½ ft^2, b = 1 ft, L = 50 ft)
(a) = 10.

C/L	V ft/sec \ X/L	0.1	0.2	0.3	0.4	0.5	0.6	0.7	0.8	0.9
0.1	Static	2.35	3.31	3.07	2.18	1.08	0.11	-0.52	-0.71	-0.49
	10	0.46	0.26	-0.07	-0.04	0.04	-0.02	-0.01	0.02	-0.02
	30	0.08	0.02	-0.03	0.01	0.01	-0.01	0.00	0.01	-0.01
	50	0.03	0.01	-0.01	0.00	0.00	-0.01	0.00	0.00	0.00
	70	0.02	0.01	-0.01	0.00	0.00	0.00	0.00	0.00	0.00
	90	0.01	0.00	0.00	0.00	0.00	0.00	0.00	0.00	0.00
0.3	Static	3.38	6.15	7.44	6.61	4.49	2.14	0.28	-0.66	-0.65
	10	1.92	3.23	3.07	1.49	-0.15	-0.81	-0.55	-0.01	0.23
	30	0.56	0.66	0.24	-0.12	-0.06	0.07	-0.02	-0.04	0.04
	50	0.29	0.23	0.03	-0.03	0.01	0.01	-0.01	0.00	0.00
	70	0.17	0.12	0.01	-0.01	0.01	0.00	0.00	0.00	0.00
	90	0.11	0.07	0.00	0.00	0.01	0.00	0.00	0.00	0.00

* The above values (in feet) to be multiplied by 10^{-2}

TABLE 5-2 (continued)

C/L	V ft/sec \ X/L	0.1	0.2	0.3	0.4	0.5	0.6	0.7	0.8	0.9
0.5	Static	1.06	2.48	4.25	5.93	6.73	5.93	4.25	2.48	1.06
	10	3.04	5.34	6.72	6.87	5.19	1.87	-1.55	-3.24	-2.47
	30	0.82	1.31	1.38	0.84	-0.03	-0.31	0.06	0.11	-0.13
	50	0.39	0.60	0.47	0.14	-0.02	0.00	0.01	-0.01	0.00
	70	0.25	0.32	0.21	0.07	0.01	0.00	0.00	0.00	0.00
	90	0.18	0.20	0.11	0.04	0.01	0.00	0.00	0.00	0.00
0.7	Static	-0.65	-0.66	0.28	2.14	4.49	6.61	7.44	6.15	3.38
	10	3.17	6.46	9.22	10.31	9.23	6.47	3.05	0.26	-0.72
	30	0.95	1.85	2.16	1.87	1.35	0.42	-0.42	-0.24	0.27
	50	0.50	0.84	0.87	0.61	0.29	0.10	0.03	-0.01	-0.02
	70	0.31	0.49	0.43	0.25	0.15	0.09	0.01	-0.02	0.01
	90	0.22	0.31	0.24	0.15	0.10	0.06	0.01	-0.01	0.01

TABLE 5-2 (continued)

C/L	V ft/sec \ X/L	0.1	0.2	0.3	0.4	0.5	0.6	0.7	0.8	0.9
0.9	Static	-0.49	-0.71	-0.52	0.11	1.08	2.18	3.07	3.31	2.35
	10	3.32	5.54	6.42	6.89	8.09	10.15	11.98	11.67	7.50
	30	1.24	2.02	2.69	2.96	2.32	1.44	0.84	0.03	-0.50
	50	0.61	1.02	1.20	1.07	0.69	0.40	0.29	0.15	0.00
	70	0.37	0.62	0.65	0.49	0.32	0.24	0.19	0.09	0.00
	90	0.26	0.40	0.38	0.26	0.19	0.16	0.11	0.04	0.01
					(b) λ = 30					
0.1	Static	1.87	2.41	1.86	0.79	-0.34	-1.21	-1.63	-1.50	-0.90
	10	0.46	0.25	-0.08	-0.05	0.03	-0.02	-0.01	0.01	-0.02
	30	0.08	0.02	-0.03	0.01	0.01	-0.01	0.00	0.01	-0.01
	50	0.03	0.01	-0.01	0.00	0.00	-0.01	0.00	0.00	0.00
	70	0.02	0.01	-0.01	0.00	0.00	0.00	0.00	0.00	0.00
	90	0.01	0.00	0.00	0.00	0.00	0.00	0.00	0.00	0.00

TABLE 5-2 (continued)

C/L	V ft/sec \ X/L	0.1	0.2	0.3	0.4	0.5	0.6	0.7	0.8	0.9
0.3	Static	1.92	3.43	3.83	2.56	0.47	-1.48	-2.64	-2.70	-1.69
	10	1.56	2.66	2.44	0.89	-0.75	-1.42	-1.19	-0.59	-0.14
	30	0.55	0.64	0.23	-0.14	-0.07	0.06	-0.03	-0.06	0.03
	50	0.29	0.23	0.03	-0.03	0.00	0.00	-0.01	0.00	0.00
	70	0.17	0.12	0.01	-0.01	0.01	0.00	0.00	0.00	0.00
	90	0.11	0.07	0.00	0.00	0.01	0.00	0.00	0.00	0.00
0.5	Static	-0.39	-0.31	0.37	1.33	1.88	1.33	0.37	-0.31	-0.39
	10	2.05	3.49	4.23	4.03	2.27	-0.92	-3.99	-5.06	-3.45
	30	0.73	1.18	1.25	0.72	-0.16	-0.43	-0.07	-0.03	-0.23
	50	0.37	0.58	0.45	0.12	-0.04	-0.02	-0.01	-0.03	-0.02
	70	0.25	0.32	0.20	0.06	0.00	0.00	-0.01	-0.01	0.00
	90	0.17	0.19	0.11	0.04	0.01	0.00	0.00	0.00	0.00

TABLE 5-2 (continued)

C/L	V ft/sec \ X/L	0.1	0.2	0.3	0.4	0.5	0.6	0.7	0.8	0.9
0.7	Static	-1.69	-2.70	-2.64	-1.48	0.47	2.56	3.83	3.43	1.92
	10	1.37	3.05	4.48	4.67	3.36	1.14	-1.16	-2.59	-2.16
	30	0.65	1.40	1.70	1.44	0.92	-0.02	-0.89	-0.70	-0.03
	50	0.44	0.76	0.79	0.54	0.22	0.03	-0.04	-0.09	-0.08
	70	0.29	0.46	0.41	0.23	0.13	0.07	-0.01	-0.04	-0.01
	90	0.22	0.30	0.23	0.14	0.09	0.05	0.00	-0.02	0.00
0.9	Static	-0.90	-1.50	-1.63	-1.21	-0.34	0.79	1.86	2.41	1.87
	10	-1.13	-2.54	-3.84	-4.11	-2.83	-0.30	2.61	4.45	3.55
	30	0.62	1.03	1.61	1.92	1.30	0.38	-0.27	-0.98	-1.13
	50	0.46	0.81	0.99	0.87	0.50	0.20	0.09	-0.06	-0.15
	70	0.32	0.55	0.59	0.43	0.25	0.18	0.13	0.02	-0.05
	90	0.24	0.38	0.36	0.24	0.16	0.14	0.09	0.01	-0.01

TABLE 5-2 (continued)

(c) $\lambda = 50$

C/L	$V_{ft/sec}$ \ X/L	0.1	0.2	0.3	0.4	0.5	0.6	0.7	0.8	0.9
0.1	Static	1.86	2.36	1.77	0.67	-0.48	-1.36	-1.75	-1.60	-0.95
	10	0.45	0.24	-0.09	-0.06	0.02	-0.03	-0.02	0.00	-0.03
	30	0.08	0.02	-0.03	0.01	0.01	-0.01	0.00	0.01	-0.01
	50	0.03	0.01	-0.01	0.00	0.00	-0.01	0.00	0.00	0.00
	70	0.02	0.01	-0.01	0.00	0.00	0.00	0.00	0.00	0.00
	90	0.01	0.00	0.00	0.00	0.00	0.00	0.00	0.00	0.00
0.3	Static	1.81	3.22	3.55	2.23	0.13	-1.80	-2.91	-2.89	-1.79
	10	1.39	2.35	2.06	0.52	-1.09	-1.79	-1.56	-0.89	-0.30
	30	0.53	0.61	0.20	-0.16	-0.10	0.03	-0.05	-0.09	0.00
	50	0.28	0.23	0.02	-0.03	0.00	0.00	-0.01	-0.01	0.00
	70	0.17	0.12	0.01	-0.01	0.01	-0.01	0.00	0.00	-0.01
	90	0.11	0.07	0.00	0.00	0.01	-0.01	0.00	0.00	0.00

TABLE 5-2 (continued)

C/L	V ft/sec \ X/L	0.1	0.2	0.3	0.4	0.5	0.6	0.7	0.8	0.9
0.5	Static	-0.52	-0.53	0.07	0.99	1.52	0.99	0.07	-0.53	-0.52
	10	2.12	3.55	4.17	3.83	2.02	-1.06	-3.94	-4.91	-3.32
	30	0.60	1.00	1.08	0.55	-0.32	-0.60	-0.25	-0.21	-0.36
	50	0.34	0.55	0.42	0.09	-0.07	-0.05	-0.04	-0.07	-0.05
	70	0.24	0.31	0.19	0.05	-0.01	-0.01	-0.02	-0.02	-0.01
	90	0.17	0.19	0.11	0.04	0.00	-0.01	-0.01	-0.01	-0.01
0.7	Static	-1.79	02.89	-2.91	-1.80	0.13	2.23	3.55	3.22	1.81
	10	0.67	1.92	3.30	3.71	2.56	0.25	-2.25	-3.63	-2.80
	30	0.42	1.01	1.26	1.04	0.55	-0.42	-1.32	-1.09	-0.25
	50	0.35	0.64	0.68	0.43	0.11	-0.08	-0.16	-0.21	-0.17
	70	0.26	0.42	0.37	0.20	0.09	0.03	-0.04	-0.08	-0.05
	90	0.20	0.28	0.22	0.12	0.07	0.04	-0.02	-0.04	-0.02

TABLE 5-2 (continued)

C/L	V ft/sec \ X/L	0.1	0.2	0.3	0.4	0.5	0.6	0.7	0.8	0.9
0.9	Static	-0.95	-1.60	-1.75	-1.36	-0.48	0.67	1.77	2.36	1.86
	10	-0.43	-1.74	-3.59	-4.55	-3.51	-0.56	3.16	5.53	4.42
	30	0.40	0.60	1.05	1.35	0.75	-0.18	-0.81	-1.39	-1.34
	50	0.28	0.55	0.74	0.64	0.27	-0.03	-0.17	-0.31	-0.33
	70	0.24	0.45	0.49	0.34	0.16	0.09	0.04	-0.09	-0.13
	90	0.20	0.34	0.32	0.20	0.12	0.10	0.05	-0.03	-0.05
	(d) λ = 70									
0.1	Static	1.90	2.40	1.78	0.65	-0.54	-1.43	-1.83	-1.66	-0.99
	10	0.43	0.23	-0.10	-0.07	0.01	-0.04	-0.03	-0.02	-0.04
	30	0.08	0.02	-0.03	0.01	0.01	-0.01	0.00	0.01	-0.01
	50	0.03	0.01	-0.01	0.00	0.00	-0.01	0.00	0.00	0.00
	70	0.02	0.01	-0.01	0.00	0.00	0.00	0.00	0.00	0.00
	90	0.01	0.00	0.00	0.00	0.00	0.00	0.00	0.00	0.00

TABLE 5-2 (continued)

C/L	V ft/sec \ X/L	0.1	0.2	0.3	0.4	0.5	0.6	0.7	0.8	0.9
0.3	Static	1.81	3.22	3.54	2.18	0.02	-1.94	-3.05	-3.01	-1.86
	10	1.40	2.36	2.05	0.48	-1.15	-1.83	-1.57	-0.88	-0.28
	30	0.50	0.58	0.17	-0.19	-0.13	0.00	-0.09	-0.12	-0.02
	50	0.28	0.22	0.02	-0.04	-0.01	-0.01	-0.02	-0.01	-0.01
	70	0.17	0.12	0.00	-0.01	0.00	-0.01	-0.01	0.00	-0.01
	90	0.11	0.07	0.00	0.00	0.00	-0.01	0.00	0.00	-0.01
0.5	Static	-0.56	-0.61	-0.02	0.91	1.45	0.91	-0.02	-0.61	-0.56
	10	2.06	3.46	4.07	3.73	1.93	-1.14	-4.02	-4.98	-3.37
	30	0.52	0.87	0.94	0.43	-0.43	-0.72	-0.39	-0.34	-0.44
	50	0.31	0.50	0.38	0.05	-0.11	-0.09	-0.08	-0.11	-0.08
	70	0.23	0.29	0.18	0.04	-0.02	-0.03	-0.03	-0.04	-0.03
	90	0.16	0.18	0.10	0.03	0.00	-0.01	-0.01	-0.01	-0.01

TABLE 5-2 (continued)

C/L	$V_{ft/sec}$ \ X/L	0.1	0.2	0.3	0.4	0.5	0.6	0.7	0.8	0.9
0.7	Static	-1.86	-3.01	-3.05	-1.94	0.02	2.18	3.54	3.22	1.81
	10	0.58	1.74	3.05	3.39	2.24	-0.01	-2.40	-3.70	-2.82
	30	0.40	0.94	1.13	0.92	0.45	-0.53	-1.44	-1.16	-0.27
	50	0.27	0.53	0.57	0.33	0.01	-0.18	-0.26	-0.32	-0.25
	70	0.22	0.37	0.33	0.16	0.04	-0.01	-0.09	-0.13	-0.08
	90	0.18	0.26	0.20	0.11	0.05	0.02	-0.03	-0.06	-0.03
0.9	Static	-0.99	-1.66	-1.83	-1.43	-0.54	0.65	1.78	2.40	1.90
	10	-0.40	-1.64	-3.47	-4.53	-3.52	-0.40	3.50	5.88	4.60
	30	0.44	0.66	1.07	1.30	0.67	-0.21	-0.77	-1.32	-1.30
	50	0.20	0.41	0.57	0.49	0.14	-0.18	-0.33	-0.46	-0.41
	70	0.17	0.35	0.40	0.25	0.07	0.00	-0.06	-0.19	-0.21
	90	0.16	0.28	0.27	0.16	0.08	0.06	0.00	-0.08	-0.09

TABLE 5-2 (continued)

(e) $\lambda = 90$

C/L	V ft/sec \ X/L	0.1	0.2	0.3	0.4	0.5	0.6	0.7	0.8	0.9
0.1	Static	1.96	2.48	1.83	0.65	-0.58	-1.50	-1.91	-1.74	-1.03
	10	0.42	0.21	-0.12	-0.08	-0.01	-0.06	-0.05	-0.03	-0.06
	30	0.08	0.02	-0.03	0.01	0.01	-0.01	0.00	0.01	-0.01
	50	0.03	0.01	-0.01	0.00	0.00	-0.01	0.00	0.00	0.00
	70	0.02	0.01	-0.01	0.00	0.00	0.00	0.00	0.00	0.00
	90	0.01	0.00	0.00	0.00	0.00	0.00	0.00	0.00	0.00
0.3	Static	1.85	3.30	3.63	2.21	-0.02	-2.05	-3.19	-3.14	-1.94
	10	1.36	2.33	2.03	0.43	-1.22	-1.87	-1.59	-0.90	-0.32
	30	0.47	0.54	0.14	-0.22	-0.16	-0.03	-0.12	-0.16	-0.05
	50	0.27	0.21	0.01	-0.05	-0.01	-0.01	-0.02	-0.02	-0.02
	70	0.16	0.12	0.00	-0.01	0.00	-0.01	-0.01	0.00	-0.01
	90	0.11	0.07	0.00	-0.01	0.00	-0.01	0.00	0.00	-0.01

TABLE 5-2 (continued)

C/L	V ft/sec \ X/L	0.1	0.2	0.3	0.4	0.5	0.6	0.7	0.8	0.9
0.5	Static	-0.60	-0.66	-0.06	0.86	1.45	0.86	-0.06	-0.66	-0.60
	10	1.96	3.36	4.02	3.64	1.80	-1.23	-4.07	-5.06	-3.47
	30	0.51	0.83	0.89	0.39	-0.46	-0.76	-0.44	-0.38	-0.45
	50	0.28	0.46	0.34	0.02	-0.15	-0.12	-0.12	-0.16	-0.11
	70	0.21	0.27	0.17	0.03	-0.04	-0.04	-0.04	-0.05	-0.04
	90	0.16	0.17	0.10	0.03	-0.01	-0.02	-0.02	-0.02	-0.02
0.7	Static	-1.94	-3.14	-3.19	-2.05	-0.02	2.21	3.63	3.30	1.85
	10	0.51	1.66	2.95	3.24	2.06	-0.12	-2.43	-3.72	-2.86
	30	0.41	0.95	1.14	0.92	0.44	-0.54	-1.43	-1.14	-0.26
	50	0.24	0.47	0.51	0.27	-0.05	-0.23	-0.33	-0.39	-0.29
	70	0.19	0.33	0.29	0.12	0.00	-0.05	-0.13	-0.18	-0.12
	90	0.16	0.24	0.18	0.08	0.03	0.00	-0.06	-0.08	-0.05

TABLE 5-2 (continued)

C/L	V ft/sec \ X/L	0.1	0.2	0.3	0.4	0.5	0.6	0.7	0.8	0.9
0.9	Static	-1.03	-1.74	-1.91	-1.50	-0.58	0.65	1.83	2.48	1.96
	10	-0.44	-1.67	-3.49	-4.56	-3.55	-0.36	3.60	5.97	4.64
	30	0.40	0.63	1.05	1.25	0.59	-0.27	-0.79	-1.35	-1.34
	50	0.21	0.39	0.53	0.46	0.12	-0.21	-0.38	-0.48	-0.40
	70	0.13	0.28	0.33	0.19	0.01	-0.06	-0.12	-0.25	-0.25
	90	0.12	0.24	0.23	0.12	0.03	0.02	-0.04	-0.13	-0.12

TABLE 5-3

Maximum Stresses of Pinned-end Shallow Circular Arches
(E = 475000 PSf, 2 = 1/96 ft^4, A = ½ ft^2, b = 1 ft, L = 50 ft)
(a) λ = 10 (psi)

C/L	V ft/sec \ X/L	0.1	0.2	0.3	0.4	0.5	0.6	0.7	0.8	0.9
0.1	Static	0.661	0.454	0.275	0.128	0.107	0.179	0.211	0.202	0.152
	10	1.056	1.228	1.162	0.904	0.713	0.602	0.445	0.281	0.152
	30	1.246	1.306	1.105	0.928	0.789	0.627	0.466	0.314	0.156
	50	1.273	1.281	1.065	0.920	0.784	0.606	0.461	0.317	0.146
	70	1.303	1.425	1.198	1.031	0.876	0.682	0.517	0.353	0.165
	90	1.301	1.377	1.149	0.997	0.848	0.655	0.500	0.344	0.157
0.3	Static	0.365	0.649	1.005	0.586	0.242	0.344	0.479	0.495	0.389
	10	0.793	1.569	2.440	2.489	2.287	1.741	1.196	0.615	0.199
	30	0.892	2.006	3.105	2.897	2.262	1.713	1.371	0.927	0.394
	50	0.933	2.148	3.168	2.812	2.268	1.825	1.381	0.906	0.455
	70	0.963	2.153	3.148	2.877	2.350	1.888	1.422	0.937	0.427
	90	0.993	2.173	3.145	2.858	2.342	1.882	1.416	0.934	0.473

TABLE 5-3 (continued)

C/L	V ft/sec \ X/L	0.1	0.2	0.3	0.4	0.5	0.6	0.7	0.8	0.9
0.5	Static	0.344	0.339	0.230	0.498	0.871	0.498	0.230	0.339	0.344
	10	0.340	0.858	1.436	1.967	2.560	2.409	2.191	1.750	1.004
	30	0.619	1.300	1.967	2.821	3.747	3.203	2.062	1.325	0.879
	50	0.718	1.374	2.191	3.120	3.726	3.051	2.242	1.494	0.759
	70	0.711	1.436	2.251	3.093	3.700	3.117	2.296	1.516	0.780
	90	0.724	1.471	2.276	3.092	3.703	3.137	2.307	1.521	0.790
0.7	Static	0.389	0.495	0.479	0.344	0.242	0.586	1.005	0.649	0.365
	10	0.070	0.250	0.413	0.301	0.225	1.020	1.846	1.565	0.906
	30	0.351	0.512	0.925	1.464	1.814	2.455	3.163	2.100	0.646
	50	0.368	0.741	1.191	1.700	2.207	2.705	3.024	2.122	1.015
	70	0.398	0.802	1.296	1.803	2.245	2.723	3.087	2.175	1.014
	90	0.402	0.840	1.337	1.809	2.244	2.736	3.093	2.191	1.032

TABLE 5-3 (continued)

C/L	V ft/sec \ X/L	0.1	0.2	0.3	0.4	0.5	0.6	0.7	0.8	0.9
0.9	Static	0.152	0.202	0.211	0.179	0.107	0.128	0.275	0.454	0.661
	10	1.075	1.674	1.757	1.583	1.427	1.398	1.413	1.191	0.433
	30	0.212	0.036	0.089	0.220	0.192	0.516	0.503	0.982	1.445
	50	0.004	0.107	0.178	0.297	0.582	0.762	0.836	1.116	1.264
	70	0.045	0.143	0.251	0.411	0.615	0.715	0.812	1.079	1.165
	90	0.081	0.217	0.369	0.542	0.723	0.838	0.982	1.240	1.270
	(b) λ = 30									
0.1	Static	0.597	0.374	0.189	0.043	0.109	0.175	0.199	0.181	0.122
	10	0.981	1.090	0.981	0.697	0.497	0.395	0.263	0.143	0.076
	30	1.234	1.285	1.077	0.897	0.757	0.595	0.439	0.293	0.144
	50	1.269	1.274	1.055	0.909	0.773	0.595	0.452	0.310	0.141
	70	1.300	1.419	1.191	1.023	0.868	0.674	0.495	0.348	0.162
	90	1.300	1.374	1.145	0.992	0.844	0.650	0.496	0.341	0.155

TABLE 5-3 (continued)

C/L	V ft/sec \ X/L	0.1	0.2	0.3	0.4	0.5	0.6	0.7	0.8	0.9
0.3	Static	0.186	0.414	0.739	0.324	0.110	0.321	0.423	0.412	0.290
	10	0.487	0.987	1.637	1.543	1.289	0.848	0.387	0.030	0.114
	30	0.738	1.724	2.732	2.470	1.818	1.287	0.998	0.643	0.239
	50	0.865	2.025	2.007	2.627	2.076	1.640	1.220	0.782	0.387
	70	0.924	2.083	3.056	2.772	2.240	1.783	1.330	0.866	0.434
	90	0.969	2.130	3.089	2.794	2.274	1.818	1.360	0.891	0.449
0.5	Static	0.238	0.272	0.171	0.205	0.561	0.205	0.171	0.272	0.238
	10	0.470	1.101	1.751	2.314	2.924	2.793	2.573	2.072	1.188
	30	0.282	0.671	1.126	1.858	2.742	2.235	1.217	0.693	0.539
	50	0.541	1.051	1.764	2.632	3.218	2.563	1.815	1.170	0.581
	70	0.606	1.246	2.001	2.808	3.403	2.831	2.046	1.325	0.675
	90	0.657	1.349	2.116	2.909	3.513	2.955	2.148	1.399	0.723

TABLE 5-3 (continued)

C/L	V ft/sec \ X/L	0.1	0.2	0.3	0.4	0.5	0.6	0.7	0.8	0.9
0.7	Static	0.290	0.412	0.423	0.321	0.110	0.324	0.739	0.414	0.186
	10	1.018	0.983	2.672	2.831	2.410	1.537	0.448	0.216	0.091
	30	0.125	0.374	0.274	0.084	0.372	1.072	1.964	1.214	0.178
	50	0.062	0.174	0.437	0.838	1.309	1.840	2.267	1.552	0.707
	70	0.207	0.452	0.833	1.275	1.695	2.195	2.624	1.824	0.822
	90	0.274	0.607	1.031	1.460	1.879	2.386	2.787	1.958	0.904
0.9	Static	0.122	0.181	0.199	0.175	0.109	0.043	0.189	0.374	0.597
	10	0.815	1.724	2.576	3.131	3.298	3.078	2.507	1.780	1.195
	30	0.557	0.707	1.033	1.346	1.008	0.617	0.444	0.313	1.095
	50	0.430	0.688	0.885	0.923	0.689	0.460	0.231	0.325	0.840
	70	0.253	0.402	0.470	0.413	0.242	0.109	0.094	0.538	0.871
	90	0.121	0.151	0.115	0.010	0.151	0.288	0.502	0.875	1.070

TABLE 5-3 (continued)

(c) $\lambda = 50$

C/L	V ft/sec \ X/L	0.1	0.2	0.3	0.4	0.5	0.6	0.7	0.8	0.9
0.1	Static	0.586	0.362	0.178	0.032	0.101	0.165	0.189	0.171	0.113
	10	0.864	0.878	0.701	0.378	0.164	0.076	0.018	0.072	0.042
	30	1.211	1.243	1.024	0.836	0.693	0.534	0.385	0.252	0.121
	50	1.261	1.259	1.036	0.887	0.750	0.574	0.432	0.295	0.133
	70	1.295	1.409	1.177	1.008	0.852	0.659	0.497	0.338	0.156
	90	1.297	1.368	1.138	0.984	0.835	0.642	0.488	0.335	0.152
0.3	Static	0.157	0.381	0.705	0.293	0.088	0.294	0.393	0.382	0.262
	10	0.716	1.413	2.194	2.162	1.928	1.479	0.961	0.468	0.128
	30	0.515	1.316	2.194	1.855	1.178	0.672	0.459	0.235	0.015
	50	0.742	1.803	2.716	2.295	1.729	1.308	0.929	0.560	0.264
	70	0.850	1.950	2.882	2.573	2.032	1.583	1.156	0.733	0.360
	90	0.922	2.046	2.980	2.669	2.144	1.693	1.251	0.807	0.403

TABLE 5-3 (continued)

C/L	$V_{ft/sec}$ \ X/L	0.1	0.2	0.3	0.4	0.5	0.6	0.7	0.8	0.9
0.5	Static	0.208	0.241	0.143	0.173	0.528	0.173	0.143	0.241	0.208
	10	0.060	0.277	0.706	1.159	1.728	1.613	1.492	1.213	0.705
	30	0.144	0.400	0.750	1.425	2.294	1.803	0.843	0.424	0.402
	50	0.299	0.608	1.178	1.964	2.522	1.894	1.229	0.726	0.339
	70	0.431	0.928	1.583	2.331	2.905	2.354	1.628	1.007	0.500
	90	0.535	1.130	1.829	2.581	3.170	2.626	1.860	1.179	0.602
0.7	Static	0.262	0.382	0.393	0.294	0.088	0.293	0.705	0.381	0.157
	10	0.531	1.135	1.643	1.760	1.311	0.429	0.653	0.705	0.445
	30	0.081	0.020	0.171	0.557	0.853	1.550	2.413	1.574	0.379
	50	0.189	0.294	0.190	0.127	0.572	1.130	1.645	1.090	0.462
	70	0.055	0.026	0.207	0.560	0.951	1.480	1.998	1.350	0.564
	90	0.069	0.235	0.542	0.901	1.297	1.827	2.297	1.586	0.699

TABLE 5-3 (continued)

C/L	V ft/sec. \ X/L	0.1	0.2	0.3	0.4	0.5	0.6	0.7	0.8	0.9
0.9	Static	0.113	0.171	0.189	0.165	0.101	0.032	0.178	0.362	0.586
	10	0.690	1.635	2.677	3.434	3.683	3.374	2.595	1.682	1.069
	30	0.036	0.254	0.223	0.056	0.439	0.795	0.822	1.279	1.626
	50	0.510	0.858	1.134	1.216	0.993	0.752	0.478	0.155	0.760
	70	0.524	0.908	1.148	1.186	1.045	0.883	0.589	0.032	0.600
	90	0.388	0.640	0.762	0.748	0.620	0.453	0.149	0.386	0.804
					(d) λ = 70					
0.1	Static	0.582	0.360	0.176	0.031	0.093	0.157	0.181	0.165	0.107
	10	0.761	0.690	0.453	0.904	0.133	0.210	0.267	0.260	0.145
	30	1.179	1.185	0.947	0.748	0.601	0.446	0.308	0.193	0.088
	50	1.249	1.238	1.008	0.855	0.717	0.542	0.405	0.274	0.121
	70	1.286	1.394	1.157	0.985	0.828	0.636	0.477	0.323	0.148
	90	1.292	1.360	1.127	0.971	0.822	0.629	0.477	0.327	0.147

TABLE 5-3 (continued)

C/L	V ft/sec \ X/L	0.1	0.2	0.3	0.4	0.5	0.6	0.7	0.8	0.9
0.3	Static	0.149	0.374	0.700	0.290	0.069	0.273	0.371	0.362	0.247
	10	0.522	1.065	1.744	1.654	1.400	0.971	0.510	0.117	0.072
	30	0.353	1.018	1.797	1.404	0.709	0.220	0.063	0.067	0.150
	50	0.590	1.527	2.355	1.882	1.299	0.895	0.568	0.285	0.111
	70	0.749	1.768	2.645	2.301	1.748	1.312	0.918	0.551	0.260
	90	0.857	1.928	2.825	2.493	1.9630	1.517	1.096	0.689	0.337
0.5	Static	0.190	0.220	0.120	0.172	0.527	0.172	0.120	0.220	0.190
	10	0.183	0.062	0.265	0.651	1.198	1.105	1.049	0.880	0.523
	30	0.412	0.877	1.365	2.121	3.020	2.502	1.461	0.904	0.673
	50	0.152	0.332	0.811	1.545	2.088	1.475	0.861	0.451	0.192
	70	0.246	0.590	1.139	1.824	2.376	1.847	1.184	0.669	0.314
	90	0.385	0.858	1.472	2.173	2.745	2.219	1.504	0.907	0.495

TABLE 5-3 (continued)

C/L	V ft/sec \ X/L	0.1	0.2	0.3	0.4	0.5	0.6	0.7	0.8	0.9
0.7	Static	0.247	0.362	0.371	0.273	0.069	0.290	0.700	0.374	0.149
	10	0.486	1.064	1.551	1.642	1.198	0.306	0.750	0.779	0.488
	30	0.201	0.228	0.507	0.922	1.218	1.917	2.754	1.823	0.499
	50	0.078	0.110	0.039	0.382	0.842	1.336	1.871	1.274	0.572
	70	0.208	0.312	0.179	0.125	0.500	1.044	1.615	1.064	0.411
	90	0.131	0.129	0.068	0.359	0.733	1.286	1.823	1.226	0.502
0.9	Static	0.107	0.165	0.181	0.157	0.093	0.031	0.176	0.360	0.582
	10	0.247	0.789	1.558	2.216	2.456	2.161	1.482	0.841	0.629
	30	0.243	0.124	0.263	0.476	0.101	0.264	0.333	0.901	1.420
	50	0.160	0.228	0.318	0.300	0.041	0.171	0.342	0.784	1.108
	70	0.479	0.845	1.080	1.109	0.960	0.805	0.520	0.094	0.644
	90	0.541	0.927	1.145	1.185	1.072	0.890	0.532	0.099	0.650

TABLE 5-3 (continued)

(e) $\lambda = 90$

C/L	V ft/sec \ X/L	0.1	0.2	0.3	0.4	0.5	0.6	0.7	0.8	0.9
0.1	Static	0.582	0.361	0.178	0.035	0.085	0.149	0.174	0.158	0.103
	10	0.716	0.604	0.338	0.038	0.268	0.340	0.381	0.345	0.190
	30	1.138	1.111	0.851	0.638	0.486	0.336	0.212	0.120	0.047
	50	1.233	1.210	0.971	0.813	0.673	0.500	0.368	0.246	0.106
	70	1.275	1.373	1.131	0.954	0.796	0.605	0.450	0.302	0.136
	90	1.286	1.349	1.112	0.954	0.804	0.613	0.463	0.315	0.141
0.3	Static	0.148	0.376	0.705	0.298	0.048	0.252	0.351	0.346	0.235
	10	0.642	1.253	1.975	1.937	1.713	1.256	0.745	0.309	0.052
	30	0.348	1.001	1.769	1.373	0.680	0.190	0.035	0.083	0.154
	50	0.439	1.254	1.997	1.473	0.872	0.487	0.210	0.012	0.042
	70	0.633	1.558	2.370	1.988	1.421	0.998	0.644	0.341	0.143
	90	0.776	1.783	2.635	2.275	1.733	1.299	0.906	0.544	0.256

TABLE 5-3 (continued)

C/L	V ft/sec \ X/L	0.1	0.2	0.3	0.4	0.5	0.6	0.7	0.8	0.9
0.5	Static	0.176	0.200	0.097	0.183	0.538	0.183	0.097	0.200	0.176
	10	0.205	0.571	1.047	1.576	2.199	2.045	1.854	1.528	0.917
	30	0.592	1.214	1.810	2.620	3.534	3.004	1.908	1.242	0.854
	50	0.201	0.412	0.908	1.658	2.209	1.588	0.959	0.531	0.242
	70	0.113	0.348	0.819	1.459	1.997	1.482	0.864	0.4268	0.182
	90	0.236	0.589	1.120	1.770	2.325	1.816	1.151	0.638	0.3024
0.7	Static	0.235	0.346	0.351	0.252	0.048	0.298	0.705	0.376	0.148
	10	0.278	0.729	1.131	1.133	0.643	0.208	1.172	1.120	0.700
	30	0.112	0.331	0.217	0.101	0.362	1.095	2.030	1.265	0.187
	50	0.238	0.452	0.765	1.208	1.703	2.213	2.598	1.834	0.885
	70	0.152	0.220	0.067	0.253	0.637	1.173	1.726	1.155	0.467
	90	0.239	0.329	0.202	0.057	0.419	0.983	1.557	1.025	0.394

TABLE 5-3 (continued)

C/L	V ft/sec \ X/L	0.1	0.2	0.3	0.4	0.5	0.6	0.7	0.8	0.9
0.9	Static	0.103	0.158	0.174	0.149	0.085	0.035	0.178	0.361	0.582
	10	0.096	0.490	1.152	1.769	2.006	1.714	1.073	0.537	0.474
	30	0.047	0.367	0.361	0.256	0.680	0.996	0.958	1.392	1.710
	50	0.136	0.164	0.222	0.201	0.049	0.267	0.439	0.849	1.043
	70	0.176	0.308	0.386	0.318	0.134	0.014	0.176	0.630	0.946
	90	0.476	0.821	1.015	0.035	0.913	0.740	0.402	0.205	0.714

TABLE 5-4

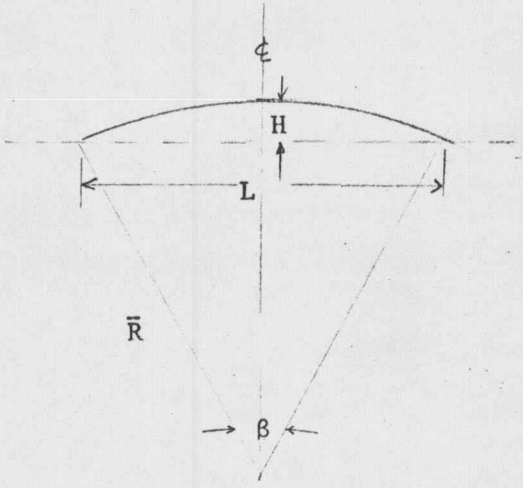
Maximum Stresses Computed by the Elastic Theory (E.T.) and by the Deflection Theory (D.T.) (λ = 50)

(psi)

P lb	C/L	0.1	0.2	0.3	0.4	0.5
P=1.0	E.T.	0.581	0.743	0.679	0.560	0.506
	D.T.	0.586	0.762	0.705	0.585	0.528
	Difference %	0.8	2.5	3.8	4.4	4.3
P=10.0	E.T.	5.806	7.433	6.786	5.600	5.063
	D.T.	6.191	8.994	9.438	7.323	5.971
	Difference %	6.5	21.1	38.9	30.7	18.0

APPENDIX B

RELATIONSHIP AMONG λ, L, H, H/L, β AND $\bar{R}$



$$H = \bar{R} - \bar{R}\cos\frac{\beta}{2}, \text{ since } \cos\frac{\beta}{2} \doteq 1 - \frac{1}{2}\left(\frac{\beta}{2}\right)^2$$

$$\Rightarrow H = R\left[1 - 1 + \frac{1}{2}\left(\frac{\beta}{2}\right)^2\right] = \frac{R\beta^2}{8} \qquad \text{----------(1)}$$

$$L = 2R\sin\frac{\beta}{2} = 4R\sin\frac{\beta}{4}\cos\frac{\beta}{4}$$

$$H = R\left(1 - \cos\frac{\beta}{2}\right) = 2R\sin^2\frac{\beta}{4}$$

$$\Rightarrow \frac{H}{L} = \frac{1}{2}\tan\frac{\beta}{4} \qquad \text{----------(2)}$$

From Eqs. (1) and (2), it is evident that if L is held fixed, β and $\bar{R}$ may be expressed in terms of H.

From Eq. (3.8),

$$\lambda = \frac{4}{\sqrt{3}} \frac{H}{R^*} \qquad \text{----------(3)}$$

Then, if R^* is constant, λ may also be expressed as a single function of H. Thus, Eqs. (1) and (3) constitute an interrelationship among the six variables. Of course, to obtain a unique solution, two of the six variables must be held constant. In this work, L and R^* are constant.

BIBLIOGRAPHY

1. S. P. Timoshenko and J. M. Gere: "Theory of Elastic Stability," Ch. 7, McGraw-Hill Book Company.

2. G. L. Rogers: "Dynamics of Frame Structures," John Wiley & Sons, p. 240.

3. J. V. Huddeston: "Finite Deflections and Snap-Through of High Circular Arches," pp. 763-769, J. of Applied Mechanics, December, 1968.

4. H. L. Shreyer and E. F. Masur: "Buckling of Shallow Arches," pp. 1-19, EM 4, ASCE, August, 1966.

5. A. Gjelsvik and S. R. Bodner: "Energy Criterion and Snap Buckling of Arches," pp. 87-135, EM 5, ASCE, October, 1962.

6. C. Oran: "Complementary Energy Method for Buckling of Arches," pp. 639-651, EM 2, ASCE, April, 1968.

7. C. Oran and R. S. Reagan: "Buckling of Uniformly Compressed Circular Arches," pp. 879-895, EM 4, ASCE, August, 1969.

8. D. A. Dadeppo and R. Schmidt: "Large Sideward Deflection of Two-Hinged Circular Arches," J. of Engineering for Industry, pp. 1-7, paper No. 71-DE-E, 1971.

9. N. J. Hoff and Victor G. Bruce: "Dynamic Analysis of the Buckling of Laterally Loaded Flat Arches," Polytechnic Institute of Brooklyn Aeronautical Laboratories (PIBAL) Report No. 191, October, 1951.

10. Y. C. Fung and A. Kaplan: "Buckling of Low Arches or Curved Beams of Small Curvature," NACA Technical Note 2840, 1952.

11. W. Stuiver: "On the Buckling of Rings Subject to Impulsive Pressures," J. of Applied Mechanics paper No. 65 - APMW - 1.

12. H. L. Langhaar, A. P. Boresi, and D. R. Carver: "Energy Theory of Buckling of Circular Elastic Rings and ARches," Proceedings of the Second U. S. National Congress of Applied Mechanics, pp. 437-444.

13. G. A. Wempner and N. E. Kesti: "On the Buckling of Circular Arches and Rings," pp. 843-849, Proceedings of the Fourth U. S. National Congress of Applied Mechanics.

14. C. S. Hsu, C. T. Kuo, and S. S. Lee: "On the Final State of Shallow Arches in Elastic Foundations Subjected to Dynamical Loads," J. of Applied Mechanics, pp. 713-723, December, 1968.

15. M. C. Cheung and C. D. Babcock, Jr.: "An Energy Approach to the Dynamic Stability of Arches," J. of Applied Mechanics, pp. 1012-1018, December, 1970.

16. R. R. Arches: "Small Vibrations of Thin Incomplete Circular Rings," Int. J. Mech. Sci. 1960 Vol. 1, pp. 45-56.

17. S. P. Timoshenko: "Vibration Problems in Engineering," pp. 351-356, D. Van Nostrand Company, Inc., 1937.

18. R. D. Mindlin and L. E. Goodman: "Beam Vibrations With Time-Dependent Boundary Conditions," J. of Applied Mechanics, pp. 377-380, December, 1950.

19. C. E. Inglis: "A Mathematical Treatise on Vibrations in Railway Bridges," Cambridge University Press, 1934.

20. W. Y. Tseng and J. Dugundji: "Nonlinear Vibrations of a Buckled Beam Under Harmonic Excitation," J. of Applied Mechanics, paper No. 70-WA/APM-48.

21. C. S. Hsu and C. T. Kuo: "Dynamic Stability Criterion for Clamped Shallow Arches Under Timewise Step Loads," J. of Applied Mechanics, pp. 1925-1931, October, 1969.

22. J. S. Humphreys: "On Dynamic Snap Buckling of Shallow Arches," AIAA J. Vol. 4, No. 5, pp. 878-886, 1966.

23. C. S. Hsu: "Equilibrium Configurations of a Shallow Arches of Arbitrary Shape and Their Dynamic Stability Character," Int. J. Non-linear Mech, Vol. 3, pp. 113-116, 1968.

24. R. K. Bernhard: "Dynamic Relations Between Moving Loads & Structures," Mechanical Engineer, p. 696, Vol. 60, September, 1938.

25. R. K. Bernhard: "Dynamic Stress Analysis of Railway Bridges," ASCE, January, 1941, Vol. 67, p. 47.

26. C. S. Hsu: "On Dynamic Stability of Elastic Bodies With Prescribed Initial Conditions," Int. J. Eng. Sci., March 1966, Vol. 4, pp. 1-21.

27. C. S. Hsu: "The Effects of Various Parameters on the Dynamic Stability of a Shallow Arch," J. of Applied Mechanics, June 1967, pp. 349-358.

28. N. M. Newmark: "Interaction Between Rib and Superstructure in Concrete Arch Bridges," ASCE, September 1936, Vol. 62.

29. D. B. Hall: "Deflection by Geometry," ASCE, December 1936, Vol. 62, p. 1952.

30. C. S. Whitney: "Design of Symmetrical Concrete Arches," ASCE, Transaction, Vol. 88, p. 931, 1952.

31. L. G. Straub: "Plastic Flow in Concrete Arches," ASCE, Structural Division, Vol. 56, p. 49, 1930.

32. "Rainbow Arch Bridge Over Niagara Gorge," Symposium, ASCE, Structural Division, October 1943.

33. J. F. Fleming and J. P. Romuldi: "Dynamic Response of Highway Bridge," ASCE, St. 7, Vol. 87, p. 31, October 1961.

34. C. F. Kee: "Lateral Inelastic Buckling of Tied Arches," ASCE, St. 1, Vol. 87, p. 23, January 1961.

35. C. A. Miller and S. A. Guralnick: "Influence Coefficients for Two-Hinged Arches," ASCE, St. 4, Vol. 88, p. 41, August 1962.

36. G. Wastiung: "Stability Problems of Compressed Steel Members and Arch Bridges," ASCE, Vol. 86, p. 47, St. 6, June 1960.

37. J. M. Biggs and H. S. Suer: "The Vibration of Simple Span Highway Bridges," ASCE, Vol. 83, p. 1186, St. 2, March 1957.

38. H. A. Miklofsky and O. J. Sotillo: "Design of Flexible Steel Arches by Interaction Diagrams," ASCE, Vol. 83, p. 1190, St. 2, March 1957.

39. A. F. Diwan: "Analysis of Open-Spandrel Arches," ASCE, Vol. 84, p. 1564, St. 2, March 1958.

40. J. S. Licari and E. N. Wilson: "Dynamic Response of a Beam Subjected to a Moving Forcing System," Proceedings of the Fourth U.S. National Congress of Applied Mechanics, pp. 419-425.

41. D. A. Dadeppo and R. Schmidt: "Nonlinear Analysis of Buckling and Postbuckling Behavior of Circular Arches, "Zeitschrift für angewandte Mathematik und Physik," Vol. 20, No. 6, 1969, pp. 847-857.

42. Y. C. Fung: "Foundations of Solid Mechanics," Prentice-Hall Book Company, 1969.

43. C. F. Lo and H. D. Conway: "The Elastic Stability of Curved Beams," Int. J. Mech. Sci. 9, pp. 527-538, 1967.

44. C. F. Lo and H. D. Conway: "Further Studies on the Elastic Stability of Curved Beams," Int. J. Mech. Sci. 9, pp. 707-718, 1967.

45. E. Reissner: "Note on the Problem of Vibrations of Slightly Curved Bars," J. of Applied Mechanics, June 1954, pp. 195-196.

46. J. F. Dickie and P. Broughton: "Stability Criterion for Shallow Arches," ASCE, Eng. Mech. Division, June 1971, pp. 951-965.

47. R. E. Fulton and F. W. Barton: "Dynamic Buckling of Shallow Arches," ASCE, Eng. Mech. Division, June 1971, pp. 865-877.

48. J. S. Kennedy and A. S. Aggarwal: "Effect of Weight on Large Deflections of Arches," ASCE, Eng. Mech. Division, June 1971, pp. 637-644.

49. C. J. Smitses: "Dynamic Snap-through Buckling of Low Arches and Shallow Spherical Caps," Ph.D. Dissertation, Department of Aeronautics and Astronautics, Stanford University, June 1965.

50. C. S. Hsu: "Stability of Shallow Arches Against Snap Through Under Timewise Step Load," J. of Applied Mechanics, Vol. 35, No. 1, March 1968, pp. 31-39.

51. M. H. Lock: "Snapping of Shallow Sinusoidal Arch Under a Step Pressure Load," AIAA, J. Vol. 4, No. 7, July 1966.

52. J. J. Stoker: "Nonlinear Vibration," Interscience Publishers, Inc.

53. Ralston and Wilf: "Mathematical Methods for Digital Computers," Wiley & Sons, New York, 1960. pp. 110-120.

54. L. C. Maugh: "Statically Inderterminate Structures," John Wiley & Sons, Inc., New York.

LIBRARY
Montana State University
Bozeman

MONTANA STATE UNIVERSITY LIBRARIES
3 1762 10010883 4

D378
L614
cop.2

Liao, Johnson
The behavior of shallo
arches subjected to
static and dynamic loads

DATE	ISSUED TO
APR	JIM WHALEY & HEDGES NI NE

D378
L614
Cop. 2